ABSTRACT

STEHLE, NICHOLAS DAVID. Spatial Domain Decomposition Methodology for Particle Transport Problems with Diffusive Subdomains. (Under the direction of Dmitriy Y. Anistratov.)

In this work we develop methodologies for domain decomposition for particle transport problems in transport and diffusive regions for 1D slab, and 2D Cartesian geometries. Here we use a set of low-order equations based off the second moment method to solve problems in the entire domain, and use a transport solver in areas of the domain where there are significant transport effects. Our methodologies are based off the Linear Discontinuous (LD) and Lumped Linear Discontinuous (LLD) transport equations for 1D, and the Simple Corner Balance method for 2D. Domains are split into diffusive and transport regions according to metrics developed based off the Quasidiffusion (Eddington) factors. To couple the domains, boundary conditions were developed from an asymptotic diffusion analysis on the transport discretization. Numerical results are presented, which show that this method can successfully identify diffusive regions, and solve the transport problem with a sufficient level of accuracy compared to one solved without using domain decomposition.

Spatial Domain Decomposition Methodology for Particle Transport Problems with Diffusive Subdomains

by
Nicholas David Stehle

A thesis submitted to the Graduate Faculty of
North Carolina State University
in partial fulfillment of the
requirements for the Degree of
Master of Science

Nuclear Engineering

Raleigh, North Carolina

2011

APPROVED BY:

Yousry Y. Azmy

John Harlim

Dmitriy Y. Anistratov
Chair of Advisory Committee

DEDICATION

To Jackie, thank you for keeping me sane these past couple of years by driving me crazy.

BIOGRAPHY

Nicholas (Nick) Stehle, was born in San Antonio TX, to Richard and Deborah Stehle. He started taking math classes at North Carolina State University in 2004 during his senior year of high school. He later enrolled in the college's Nuclear Engineering program after graduation starting courses full-time in 2005. After graduating Magna Cum Laude in 2009 with B.S. degrees in Nuclear Engineering and Applied Mathematics, he continued his coursework by pursing a MS in Nuclear Engineering.

ACKNOWLEDGEMENTS

I would like to thank the Nuclear Engineering Department and all the associated professors who helped me get where I am today. First, I would like to thank my advisor, Dr. Dmitriy Y. Anistratov for the countless hours in his office where he answered all the questions I never knew I had. I would also like to make a special note of the rest of my committee, Dr. Azmy, and Dr. Harlim, who were both very patient and flexible for my last minute defense. I would also like to thank each of the professors that gave me opportunities to better myself, which include, but are not limited to, Dr. Paul Turinsky, Dr. Man-Sung Yim, and Dr. Steve Shannon. I would also like to mention the staff of the reactor program, Larry, Kerry, Andrew, and Scott, for their patience with me while I learned the ins and outs of the PULSTAR reactor. I would especially like to thank all my peers, that endured this program with me, including Wes, Ross, Andrew, Steve, Jason, and all the various other people who came into the back office and provided yet another distraction from what I should have been working on.

I would also like to thank the people outside of the department who helped me with my work. Dr. Marvin L. Adams at Texas A&M University provided several suggestions for improving the work presented here. I would also like to thank the members of CCS-2 at Los Alamos National Laboratory, including Jeff Densmore, and Todd Urbatsch, who helped me get started on this work. Finally, I would like to thank my family for the support all these years, I wouldn't be where I am without you.

TABLE OF CONTENTS

LIST OF TABLES

LIST OF FIGURES

Chapter 1

Introduction

Simulating the interaction of radiation with matter has been a major subject of study in computational physics for many years. This is a complex task where particles (x-rays, neutrons, etc.) that interact with the surrounding material, but not each other, are modeled to see their distribution through various mediums. Most of these problems can be solved using a linear Boltzmann equation, which can be solved either using deterministic or stochastic methods. Deterministic algorithms require that the equation is discretized and the resulting system of equations is solved. This resulting system is relatively large and complex, so iterative methods must be used to solve it. Stochastic methods solve this problem using Monte Carlo techniques. [1]

For several decades the nuclear industry has been the driving motivation for solving and analyzing discrete ordinate problems. Simulating neutron movement in reactors answers questions about power distribution, heat transfer, cycling schemes, and so on. These methods can be expanded from neutron transport into electron and thermal radiation transport problems.

Using the source iteration approach in a deterministic method, the nth iteration can be interpreted in terms of angular fluxes of particles that had exactly n collisions if the initial guess is zero. It follows that optically thick, highly scattering problems will take a long time to converge because the particles will experience numerous scattering interactions. Similar problems will arise in stochastic methods too. Transport problems in such domains can be solved using a diffusion approximation, which are highly accurate and have a significantly smaller computational demand.

A diffusion approximation can be coupled with transport sweeps to "accelerate" the convergence of an iterative method. This is done by following each transport iteration with solving a set of low order (diffusion-like) equations designed to improve the result. The set of low order equations must be carefully developed to avoid stability difficulties which can greatly reduce their usefulness [2]. Well known techniques such as Diffusion Synthetic Acceleration

(DSA), Quasidiffusion (QD), and the second moment method (SM) have shown to be robust and accurate for solving optically thick problems with high scattering. [3] [4]

A method for analyzing a set of discrete equations is to preform an asymptotic diffusion analysis of the transport equation discretization. [5] This is where the total cross section is made arbitrarily large, while the source and absorption cross sections are inversely scaled. Following an expansion of the angular flux, the leading order solution to this problem becomes the diffusion approximation for a given discretization. This analysis proves a given discretization of the transport equation will have an accurate diffusion approximation that can be solved efficiently.

Diffusion approximations tend to lose accuracy where transport effects are dominant, for example, near boundaries or areas with significant absorption. Therefore a domain decomposition method can be employed so that the transport equation is used in areas where transport effects are significant, and the diffusion approximation elsewhere. [4] This method can therefore be used to significantly reduce CPU time to solve radiative transfer problems while still retaining an accurate solution to the problem compared to if it were solved only using the transport equation.

We should note that this domain decomposition method is not used in the traditional sense of computer science, where parallel architecture is used to solve the same set of equations in different parts of the domain. These methods methods of domain decompositions have been used to split either the spatial, angular or energy domains into subregions to be solved independently. [6], [7] [8] This allows computers to solve each region on a separate processor with a goal of spending less time solving the transport equation. Some of these methods typically showed a degradation in performance due to communication between processors.

Another form of domain decomposition is used where two different sets of equations are used to solve the transport problem. Klar has suggested method for solving radiative heat transfer problems using both the transport equation and a diffusion approximation; and a similar method is proposed for gas hydrodynamics. [9] Here all the spacial domains are decoupled, where they are solved independently of one another and connected by interface conditions.

To effectively utilize a domain decomposition method, regions where transport effects are significant have to be determined. This can be done using a variety of methods that quantify if the flux in a region is linearly anisotropic. These metrics for transport effects can then be used to determine if a region should be solved using either the transport equation or if a low-order diffusion approximation is sufficient. In his paper, Klar uses a similar method where he looks at how a density function deviates from the local Maxwellian in the transition from kinetic theory to macroscopic fluid equations. A conundrum arises here because evaluating the flux in a region requires the solution to the problem, that is, the solution to a problem is needed before solving the problem itself. Any measure of transport effects to split the domain will then need to be estimated on the fly, or diffusion areas will need to be predetermined based off intuition.

In this thesis, computational methods are developed for solving transport problems using a domain decomposition method. We show that a reasonably accurate solution can be obtained using multiple domains compared to a single domain for a set of representative test problems. We start by looking at the transport problem in 1D slab geometry, and 2D Cartesian geometry. We then develop a set of low-order equations that will both accelerate the transport solution and solve the problem for both types of domains. Metrics are developed to analyze transport effects and numerical results are provided to demonstrate the performance of the proposed approach.

In the first chapter of this thesis we provide a general framework for the tools that will be needed for using a domain decomposition algorithm. In the second chapter, we develop more specific equations and methodologies for 1D slab geometry. In the third chapter, we present numerical results from the methods developed in the previous chapter. In the fourth chapter, we develop derive the equations needed for domain decomposition in 2D slab geometry. We present the numerical results for this methodology in chapter five. In the last chapter we give our conclusions of the work presented. The 1D results for this paper will be presented at the 22nd International Conference on Transport Theory in Portland. [10] A summary of the 2D results will be presented at the ANS winter meeting. [11]

1.1 The Transport Problem

Here we look at various forms of the transport problem. The general equation for steady-state, one group, particle transport is

$$\vec{\Omega} \cdot \nabla\psi(\vec{r},\vec{\Omega}) + \sigma_t(\vec{r},\vec{\Omega})\psi(\vec{r},\vec{\Omega}) = \int_{4\pi} \sigma_s(\vec{r},\vec{\Omega}' \to \vec{\Omega})\psi(\vec{r},\vec{\Omega}')d\vec{\Omega}' + Q(\vec{r},\vec{\Omega}), \tag{1.1}$$

$$\psi(\vec{r}_s,\vec{\Omega}) = \psi_{in}(\vec{r}_s,\vec{\Omega}) \text{ for } \vec{\Omega}\cdot\vec{e}_s < 0. \tag{1.2}$$

ψ is the angular flux, σ_t and σ_s are the total and scattering cross sections. The first term in the balance equation, $\vec{\Omega} \cdot \nabla\psi(\vec{r},\vec{\Omega})$, represents the streaming operator. The second term, $\sigma_t(\vec{r},\vec{\Omega})\psi(\vec{r},\vec{\Omega})$, describes the collision rate density in the phase space of particles in the domain. The scattering term, $\int_{4\pi} \sigma_s(\vec{r},\vec{\Omega}' \to \vec{\Omega})\psi(\vec{r},\vec{\Omega}')d\vec{\Omega}'$, describes particles scattering thus changing direction. The last term is the external source, $Q(\vec{r},\vec{\Omega})$, which accounts for all particles appearing in the problem domain from sources in the domain itself. The boundary condition, Eq. 1.2, describes the incoming flux at the surface of the boundary $\vec{r}_s$. [12]. Other variables of note should be the scalar flux :

$$\phi(\vec{r}) = \int_{4\pi} \psi(\vec{r},\vec{\Omega})d\vec{\Omega} \tag{1.3}$$

and particle current

$$\vec{J}(\vec{r}) = \int_{4\pi} \vec{\Omega}\psi(\vec{r},\vec{\Omega})d\vec{\Omega} \tag{1.4}$$

For the rest of this study we will assume isotropic scattering, that is $\sigma_s(\vec{r},\vec{\Omega}) = \frac{1}{4\pi}\sigma_s(\vec{r})$. The equations presented here are general and can be used for a variety geometries. We will consider both 1D and 2D cases in this paper.

1.1.1 1D Slab Geometry

Here we use Eq. 1.1 for single dimensional slab geometry. The equations simplify to

$$\mu\frac{\partial}{\partial x}\psi(x,\mu) + \sigma_t\psi(x,\mu) = \frac{1}{2}\sigma_s\int_{-1}^{1}\psi(x,\mu')d\mu + \frac{1}{2}Q(x), \tag{1.5a}$$

$$0 \le x \le L, \quad -1 \le \mu \le 1, \tag{1.5b}$$

$$\psi|_{x=0} = \psi_{in}^{+}(\mu), \quad \mu > 0 \tag{1.5c}$$

$$\psi|_{x=L} = \psi_{in}^{-}(\mu), \quad \mu < 0 \tag{1.5d}$$

The angular direction μ is described as the cosine of the azimuthal angle θ, i.e. $\mu = \cos(\theta)$. The scalar flux for slab geometry would then be

$$\phi(x) = \int_{-1}^{1}\psi(x,\mu)d\mu. \tag{1.6}$$

These equations will be discretized by the Linear Discontinuous (LD) and Lumped Linear Discontinuous (LLD) method used in this paper. [13]

1.1.2 2D Cartesian Geometry

Evaluating Eq. 1.1 for 2D Cartesian geometry would become

$$\mu\frac{\partial}{\partial x}\psi(\vec{r},\vec{\Omega}) + \eta\frac{\partial}{\partial y}\psi(\vec{r},\vec{\Omega}) + \sigma_t(\vec{r})\psi(\vec{r},\vec{\Omega}) = \frac{1}{4\pi}\sigma_s(\vec{r})\int_{4\pi}\psi(\vec{r},\vec{\Omega}')d\vec{\Omega}' + \frac{1}{4\pi}Q(\vec{r}) \tag{1.7}$$

Here $\vec{\Omega} = [\mu,\eta]$ where $\mu = \sin(\theta)\cos(\gamma)$, and $\eta = \sin(\theta)\sin(\gamma)$. The angles θ and γ are the azimuthal and the polar angle respectively, where they are defined for $0 \le \theta \le \pi$ and $0 \le \gamma \le 2\pi$. Note that $\vec{r} = [x,y]$. The boundary conditions for this problem are

$$\psi(\vec{r},\vec{\Omega})|_{x=0} = \psi_{left}^{in}(\vec{\Omega}), \text{ for } \mu > 0, \tag{1.8a}$$

$$\psi(\vec{r},\vec{\Omega})|_{x=X} = \psi^{in}_{right}(\vec{\Omega}),\ \text{for } \mu < 0, \tag{1.8b}$$

$$\psi(\vec{r},\vec{\Omega})|_{y=0} = \psi^{in}_{bottom}(\vec{\Omega}),\ \text{for } \eta > 0, \tag{1.8c}$$

$$\psi(\vec{r},\vec{\Omega})|_{y=Y} = \psi^{in}_{top}(\vec{\Omega}),\ \text{for } \eta < 0. \tag{1.8d}$$

The problem domain here would be defined for $0 \leq x \leq X$, $0 \leq y \leq Y$. These equations will be approximated by the Simple Corner Balance Method (SCB) that will be derived later. [14] [15].

1.2 Second Moment Method

There are several ways to solve the transport problem, the most basic is the source iteration method. [1] This is an iterative technique where the transport equation is iterated by

$$L\psi^{s+1} = S\psi^{s} + Q. \tag{1.9}$$

The operator L, represents the streaming and collision terms, while the S operator represents the scattering term; this is a generalization of Eq. 1.1. Here the superscript s is the iteration index. The solution for the angular flux is calculated iteratively by continually updating the scattering term. This method can be very slow to converge in areas of high scattering, so often times a low order acceleration method is used. This can be done through DSA like algorithms such as the second moment (SM) method [16]. These methods calculate the scalar flux and currents explicitly through a set of low order equations. These equations are formed by taking moments of the transport equation. The acceleration method can then be described as a two step process,

$$L\psi^{s+1/2} = S\psi^{s} + Q, \tag{1.10a}$$

$$\phi^{s+1} = D\psi^{s+1/2}. \tag{1.10b}$$

The angular flux to the solution of the transport problem is used to calculate the scalar flux through a diffusion approximation. This solution is then fed back into the scattering term of the high order transport problem. Diffusion Synthetic Acceleration (DSA) techniques for solving this problem would involve estimating the difference in the solution and the iteration and using that to accelerate the problem. This SM method will be applied to both the 1D slab, and the 2D Cartesian balance equations.

1.2.1 1D Slab Geometry

Consider Eq. 1.5a. To form the low order equations we will integrate the transport equation over all directional angles, μ, which yields,

$$\frac{d}{dx}J(x) + \sigma_a \phi(x) = Q(x). \tag{1.11}$$

The absorption cross section is defined as $\sigma_a = \sigma_t - \sigma_s$. We can again integrate the transport equation, Eq. 1.5a, with respect to the angular direction μ, to take another moment giving

$$\frac{d}{dx}\int_{-1}^{1} \mu^2 \psi(x,\mu) d\mu + \sigma_t J(x) = 0. \tag{1.12}$$

The first term in this equation can be expanded by defining a second moment closure term F as:

$$F(x) = \int_{-1}^{1} \left(\frac{1}{3} - \mu^2\right) \psi(x,\mu) d\mu. \tag{1.13}$$

Using this definition, Eq. 1.12 is rewritten as:

$$\frac{1}{3}\frac{d}{dx}\phi(x) + \sigma_t J(x) = \frac{\partial}{\partial x}F(x). \tag{1.14}$$

Using Eq. 1.11 and Eq. 1.14, we can solve explicitly for the scalar flux $\phi(x)$ and the current $J(x)$. To do this, however, we need to develop boundary conditions to close the system of equations. This can be done by finding the incoming current at either end of the slab; first consider the right boundary Eq. 1.5d:

$$J_{in}^{-} = \int_{-1}^{0} \mu\psi\left(L,\mu\right) d\mu. \tag{1.15}$$

This can then be expanded:

$$
\begin{aligned}
J_{in}^{-} &= \int_{-1}^{0} \mu \left(\psi - \frac{1}{2}\phi - \frac{3}{2}\mu J \right) d\mu + \int_{-1}^{0} \mu \left(\frac{1}{2}\phi + \frac{3}{2}\mu J \right) d\mu \\
&= \int_{-1}^{0} \mu\psi d\mu + \frac{1}{4}\phi - \frac{1}{2}J - \frac{1}{2}\phi + \frac{1}{2}J \\
&= \int_{-1}^{0} \mu\psi d\mu + \frac{1}{4}\int_{-1}^{1} \psi d\mu - \frac{1}{2}\int_{-1}^{1} \mu\psi d\mu - \frac{1}{4}\phi + \frac{1}{2}J \\
&= \frac{1}{4}\int_{-1}^{1} \psi d\mu - \frac{1}{2}\int_{0}^{1} \mu\psi d\mu + \frac{1}{2}\int_{-1}^{0} \mu\psi d\mu - \frac{1}{4}\phi + \frac{1}{2}J \\
&= \frac{1}{4}\int_{-1}^{1} \psi d\mu - \frac{1}{2}\int_{-1}^{1} |\mu|\psi d\mu - \frac{1}{4}\phi + \frac{1}{2}J \\
&= \frac{1}{4}\int_{-1}^{1} \left(1 - 2|\mu|\right) \psi d\mu - \frac{1}{4}\phi + \frac{1}{2}J.
\end{aligned}
$$

Rearranging this equation, we arrive at,

$$
\frac{1}{4}\phi(L) - \frac{1}{2}J(L) = \frac{1}{4}\int_{-1}^{1} \left(1 - 2|\mu|\right) \psi(L,\mu) d\mu - J_{in}^{-}. \tag{1.16}
$$

A similar method can be used for the left boundary condition at $x = 0$ arriving at:

$$
\frac{1}{4}\phi(0) + \frac{1}{2}J(0) = J_{in}^{+} + \frac{1}{4}\int_{-1}^{1} \left(1 - 2|\mu|\right) \psi(0,\mu) d\mu. \tag{1.17}
$$

We now have a complete set of equations that can be solved. This is done by solving the transport equation, Eq. 1.5a

$$
\mu \frac{\partial}{\partial x}\psi^{s+1/2}(x,\mu) + \sigma_t \psi^{s+1/2}(x,\mu) = \frac{1}{2}\sigma_s \phi^{s}(x) + \frac{1}{2}Q(x). \tag{1.18}
$$

This solution, $\psi^{s+1/2}$, is then used to calculate the closure term, from Eq. 1.14,

$$
F^{s+1/2}(x) = \int_{-1}^{1} \left(\frac{1}{3} - \mu^2 \right) \psi^{s+1/2}(x,\mu) d\mu. \tag{1.19}
$$

Now we solve the low-order second moment (LOSM) equations:

$$
\frac{d}{dx}J^{s+1}(x) + \sigma_a \phi^{s+1}(x) = Q(x), \tag{1.20a}
$$

$$
\frac{1}{3}\frac{d}{dx}\phi^{s+1}(x) + \sigma_t J^{s+1}(x) = \frac{d}{dx}F^{s+1/2}(x). \tag{1.20b}
$$

The solution to the low-order second moment equations, is then fed back into the transport equation, Eq. 1.18, and the process is repeated until the solution has converged.

1.2.2 2D Cartesian Geometry

To develop the set of low-order equations, the same method is used of integrating the transport equation, Eq. 1.7, over all angular directions. The zeroth moment would then be,

$$\frac{\partial}{\partial x}J_x(x,y) + \frac{\partial}{\partial y}J_y(x,y) + \sigma_a\phi(x,y) = Q(x,y). \tag{1.21}$$

J_x and J_y, denote the components of the current. We will then integrate the equation two more times with weights μ and η, which will yield,

$$\frac{\partial}{\partial x}\int_{4\pi}\mu^2\psi(x,y,\vec{\Omega})d\vec{\Omega} + \frac{\partial}{\partial y}\int_{4\pi}\mu\eta\psi(x,y,\vec{\Omega})d\vec{\Omega} + \sigma_t J_x(x,y) = 0, \tag{1.22a}$$

$$\frac{\partial}{\partial x}\int_{4\pi}\mu\eta\psi(x,y,\vec{\Omega})d\vec{\Omega} + \frac{\partial}{\partial y}\int_{4\pi}\eta^2\psi(x,y,\vec{\Omega})d\vec{\Omega} + \sigma_t J_y(x,y) = 0. \tag{1.22b}$$

Defining other second moment closure terms,

$$F_{xx}(x,y) = \int_{4\pi}\left(\frac{1}{3} - \mu^2\psi(x,y,\vec{\Omega})\right)d\vec{\Omega} \tag{1.23a}$$

$$F_{yy}(x,y) = \int_{4\pi}\left(\frac{1}{3} - \eta^2\psi(x,y,\vec{\Omega})\right)d\vec{\Omega} \tag{1.23b}$$

$$F_{xy}(x,y) = -\int_{4\pi}\eta\ \mu\psi(x,y,\vec{\Omega})d\vec{\Omega} \tag{1.23c}$$

Expanding these equations we can now simplify Eq. 1.22

$$\frac{1}{3}\frac{\partial}{\partial x}\phi(x,y) + \sigma_t J_x(x,y) = \frac{\partial}{\partial x}F_{xx}(x,y) + \frac{\partial}{\partial y}F_{xy}(x,y), \tag{1.24a}$$

$$\frac{1}{3}\frac{\partial}{\partial y}\phi(x,y) + \sigma_t J_y(x,y) = \frac{\partial}{\partial x}F_{xy}(x,y) + \frac{\partial}{\partial y}F_{yy}(x,y). \tag{1.24b}$$

Similar to the 1D version, this set of low order equations is explicitly solved for both the scalar flux, $\phi(x,y)$, and the current, $\vec{J}(x,y)$. To close this system we need to develop boundary conditions. This is done by finding the incoming current from Eq. 1.8; for the left cells we would have:

$$J^{left}_{x,in}(y) = \int_0^1\int_{-1}^1 \mu\psi(\vec{r},\vec{\Omega})|_{x=0}d\mu d\eta. \tag{1.25}$$

Making a linear anisotropic expansion of the angular flux we have

$$J_{x,in}^{left}(y) = \frac{1}{4\pi}\int_0^1 = \int_{-1}^{1} \mu\left[\phi(1,y) + 3\mu J_x(1,y) + 3\eta J_y(1,y)\right] d\mu d\eta + r_{left}(y), \tag{1.26}$$

which can be simplified to,

$$J_{x,in}^{left}(y) = \frac{1}{4\pi}\left[\phi(1,y) + 2J_x(1,y)\right] + r_{left}(y). \tag{1.27}$$

The difference in the angular flux and the approximation, r_{left} is defined by,

$$r_{left}(y) = \int_0^1\int_{-1}^{1} \mu\psi(\vec{r},\vec{\Omega})|_{x=0} d\mu d\eta - \frac{1}{4\pi}\left[\tilde{\phi}(1,y) + 2\tilde{J}_x(1,y)\right]$$

Note that we have defined $\tilde{\phi}$ and $\tilde{\vec{J}}$ in the residual to be the solution from the transport equation. Doing a similar method for the other boundaries we get,

$$J_{x,in}^{right}(y) = \frac{1}{4\pi}\left[-\phi(X,y) + 2J_x(X,y)\right] + r_{right}(y), \tag{1.28}$$

$$J_{y,in}^{bottom}(y) = \frac{1}{4\pi}\left[-\phi(x,1) + 2J_y(x,1)\right] + r_{bottom}(x), \tag{1.29}$$

$$J_{y,in}^{top}(y) = \frac{1}{4\pi}\left[-\phi(x,Y) + 2J_y(x,Y)\right] + r_{top}(x). \tag{1.30}$$

Each of the residuals of the P_1 expansion are defined using the transport solution. The complete iteration process is defined by first solving the transport equation, Eq. 1.7,

$$\mu\frac{\partial}{\partial x}\psi^{s+1/2}(\vec{r},\vec{\Omega}) + \eta\frac{\partial}{\partial y}\psi^{s+1/2}(\vec{r},\vec{\Omega}) + \sigma_t(\vec{r})\psi^{s+1/2}(\vec{r},\vec{\Omega}) = \frac{1}{4\pi}\sigma_s(\vec{r})\phi^s(\vec{r}) + \frac{1}{4\pi}Q(\vec{r}). \tag{1.31}$$

Then, we calculate the second moment closure terms, Eq. 1.23,

$$F_{xx}^{s+1/2}(x,y) = \int_{4\pi}\left(\frac{1}{3} - \mu^2\psi^{s+1/2}(x,y,\vec{\Omega})\right) d\vec{\Omega} \tag{1.32a}$$

$$F_{yy}^{s+1/2}(x,y) = \int_{4\pi}\left(\frac{1}{3} - \eta^2\psi^{s+1/2}(x,y,\vec{\Omega})\right) d\vec{\Omega} \tag{1.32b}$$

$$F_{xy}^{s+1/2}(x,y) = -\int_{4\pi} \eta\ \mu^2\psi^{s+1/2}(x,y,\vec{\Omega}) d\vec{\Omega} \tag{1.32c}$$

This step is followed by solving the low-order second moment equations,Eq. 1.21 and Eq. 1.24,

$$\frac{1}{3}\frac{\partial}{\partial x}\phi^{s+1}(x,y) + \sigma_t J_x^{s+1}(x,y) = \frac{\partial}{\partial x}F_{xx}^{s+1/2}(x,y) + \frac{\partial}{\partial y}F_{xy}^{s+1/2}(x,y), \tag{1.33a}$$

$$\frac{1}{3}\frac{\partial}{\partial y}\phi^{s+1}(x,y) + \sigma_t J_y^{s+1}(x,y) = \frac{\partial}{\partial x}F_{xy}^{s+1/2}(x,y) + \frac{\partial}{\partial y}F_{yy}^{s+1/2}(x,y). \tag{1.33b}$$

Here, the second moment terms F , and residuals for the boundary conditions r_* are calculated from the transport iteration. These equations are solved for over the whole domain, and the solution is used in the transport equation. This iteration process continues until we arrive at a solution.

1.3 Algorithm

The method for domain decomposition used in this paper is based off the Second Moment method outlined earlier. A problem domain will be split into multiple regions where the transport equation will be solved, hereafter referred to as transport subdomains, and diffusion subdomains. The LOSM equations will be used for multiple purposes,

1. To solve for the scalar flux and current everywhere in the problem domain.
2. To accelerate the solution of highly diffusive areas
3. To provide an approximation of the angular flux *in the diffusion subdomain* to the transport subdomain.

The angular approximations for the interfaces between subdomains will be estimated using either a P_1 approximation or from an asymptotic diffusion analysis of a transport discretization scheme. These approximations will then be used as transport boundary conditions at the interface of transport and diffusion subdomains. The algorithm for this method can be seen in Figure 1.1.

This method of domain decomposition method includes a few unique aspects. For one, the code automatically evaluates which areas in the problem domain are diffusive and does not solve the transport equation in those areas. The primary difference is this algorithm uses a fully consistent low-order discretization of the transport problem over the whole domain. By doing this we solve for the scalar flux everywhere without having to solve the transport problem everywhere. The low order set of equations is used everywhere, so production codes only have to modify the boundary conditions on their transport solvers by using the set of low order equations presented.

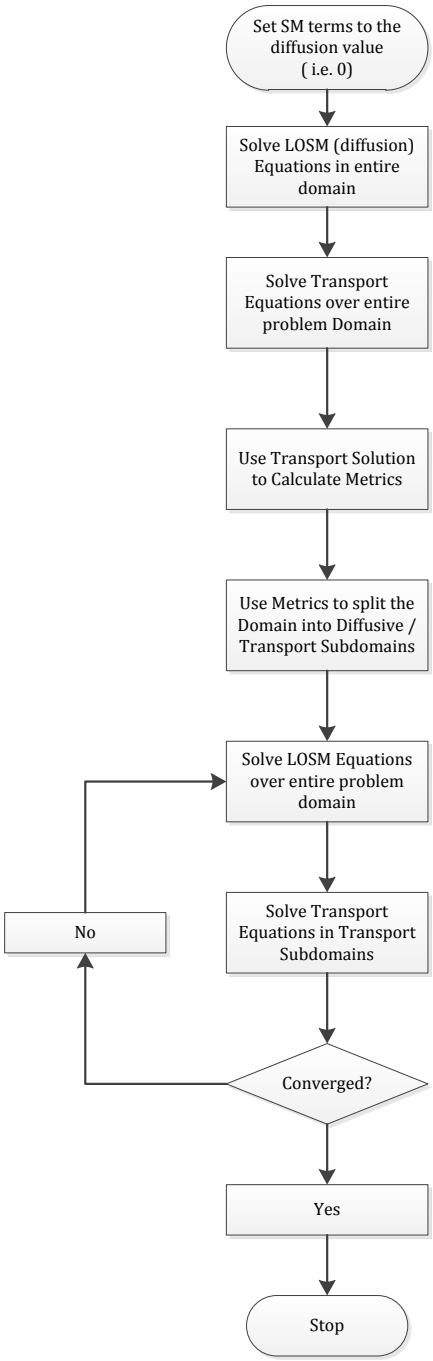

Figure 1.1: Proposed Algorithm for Solving Transport Problems

Chapter 2

Methodology for the LD Scheme in 1D Slab Geometry

In this chapter we look at how to develop discretized versions of the transport equation developed in Sec. 1.1.1. Here we use the Linear Discontinuous (LD) / Lumped Linear Discontinuous (LLD) Methods. We then develop the low-order second moment equations for the LD/LLD using the methods outlined in Sec. 1.2.1. We also consider an alternative set of low order equations that we develop from the Quasidiffusion (QD) method. We also develop a set of metrics for evaluating transport effects, and their associated discretized versions. We conclude this chapter by developing a set of boundary conditions to estimate the angular flux in the transport subdomains at the interfaces between subdomains.

2.1 LD / LLD Method

The transport equation for 1D slab geometry used is given by Eq. 1.5a. This problem is discretized by dividing the spacial domain into N spatial cells, and using a quadrature set to define the angular directions. The abscissa of the quadrature will be the angular direction. The spacial coordinates x will be subscripted by $i + 1/2$ for cell-edge values while cell average coordinates, and width will be defined as

$$x_i = \frac{1}{2}\left(x_{i+1/2} + x_{i-1/2}\right),$$

$$\Delta x_i = x_{i+1/2} - x_{i-1/2}, \qquad \Delta x_{i+1 1/2} = x_{i+1} - x_i,$$

where

$$i = 1 \ldots N, \quad 0 = x_{1/2} < \ldots < x_{i+1/2} < \ldots < x_{N+1/2} = X.$$

Similarly the angular direction μ_m will be defined for $m = 1 \ldots M$, for a given quadrature set. The cell-edge angular flux will be defined by:

$$\psi_{m,i+1/2} = \psi\left(x_{i+1/2}, \mu_m\right), \tag{2.1}$$

while the cell-average flux is given by

$$\psi_{m,i} = \frac{1}{\Delta x_i} \int_{x_{i-1/2}}^{x_{i+1/2}} \psi\left(x, \mu_m\right) dx. \tag{2.2}$$

The linear (first) spatial moment of the angular flux is

$$\hat{\psi}_{m,i} = \frac{6}{\Delta x_i^2} \int_{x_{i-1/2}}^{x_{i+1/2}} (x - x_i) \psi\left(x, \mu_m\right) dx. \tag{2.3}$$

The LD method [17] approximates the angular flux in the ith cell as

$$\psi_m(x) = \psi_{m,i} + \frac{2}{\Delta x_i}(x - x_i)\hat{\psi}_{m,i} \quad x_{i-1/2} \leq x \leq x_{i-1/2}. \tag{2.4}$$

The complete set of LD equations are

$$\mu_m\left(\psi_{m,i+1/2} - \psi_{m,i-1/2}\right) + \sigma_{t,i}\Delta x_i \psi_{m,i} = \frac{1}{2}\left(\sigma_{s,i}\phi_i + Q_i\right)\Delta x_i, \tag{2.5a}$$

$$\theta_i \mu_m\left(\psi_{m,i+1/2} + \psi_{m,i-1/2} - 2\psi_{m,i}\right) + \sigma_{t,i}\Delta x_i \hat{\psi}_{m,i} = \frac{1}{2}\left(\sigma_{s,i}\hat{\phi}_i + \hat{Q}_i\right)\Delta x_i, \tag{2.5b}$$

$$\begin{cases} \psi_{m,i+1/2} = \psi_{m,i} + \hat{\psi}_{m,i}, & \mu_m > 0 \\ \psi_{m,i-1/2} = \psi_{m,i} - \hat{\psi}_{m,i}, & \mu_m < 0 \end{cases} \tag{2.5c}$$

$$\theta_i = \begin{cases} 3, & \sigma_{t,i}\Delta x_i \leq \tau^* \\ 1, & \sigma_{t,i}\Delta x_i \geq \tau^* \end{cases} \tag{2.5d}$$

Here τ^* is a parameter used to define diffusive regions for the lumping parameter θ. This determines if the LD method ($\theta = 3$) or the LLD method ($\theta = 1$) is used. The scalar flux, $\phi(x)$, is calculated for cell average and cell edge by:

$$\phi_i = \sum_{m=1}^{M} \psi_{i,m} w_m, \quad \phi_{i+1/2} = \sum_{m=1}^{M} \psi_{i+1/2,m} w_m. \tag{2.6}$$

Here w_m is the quadrature weight. Similarly the first linear moment of the scalar flux is defined by:

$$\hat{\phi}_i = \sum_{m=1}^{M} \hat{\psi}_{i,m} w_m. \tag{2.7}$$

2.2 The Second Moment Method for the LD Scheme

Here we will develop the SM method for the LD/LLD equations for slab geometry using low order equations. [17] Starting with the discrete equations for LD/LLD defined by Eq. 2.5 and using the method outlined in Sec. 1.2, we can solve Eq. 2.5c for $\hat{\psi}_{i,m}$ and substitute this into Eq. 2.5b for $\mu_m > 0$.

$$\theta_i \mu_m \left(\psi_{m,i+1/2} + \psi_{m,i-1/2} - 2\psi_{m,i}\right) + \sigma_{t,i}\Delta x_i \left(\psi_{m,i+1/2} - \psi_{m,i}\right) = \frac{1}{2}\left(\sigma_{s,i}\hat{\phi}_i + \hat{Q}_i\right)\Delta x_i.$$

Solving for $\psi_{m,i}$, we have

$$\psi_{m,i} = \frac{\theta_i\mu_m + \sigma_{t,i}\Delta x_i}{2\theta_i\mu_m + \sigma_{t,i}\Delta x_i}\psi_{m,i+1/2} + \frac{\theta_i\mu_m}{2\theta_i\mu_m + \sigma_{t,i}\Delta x_i}\psi_{m,i-1/2} - \frac{1}{2}\frac{\left(\sigma_{s,i}\hat{\phi}_i + \hat{Q}_i\right)\Delta x_i}{\sigma_{t,i}\Delta x_i + 2\theta_i\mu_m}. \tag{2.8}$$

Similarly for $\mu_m < 0$ we can substitute $\hat{\psi}_{i,m}$ from Eq. 2.5c into Eq. 2.5b

$$\theta_i \mu_m \left(\psi_{m,i+1/2} + \psi_{m,i-1/2} - 2\psi_{m,i}\right) + \sigma_{t,i}\Delta x_i \left(\psi_{m,i} - \psi_{m,i+1/2}\right) = \frac{1}{2}\left(\sigma_{s,i}\hat{\phi}_i + \hat{Q}_i\right)\Delta x_i.$$

Again, solving for $\psi_{m,i}$, we get something analogous to Eq. 2.8,

$$\psi_{m,i} = -\frac{\theta_i\mu_m - \sigma_{t,i}\Delta x_i}{\sigma_{t,i}\Delta x_i - 2\theta_i\mu_m}\psi_{m,i-1/2} + \frac{\theta_i\mu_m}{\sigma_{t,i}\Delta x_i - 2\theta_i\mu_m}\psi_{m,i+1/2} + \frac{1}{2}\frac{\left(\sigma_{s,i}\hat{\phi}_i + \hat{Q}_i\right)\Delta x_i}{\sigma_{t,i}\Delta x_i - 2\theta_i\mu_m}. \tag{2.9}$$

We now make the following definitions:

$$\tau_{m,i} = \frac{\sigma_{t,i}\Delta x_i}{\mu_i}, \tag{2.10}$$

$$\alpha^{\pm}_{m,i} = \frac{\tau_{m,i}}{2\theta_i \pm \tau_{m,i}}. \tag{2.11}$$

Note some of the properties of Eq. 2.11

$$1+\alpha^{-}_{m,i}=\frac{2\theta_i}{2\theta_i-\tau_{m,i}}, \qquad 1+\alpha^{+}_{m,i}=\frac{2\left(\theta_i+\tau_{m,i}\right)}{2\theta_i-\tau_{m,i}},$$

$$1-\alpha^{-}_{m,i}=\frac{2\left(\tau_{m,i}-\theta_i\right)}{2\theta_i-\tau_{m,i}}, \qquad 1-\alpha^{+}_{m,i}=\frac{2\theta_i}{2\theta_i+\tau_{m,i}}.$$

Using the above relations and substituting our definitions from Eq. 2.11 and Eq. 2.10 into Eq. 2.8 and Eq. 2.9 we can arrive at:

$$\psi_{m,i}=\frac{1}{2}\left(1+\alpha^{+}_{m,i}\right)\psi_{m,i+1/2}+\frac{1}{2}\left(1-\alpha^{+}_{m,i}\right)\psi_{m,i-1/2}-\frac{\alpha^{+}_{m,i}}{2\sigma_{t,i}}\left(\sigma_{t,i}\hat{\phi}_i+\hat{Q}_i\right), \quad \mu_m>0, \tag{2.12a}$$

$$\psi_{m,i}=\frac{1}{2}\left(1+\alpha^{-}_{m,i}\right)\psi_{m,i+1/2}+\frac{1}{2}\left(1-\alpha^{-}_{m,i}\right)\psi_{m,i-1/2}-\frac{\alpha^{-}_{m,i}}{2\sigma_{t,i}}\left(\sigma_{t,i}\hat{\phi}_i+\hat{Q}_i\right), \quad \mu_m<0. \tag{2.12b}$$

We can now define:

$$\alpha_{m,i}=\frac{\tau_{m,i}}{2\theta_i+\left|\tau_{m,i}\right|}. \tag{2.13}$$

Since $\alpha_{m,i}$ is an odd function i.e. $\alpha_{m,i}\left(-\tau_{m,i}\right)=-\alpha_{m,i}\left(\tau_{m,i}\right)$ we can condense Eq. 2.12a and Eq. 2.12b to arrive at a new set of closed equations for the LD/LLD method:

$$\mu_m\left(\psi_{m,i+1/2}-\psi_{m,i-1/2}\right)+\sigma_{t,i}\Delta x_i\psi_{m,i}=\frac{1}{2}\left(\sigma_{s,i}\phi_i+Q_i\right)\Delta x_i, \tag{2.14a}$$

$$\theta_i\mu_m\left(\psi_{m,i+1/2}+\psi_{m,i-1/2}-2\psi_{m,i}\right)+\sigma_{t,i}\Delta x_i\hat{\psi}_{m,i}=\frac{1}{2}\left(\sigma_{s,i}\hat{\phi}_i+\hat{Q}_i\right)\Delta x_i, \tag{2.14b}$$

$$\psi_{m,i}=\frac{1}{2}\left(1+\alpha_{m,i}\right)\psi_{m,i+1/2}+\frac{1}{2}\left(1-\alpha_{m,i}\right)\psi_{m,i-1/2}-\frac{\alpha_{m,i}}{2\sigma_{t,i}}\left(\sigma_{s,i}\hat{\phi}_i+\hat{Q}_i\right). \tag{2.14c}$$

From our definition of $\alpha_{m,i}$ we make further definitions:

$$\rho_i=\frac{1}{2}\sum_{m=1}^{M}\mu_m\alpha_{m,i}w_m. \tag{2.15}$$

$$\gamma_{m,i}=\alpha_{m,i}-3\rho_i\mu_m \tag{2.16}$$

Notice some properties of $\gamma_{m,i}$; first by numerically integrating it over all μ

$$\sum_{m=1}^{M}\gamma_{m,i}w_m=\sum_{m=1}^{M}\alpha_{m,i}w_m-3\rho_i\sum_{m=1}^{M}\mu_m w_m=0.$$

Secondly, note that taking the first moment of $\gamma_{m,i}$ will yield:

$$\sum_{m=1}^{M} \mu_m \gamma_{m,i} w_m = \sum_{m=1}^{M} \mu_m \alpha_{m,i} w_m - 3\rho_i \sum_{m=1}^{M} \mu_m^2 w_m = 0.$$

Making further definitions for the cell-edge and cell-average currents, along with the first linear moment of current we say:

$$J_i = \sum_{m=1}^{M} \mu_m \psi_{m,i} w_m, \quad J_{i+1/2} = \sum_{m=1}^{M} \mu_m \psi_{m,i+1/2} w_m, \tag{2.17}$$

$$\hat{J}_i = \sum_{m=1}^{M} \mu_m \hat{\psi}_{m,i} w_m. \tag{2.18}$$

We can now define the cell-edge and cell average second moments of the angular flux

$$\tilde{F}_{i+1/2} = \sum_{m=1}^{M} \mu_m^2 \psi_{m,i+1/2} w_m, \quad \tilde{F}_i = \sum_{m=1}^{M} \mu_m^2 \psi_{m,i} w_m. \tag{2.19}$$

Having these definitions we can now integrate Eq. 2.5a and Eq. 2.5b over all angular directions and get:

$$J_{i+1/2} - J_{i-1/2} + \sigma_{a,i} \Delta x_i \phi_i = Q_i \Delta x_i, \tag{2.20a}$$

$$\theta_i \left(J_{i+1/2} + J_{i-1/2} - J_i \right) + \sigma_{a,i} \Delta x_i \hat{\phi}_i = \hat{Q}_i \Delta x_i. \tag{2.20b}$$

Taking the first angular moments of Eq. 2.5a and Eq. 2.5b by integrating them with respect to μ yields:

$$\tilde{F}_{i+1/2} - \tilde{F}_{i-1/2} + \sigma_{t,i} \Delta x_i J_i = 0, \tag{2.21a}$$

$$\theta_i \left(\tilde{F}_{i+1/2} + \tilde{F}_{i-1/2} - 2\tilde{F}_i \right) + \sigma_{t,i} \Delta x_i \hat{J}_i = 0. \tag{2.21b}$$

From here we make the definitions,

$$F_i = \sum_{m=1}^{M} \left(\frac{1}{3} - \mu_m^2 \right) \psi_{m,i} w_m, \tag{2.22a}$$

$$F_{i+1/2} = \sum_{m=1}^{M} \left(\frac{1}{3} - \mu_m^2 \right) \psi_{m,i+1/2} w_m, \tag{2.22b}$$

noting that,

$$F_i = \frac{1}{3} \phi_i - \tilde{F}_i$$

$$F_{i+1/2} = \frac{1}{3}\phi_{i+1/2} - \tilde{F}_{i+1/2}$$

Rewriting Eq. 2.21a and Eq. 2.21b using the above definition:

$$\frac{1}{3}\left(\phi_{i+1/2} - \phi_{i-1/2}\right) + \sigma_{t,i}\Delta x_i J_i = F_{i+1/2} - F_{i-1/2}, \tag{2.23a}$$

$$\frac{\theta_i}{3}\left(\phi_{i+1/2} + \phi_{i-1/2} - 2\phi_i\right) + \sigma_{t,i}\Delta x_i \hat{J}_i = \theta_i\left(F_{i+1/2} + F_{i-1/2} - 2F_i\right). \tag{2.23b}$$

Taking Eq. 2.14c and integrating it over all μ_m we get

$$\phi_i = \frac{1}{2}\left(\phi_{i+1/2} + \phi_{i-1/2}\right) + \frac{3}{2}\rho_i\left(J_{i+1/2} - J_{i-1/2}\right) + \Gamma_{0,i}, \tag{2.24}$$

where

$$\Gamma_{n,i} = \frac{1}{2}\sum_{m=1}^{M}\mu_m^n\gamma_{m,i}\left(\psi_{m,i+1/2} - \psi_{m,i-1/2}\right)w_m, \quad n = 0, 1. \tag{2.25}$$

Similarly, taking Eq. 2.14c and integrating it over all μ with respect to μ we get:

$$J_i = \frac{1}{2}\left(J_{i+1/2} + J_{i-1/2}\right) + \frac{\rho_i}{2}\left(\phi_{i+1/2} - \phi_{i-1/2}\right) - \frac{3\rho_i}{2}\left(F_{i+1/2} - F_{i-1/2}\right) - \frac{\rho_i}{\sigma_{t,i}}\left(\sigma_{s,i}\hat{\phi}_i + \hat{Q}_i\right) + \Gamma_{1,i}. \tag{2.26}$$

We now have the resulting set of six low order equations for each cell, to solve for the scalar flux, ϕ, and the current J, for both the cell-average, and cell-edge values. To close the system we need to develop boundary conditions. This method is described in Sec. 1.2.1, where we take the discrete forms of Eq. 1.17 and Eq. 1.16. Doing this, we get the equations needed to close our low-order set:

$$\frac{1}{4}\phi_{1/2} + \frac{1}{2}J_{1/2} = J_{in}^{+} + \frac{1}{4}B_{left}, \tag{2.27a}$$

$$\frac{1}{4}\phi_{N+1/2} - \frac{1}{2}J_{N+1/2} = \frac{1}{4}B_{right} - J_{in}^{-}, \tag{2.27b}$$

where,

$$B_{left} = \sum_{m=1}^{M}\left(1 - 2|\mu_m|\right)\psi_{m,1/2}w_m, \tag{2.28a}$$

$$B_{right} = \sum_{m=1}^{M}\left(1 - 2|\mu_m|\right)\psi_{m,N+1/2}w_m, \tag{2.28b}$$

In conclusion, our low-order equations can be summarized using the following equations:

$$J_{i+1/2} - J_{i-1/2} + \sigma_{a,i}\Delta x_i\phi_i = Q_i\Delta x_i \tag{2.29a}$$

$$\theta_i \left(J_{i+1/2} + J_{i-1/2} - J_i\right) + \sigma_{a,i}\Delta x_i \hat{\phi}_i = \hat{Q}_i \Delta x_i \tag{2.29b}$$

$$\frac{1}{3}\left(\phi_{i+1/2} - \phi_{i-1/2}\right) + \sigma_{t,i}\Delta x_i J_i = F_{i+1/2} - F_{i-1/2} \tag{2.29c}$$

$$\frac{\theta_i}{3}\left(\phi_{i+1/2} + \phi_{i-1/2} - 2\phi_i\right) + \sigma_{t,i}\Delta x_i \hat{J}_i = \theta_i \left(F_{i+1/2} + F_{i-1/2} - 2F_i\right) \tag{2.29d}$$

$$\phi_i = \frac{1}{2}\left(\phi_{i+1/2} + \phi_{i-1/2}\right) + \frac{3}{2}\rho_i \left(J_{i+1/2} - J_{i-1/2}\right) + \Gamma_{0,i} \tag{2.29e}$$

$$J_i = \frac{1}{2}\left(J_{i+1/2} + Ji - 1/2\right) + \frac{\rho_i}{2}\left(\phi_{i+1/2} - \phi_{i-1/2}\right) - \frac{3\rho_i}{2}\left(F_{i+1/2} - F_{i-1/2}\right) - \frac{\rho_i}{\sigma_{t,i}}\left(\sigma_{s,i}\hat{\phi}_i + \hat{Q}_i\right) + \Gamma_{1,i} \tag{2.29f}$$

$$\frac{1}{4}\phi_{1/2} + \frac{1}{2}J_{1/2} = J_{in}^{+} + \frac{1}{4}B_{left} \tag{2.29g}$$

$$\frac{1}{4}\phi_{N+1/2} - \frac{1}{2}J_{N+1/2} = \frac{1}{4}B_{right} - J_{in}^{-} \tag{2.29h}$$

Notice that the set can be condensed by substituting Eq. 2.29e into Eq. 2.29a and Eq. 2.29d, also substituting in Eq. 2.29f into Eq. 2.29b and Eq. 2.29c. This method is fully consistent with the transport equations.

2.3 The Quasidiffusion Method

Here we look at low-order quasidiffusion equations that can be used to solve transport problems [18]. Similar to the Second Moment method, the equations derived here are fully consistent with the LD/LLD method presented in Section 2.1. Each method has its individual advantages for solving transport problems which will be discussed later. Starting with the modified set of LD/LLD equations, Eq. 2.14, we integrate over all directions with respect to μ to arrive at Eq. 2.20. However, here we define the cell average and cell-edge quasidiffusion (Eddington) factors as:

$$E_i = \frac{\sum_{m=1}^{M} \mu_m^2 \psi_{m,i} w_m}{\sum_{m=1}^{M} \psi_{m,i} w_m}, \tag{2.30a}$$

$$E_{i+1/2} = \frac{\sum_{m=1}^{M} \mu_m^2 \psi_{m,i+1/2} w_m}{\sum_{m=1}^{M} \psi_{m,i+1/2} w_m}, \tag{2.30b}$$

Using the above definitions we can now rewrite Eq. 2.21 as

$$E_{i+1/2}\phi_{i+1/2} - E_{i-1/2}\phi_{i-1/2} + \sigma_{t,i}\Delta x_i J_i = 0, \tag{2.31a}$$

$$\theta_i \left(E_{i+1/2}\phi_{i+1/2} + E_{i-1/2}\phi_{i-1/2} - 2E_i\phi_i\right) + \sigma_{t,i}\Delta x_i \hat{J}_i = 0. \tag{2.31b}$$

Once again, we can integrate Eq. 2.14c over all μ however, we will rewrite it this time as

$$\phi_i = \frac{1}{2}\left(1 + G_i^+\right)\phi_{i+1/2} + \frac{1}{2}\left(1 - G_i^-\right)\phi_{i-1/2} + \frac{3}{2}\rho_i\left(J_{i+1/2} - J_{i-1/2}\right). \tag{2.32}$$

Here we have defined $G_i^{\pm}$ as

$$G_i^{\pm} = \frac{\sum_{m=1}^{M} \gamma_{m,i}\psi_{m,i\pm1/2} w_m}{\sum_{m=1}^{M} \psi_{m,i\pm1/2} w_m}. \tag{2.33}$$

Once again, we will take Eq. 2.14c and take the first moment of it. By using our definition of $\gamma_{m,i}$ in Eq. 2.16, we can expand $\alpha_{m,i}$ in terms of $\gamma_{m,i}$ and ρ_i.

$$\begin{aligned} J_i = \frac{1}{2}\left(J_{i+1/2} + J_{i-1/2}\right) - \frac{\rho_i}{\sigma_{t,i}}\left(\sigma_{s,i}\hat{\phi}_i + \hat{Q}_i\right) + \\ \frac{1}{2}\sum_{m=1}^{M} \mu_m\gamma_{m,i}\left(\psi_{m,i+1/2} - \psi_{m,i-1/2}\right) w_m + \frac{3}{2}\rho_i \sum_{m=1}^{M} \mu_m^2\left(\psi_{m,i+1/2} - \psi_{m,i-1/2}\right) w_m \end{aligned} \tag{2.34}$$

Using our definition of quasidiffusion (Eddington) factors defined in Eq. 2.30, and the following definition we can simplify the above equation to

$$H_i^{\pm} = \frac{\sum_{m=1}^{M} \mu_m\gamma_{m,i}\psi_{m,i\pm1/2}}{\sum_{m=1}^{M} \psi_{m,i\pm1/2} w_m}. \tag{2.35}$$

The final form of the equation is then,

$$J_i = \frac{1}{2}\left(J_{i+1/2} + J_{i-1/2}\right) + \frac{1}{2}\left(H_i^+ + 3\rho_i E_{i+1/2}\right)\phi_{i+1/2} - \frac{1}{2}\left(H_i^- + 3\rho_i E_{i-1/2}\right)\phi_{i-1/2} - \frac{\rho_i}{\sigma_{t,i}}\left(\sigma_{s,i}\hat{\phi}_i + \hat{Q}_i\right). \quad (2.36)$$

We have now developed all the low order Quasidiffusion equations. However, to close the set of equations we need to develop the proper boundary conditions. The boundary conditions to the QD method are the following [18]

$$J_{1/2} = C_L\left(\phi_{1/2} - \phi_{in}^+\right) + J_{in}^+, \quad (2.37a)$$

$$J_{N+1/2} = C_R\left(\phi_{N+1/2} - \phi_{in}^-\right) + J_{in}^-, \quad (2.37b)$$

where we have defined,

$$C_L = \frac{\sum_{\mu_m \le 0} \mu_m \psi_{m,1/2} w_m}{\sum_{\mu_m \le 0} \psi_{m,1/2} w_m}, \quad (2.38a)$$

$$C_R = \frac{\sum_{\mu_m \ge 0} \mu_m \psi_{m,N+1/2} w_m}{\sum_{\mu_m \ge 0} \psi_{m,N+1/2} w_m}. \quad (2.38b)$$

and $\phi_{in}^{\pm}$ is defined as the incoming scalar flux at either side of the domain as defined by

$$\phi_{in}^+ = \sum_{\mu_m \ge 0} \psi_{m,1/2} w_m, \quad (2.39a)$$

$$\phi_{in}^- = \sum_{\mu_m \le 0} \psi_{m,N+1/2} w_m. \quad (2.39b)$$

The complete set of low-order QD equations are defined by Eq. 2.20, Eq. 2.31, Eq. 2.32, Eq. 2.36, and with boundary conditions given by Eq. 2.37. Similar to the SM method we solve this set of equations for the scalar flux and current everywhere in the problem domain.

2.4 Metrics for Evaluating Transport Effects

Metrics for measuring transport effects can be developed by looking at various derivations of the diffusion equation [19]. The diffusion equation can be derived in a number of ways, and typically have higher order terms that can be neglected in diffusive regions, or factors that will

develop certain properties. The idea presented here is to observe these higher order terms and factors to measure how they deviate from their "ideal" values for diffusive regions. We consider two different low-order equations and analyze how they tend to the diffusion equation.

First consider the P_N equations, where we expand the transport equation, Eq. 1.5a, using spherical harmonics. [20] Taking the zeroth and first Legendre polynomial moments of the transport equation we develop the P_1 equations.

$$\frac{d\phi_1}{dx} + \sigma_a \phi_0 = Q \tag{2.40a}$$

$$\frac{2}{3}\frac{d\phi_2}{dx} + \frac{1}{3}\frac{d\phi_0}{dx} + \sigma_t \phi_1 = 0 \tag{2.40b}$$

$$\phi_n = \int_{-1}^{1} P_n(\mu)\psi(x,\mu)d\mu \tag{2.40c}$$

We can note that the first two Legendre moments, i.e. ϕ_0, and ϕ_1 correspond to the scalar flux ϕ and the current J respectively. Generally by setting the derivative of the higher moment terms to zero i.e. $\frac{d\phi_2}{dx} = 0$ we can close the set of equations. The result is the one dimensional steady state balance equation and Fick's Law or the P_1 equations.

$$\frac{dJ}{dx} + \sigma_a \phi = Q \tag{2.41a}$$

$$\frac{1}{3}\frac{d\phi}{dx} + \sigma_t J = 0 \tag{2.41b}$$

We now can develop a ratio between the higher moment's derivative ($\frac{d\phi_2}{dx}$) and the other leading order terms, in Eq. 2.40b, to see if it is sufficiently small to be neglected.

$$M_1(x) = 2\left|\frac{d\phi_2}{dx}\Big/\frac{d\phi}{dx}\right|. \tag{2.42}$$

If $M_1 \ll 1$ then that term is negligible and the resulting P_1 equations (Eq. 2.41a, Eq. 2.41b) are valid in that area.

Using the Low-Order Quasidiffusion (LOQD) equations [18], we can develop other metrics to further study the properties of a problem domain. These equations are given by

$$\frac{dJ}{dx} + \sigma_a \phi = q, \tag{2.43a}$$

$$\frac{dE\phi}{dx} + \sigma_t J = 0, \tag{2.43b}$$

$$E(x) = \frac{\int_{-1}^{1} \mu^2 \psi(x,\mu) d\mu}{\int_{-1}^{1} \psi(x,\mu) d\mu}. \tag{2.43c}$$

Where $E(x)$ is defined to be the quasidiffusion factor which provides closure to this set of equations. Notice in Eq. 2.43b, if $E = \frac{1}{3}$ then this equation reduces to Fick's law. One can note that the second LOQD equation 2.43b can be rewritten as

$$E\frac{d\phi}{dx} + \frac{dE}{dx}\phi + \sigma_t J = 0. \tag{2.44}$$

This allows us to construct another two metrics to test for transport effects,

$$M_2(x) = \left| E(x) - \frac{1}{3} \right|. \tag{2.45}$$

$$M_3(x) = \left| \frac{dE}{dx} \right|. \tag{2.46}$$

Similar to $M_1(x)$, if $M_2(x) \ll 1$ and $M_3(x) \ll 1$ then there are minimal transport effects and the diffusion equation is valid. It should be noted that using the LOQD method, the Eddington factor (E) may be deemed constant by M_3, however it may not be equal to $\frac{1}{3}$ as indicated by M_2. This can lead to a so-called modified diffusion approximation, where the diffusion equation can be used, however $E \neq \frac{1}{3}$. This indicates the need to apply all transport metrics and not just one.

2.5 Calculation of Metrics

This section develops the discrete version of the metrics used in case of LD/LLD method. First consider $M_2(x)$, which requires the calculation of the Quasidiffusion factor Eq. 2.43c. This is done numerically for cell average and cell edge values by Eq. 2.30. Having $E(x)$ defined, cell-average and cell-edge $M_2(x)$ are given by

$$M_{2,i} = \left| E_i - \frac{1}{3} \right|, \tag{2.47a}$$

$$M_{2,i+1/2} = \left| E_{i+1/2} - \frac{1}{3} \right|. \tag{2.47b}$$

To evaluate M_1 we use the following finite difference derivatives,

$$\left.\frac{d\phi}{dx}\right|_{x=x_i} = \frac{\phi_{i+1/2} - \phi_{i-1/2}}{\Delta x_i}, \tag{2.48}$$

$$\left.\frac{d\phi}{dx}\right|_{x=x_{i+1/2}} = \frac{\phi_{i+1} - \phi_i}{\Delta x_{i+1/2}}. \tag{2.49}$$

A similar finite differencing scheme can be used for the second Legendre moment, ϕ_2, thus allowing us to numerically approximate M_1 in a cell by

$$M_{1,i} = 2\left|\frac{\phi_{2,i+1/2} - \phi_{2,i-1/2}}{\phi_{i+1/2} - \phi_{i-1/2}}\right|, \tag{2.50}$$

where the high-order Legendre moment,

$$\phi_{2,i+1/2} = \sum_{m=1}^{M} \frac{1}{2}\left(3\mu_m^2 - 1\right)\psi_{m,i+1/2} w_m. \tag{2.51}$$

From Eq. 2.4 we can approximate the derivative of angular flux by:

$$\left.\widehat{\frac{d\psi_m}{dx}}\right|_{x=x_i} = \frac{2}{\Delta x_i}\hat{\psi}_{m,i}. \tag{2.52}$$

With this we can approximate the spatial derivatives of the scalar flux and the P_2 moment at the cell center in the following way

$$\left.\widehat{\frac{d\phi}{dx}}\right|_{x=x_i} = \frac{2}{\Delta x_i}\hat{\phi}_i, \tag{2.53}$$

$$\left.\widehat{\frac{d\phi_2}{dx}}\right|_{x=x_i} = \frac{2}{\Delta x_i}\hat{\phi}_{2,i}. \tag{2.54}$$

As a result, we have an alternative way of calculating M_1

$$\hat{M}_{1,i} = 2\left|\left.\widehat{\frac{d\phi_2}{dx}}\right|_{x=x_i} \Bigg/ \left.\widehat{\frac{d\phi}{dx}}\right|_{x=x_i}\right| = 2\left|\frac{\hat{\phi}_{2,i}}{\hat{\phi}_i}\right|. \tag{2.55}$$

We can now calculate $M_3(x)$ using a finite differencing scheme for either the cell edge or cell-average values.

$$\left.\frac{dE}{dx}\right|_{x=x_i} = \frac{E_{i+1/2} - E_{i-1/2}}{\Delta x_i} \tag{2.56}$$

$$\left.\frac{dE}{dx}\right|_{x=x_{i+1/2}} = \frac{E_{i+1} - E_i}{\Delta x_{i+1/2}} \tag{2.57}$$

From here it is a simple substitution of

$$M_{3,i} = \left|\frac{dE}{dx}\right|_{x=x_i}, \tag{2.58a}$$

$$M_{3,i+1/2} = \left|\frac{dE}{dx}\right|_{x=x_{i+1/2}}. \tag{2.58b}$$

If we define

$$\varphi_2(x) = \int_{-1}^{1} \mu^2 \psi(x,\mu) d\mu \tag{2.59}$$

Then the QD factor, Eq. 2.43c, can be rewritten as

$$E(x) = \frac{\varphi_2(x)}{\phi(x)}, \tag{2.60}$$

and the derivative is,

$$\frac{dE}{dx} = \frac{1}{\phi^2}\left(\phi\frac{d\varphi_2}{dx} - \varphi_2\frac{d\phi}{dx}\right) = \frac{1}{\phi}\left(\frac{d\varphi_2}{dx} - E\frac{d\phi}{dx}\right). \tag{2.61}$$

Using a similar method to that of Eq. 2.52, we integrate Eq. 2.4 over all μ with respect to μ^2 and take the derivate. To calculate the derivative we say

$$\left.\widehat{\frac{d\varphi_2}{dx}}\right|_{x=x_i} = \frac{2}{\Delta x_i}\hat{\varphi}_{2,i}, \tag{2.62}$$

$$\hat{\varphi}_{2,i} = \sum_{m=1}^{M} \mu_m^2 \hat{\psi}_{m,i} w_m. \tag{2.63}$$

Using the alternative forms of the derivatives we can calculate Eq. 2.61 using Eq. 2.62 and Eq. 2.53 to get

$$\hat{M}_{3,i} = \left|\left.\widehat{\frac{dE}{dx}}\right|_{x=x_i}\right| = \left|\frac{2}{\phi_i \Delta x_i}\left(\hat{\varphi}_{2,i} - E_i\hat{\phi}_i\right)\right|. \tag{2.64}$$

2.6 Boundary Conditions at Subdomain Interfaces

To solve the transport equation in a transport subdomain we need to develop proper boundary conditions to use at the interface of transport and diffusion subdomains. One way to formulate boundary conditions is to use the P_1 approximation of the angular flux:

$$\psi(x,\mu) = \frac{1}{2}\phi(x) + \frac{3}{2}\mu J(x). \tag{2.65}$$

ϕ and J are from the solution of a low-order problem. Hereafter, we refer to this boundary condition as the P_1 boundary condition. Evaluating this at the cell edge in discrete coordinates,

$$\psi_{m,i+1/2} = \frac{1}{2}\phi_{i+1/2} + \frac{3}{2}\mu_m J_{i+1/2}. \tag{2.66}$$

This linear anisotropic approximation is a suitable estimate, however the asymptotic diffusion analysis of the LD/LLD method in the interior of the diffusion domain gives something slightly different. Asymptotic analyses have been done before and have proven that the LD/LLD method does limit to a discretization of the diffusion equation for discrete ordinate problems. [17] Here we expand on this concept to develop an approximation of the angular flux at the cell boundaries. We start with the LD/LLD equations stated in Eq. 2.5. We start by introducing the ansatz,

$$\psi_{m,j} = \sum_{k=0}^{\infty} \varepsilon^k \psi_{m,j}^{[k]}, \tag{2.67}$$

For optically thick problems, we scale the cross sections accordingly to see the limit of the equations. We do this by

$$\sigma_{t,i} = \frac{\tilde{\sigma}_{t,i}}{\varepsilon}, \quad \sigma_{a,i} = \varepsilon\tilde{\sigma}_{a,i}, \quad \tilde{q}_i = \varepsilon Q_i$$

Therefore we rewire the LD/LLD set of equations,

$$\mu_m\left(\psi_{m,i+1/2} - \psi_{m,i-1/2}\right) + \frac{\tilde{\sigma}_{t,i}}{\varepsilon}\Delta x_i \psi_{m,i} = \frac{\Delta x_i}{2}\left(\left[\frac{\tilde{\sigma}_{t,i}}{\varepsilon} - \tilde{\sigma}_{a,i}\varepsilon\right]\sum_{n=1}^{M}\psi_{n,i}w_n + \tilde{q}_i\right), \tag{2.68a}$$

$$\theta_i\mu_m\left(\psi_{m,i+1/2} + \psi_{m,i-1/2} - 2\psi_{m,i}\right) + \frac{\tilde{\sigma}_{t,i}}{\varepsilon}\Delta x_i \hat{\psi}_{m,i} = \frac{\Delta x_i}{2}\left(\left[\frac{\tilde{\sigma}_{t,i}}{\varepsilon} - \tilde{\sigma}_{a,i}\varepsilon\right]\sum_{n=1}^{M}\hat{\psi}_{n,i}w_n + \hat{\tilde{q}}_i\right), \tag{2.68b}$$

$$\begin{cases} \psi_{m,i+1/2} = \psi_{m,i} + \hat{\psi}_{m,i}, & \mu_m > 0 \\ \psi_{m,i-1/2} = \psi_{m,i} - \hat{\psi}_{m,i}, & \mu_m < 0 \end{cases} \tag{2.68c}$$

By taking the $O(\varepsilon^{-1})$ equations we can see from Eq. 2.68a and Eq. 2.68b that

$$\tilde{\sigma}_{t,i}\Delta x_i\left(\psi_{m,i}^{[0]} - \frac{1}{2}\sum_{n=1}^{M}\psi_{n,i}^{[0]}w_n\right) = 0 \tag{2.69a}$$

$$\tilde{\sigma}_{t,i}\Delta x_i\left(\hat{\psi}^{[0]}_{m,i}-\frac{1}{2}\sum_{n=1}^{M}\hat{\psi}^{[0]}_{n,i}w_n\right)=0 \tag{2.69b}$$

Which tells us that the cell average angular flux has the isotropic solution,

$$\psi^{[0]}_{m,i}=\frac{1}{2}\phi^{[0]}_i, \tag{2.70a}$$

$$\hat{\psi}^{[0]}_{m,i}=\frac{1}{2}\hat{\phi}^{[0]}_i. \tag{2.70b}$$

Taking the $O(\varepsilon^0)$ equations we see

$$\mu_m\left(\psi^{[0]}_{m,i+1/2}-\psi^{[0]}_{m,i-1/2}\right)+\tilde{\sigma}_{t,i}\Delta x_i\psi^{[1]}_{m,i}=\frac{\Delta x_i\tilde{\sigma}_{t,i}}{2}\sum_{n=1}^{M}\psi^{[1]}_{n,i}w_n, \tag{2.71a}$$

$$\theta_i\mu_m\left(\psi^{[0]}_{m,i+1/2}+\psi^{[0]}_{m,i-1/2}-\phi^{[0]}_i\right)+\tilde{\sigma}_{t,i}\Delta x_i\hat{\psi}^{[1]}_{m,i}=\frac{\Delta x_i\tilde{\sigma}_{t,i}}{2}\sum_{n=1}^{M}\hat{\psi}^{[1]}_{n,i}w_n, \tag{2.71b}$$

$$\psi^{[0]}_{m,i+1/2}=\begin{cases}\frac{1}{2}\left(\phi^{[0]}_i+\hat{\phi}^{[0]}_i\right), & 1\le i\le N,\quad \mu_m>0,\\ \frac{1}{2}\left(\phi^{[0]}_{i+1}-\hat{\phi}^{[0]}_{i+1}\right), & 0\le i\le N-1,\quad \mu_m<0.\end{cases} \tag{2.71c}$$

By making the following definitions:

$$\phi^{[0]}_{1/2}=\phi^{[0]}_1-\hat{\phi}^{[0]}_1, \tag{2.72a}$$

$$\phi^{[0]}_{i+1/2}=\phi^{[0]}_i+\hat{\phi}^{[0]}_i=\phi^{[0]}_{i+1}-\hat{\phi}^{[0]}_{i+1}, \qquad 1\le i\le N-1 \tag{2.72b}$$

$$\phi^{[0]}_{N+1/2}=\phi^{[0]}_N+\hat{\phi}^{[0]}_N, \tag{2.72c}$$

we can now rewrite Eq. 2.71c as

$$\psi^{[0]}_{m,i+1/2}=\frac{1}{2}\phi^{[0]}_{i+1/2},\begin{cases}1\le i\le N, & \mu_m>0\\ 0\le i\le N-1, & \mu_m<0.\end{cases} \tag{2.73}$$

Note that from our definition,

$$\phi^{[0]}_{i+1/2}-\phi^{[0]}_{i-1/2}=2\hat{\phi}^{[0]}_i.$$

Now solving for $\psi^{[1]}_{m,i}$ and $\hat{\psi}^{[1]}_{m,i}$ in Eq. 2.71a and Eq. 2.71b gives,

$$\psi^{[1]}_{m,i}=\frac{1}{2}\phi^{[1]}_i-\frac{\mu_m}{\tilde{\sigma}_{t,i}\Delta x_i}\left(\psi^{[0]}_{m,i+1/2}-\psi^{[0]}_{m,i-1/2}\right), \tag{2.74a}$$

$$\hat{\psi}^{[1]}_{m,i}=\frac{1}{2}\hat{\phi}^{[1]}_i-\frac{\theta_i\mu_m}{\tilde{\sigma}_{t,i}\Delta x_i}\left(\psi^{[0]}_{m,i+1/2}+\psi^{[0]}_{m,i-1/2}-\phi^{[0]}_i\right). \tag{2.74b}$$

Taking the $O(\varepsilon^1)$ terms of Eq. 2.68c we see,

$$\psi^{[1]}_{m,i+1/2} = \psi^{[1]}_{m,i} + \hat{\psi}^{[1]}_{m,i}, \quad \mu_m > 0, \tag{2.75a}$$

$$\psi^{[1]}_{m,i-1/2} = \psi^{[1]}_{m,i} - \hat{\psi}^{[1]}_{m,i}, \quad \mu_m < 0. \tag{2.75b}$$

By taking Eq. 2.74 and putting it into Eq. 2.75a, we find,

$$\psi^{[1]}_{m,i+1/2} = \begin{cases} \frac{1}{2}\left(\phi^{[1]}_i + \hat{\phi}^{[1]}_i\right) - \\ \quad \frac{\mu_m}{\tilde{\sigma}_{t,i}\Delta x_i}\left[\psi^{[0]}_{m,i+1/2} - \psi^{[0]}_{m,i-1/2} + \theta_i\left(\psi^{[0]}_{m,i+1/2} + \psi^{[0]}_{m,i-1/2} - \phi^{[0]}_i\right)\right], & \mu_m > 0 \\ \\ \frac{1}{2}\left(\phi^{[1]}_{i+1} - \hat{\phi}^{[1]}_{i+1}\right) - \\ \quad \frac{\mu_m}{\tilde{\sigma}_{t,i+1}\Delta x_{i+1}}\left[\psi^{[0]}_{m,i+3/2} - \psi^{[0]}_{m,i+1/2} - \theta_i\left(\psi^{[0]}_{m,i+3/2} + \psi^{[0]}_{m,i+1/2} - \phi^{[0]}_{i+1}\right)\right], & \mu_m < 0. \end{cases} \tag{2.76}$$

Since we are finding the diffusion limit we can set $\theta_i = 1$ by definition of the LLD method. Using this, Eq. 2.73, and our definition of $\phi^{[0]}_{i+1/2}$, Eq. 2.72a, we can simplify the above equation for the interior of the problem.

$$\psi^{[1]}_{m,i+1/2} = \begin{cases} \frac{1}{2}\left(\phi^{[1]}_i + \hat{\phi}^{[1]}_i\right) - \frac{\mu_m}{2\tilde{\sigma}_{t,i}\Delta x_i}\left(\phi^{[0]}_{i+1/2} - \phi^{[0]}_{i-1/2}\right), & \mu > 0, \\ \frac{1}{2}\left(\phi^{[1]}_{i+1} - \hat{\phi}^{[1]}_{i+1}\right) - \frac{\mu_m}{2\tilde{\sigma}_{t,i+1}\Delta x_{i+1}}\left(\phi^{[0]}_{i+3/2} - \phi^{[0]}_{i+1/2}\right). & \mu > 0, \end{cases} \tag{2.77}$$

Using the anstaz expansion from earlier we can rewrite the angular flux now to $O(\varepsilon^2)$ by

$$\psi_{m,i+1/2} = \psi^{[0]}_{m,i+1/2} + \varepsilon\psi^{[1]}_{m,i+1/2} + O(\varepsilon^2)\ldots$$

From our definitions in Eq. 2.73 and Eq. 2.77 we can solve for the limit.

$$\psi_{m,i+1/2} = \begin{cases} \frac{1}{2}\left(\phi^{[0]}_i + \hat{\phi}^{[0]}_i\right) - \frac{\mu_m}{2\sigma_{t,i}\Delta x_i}\left(\phi^{[0]}_{i+1/2} - \phi^{[0]}_{i-1/2}\right) + O(\varepsilon), & \mu_m > 0, \\ \frac{1}{2}\left(\phi^{[0]}_{i+1} - \hat{\phi}^{[0]}_{i-1}\right) - \frac{\mu_m}{2\sigma_{t,i+1}\Delta x_{i+1}}\left(\phi^{[0]}_{i+3/2} - \phi^{[0]}_{i+1/2}\right) + O(\varepsilon), & \mu_m < 0, \end{cases} \tag{2.78}$$

It has been previously shown [17] that $\phi^{[0]}$ meets the diffusion equation. Therefore we can approximate the cell-edge angular flux on the interior of the diffusion domain as:

$$\psi_{m,i+1/2} = \begin{cases} \frac{1}{2}\left(\phi_i + \hat{\phi}_i\right) - \frac{\mu_m}{2\sigma_{t,i}\Delta x_i}\left(\phi_{i+1/2} - \phi_{i-1/2}\right), & \mu_m > 0, \\ \frac{1}{2}\left(\phi_{i+1} - \hat{\phi}_{i+1}\right) - \frac{\mu_m}{2\sigma_{t,i+1}\Delta x_{i+1}}\left(\phi_{i+3/2} - \phi_{i+1/2}\right), & \mu_m < 0, \end{cases} \tag{2.79}$$

These equations are used to formulate the boundary conditions and define the angular flux coming from the diffusion domain and going into the transport subdomain. These will be our boundary conditions.

2.7 Domain Decomposition in 1D Slab Geometry

All the equations needed for our domain decomposition algorithm defined in Sec. 1.3 have been developed. Here we present the equations used in each step of our method used for solving transport problems. In the transport iterations we use the set of LD/LLD equations, Eq. 2.5,

$$\mu_m \left(\psi_{m,i+1/2}^{s+1/2} - \psi_{m,i-1/2}^{s+1/2}\right) + \sigma_{t,i}\Delta x_i \psi_{m,i}^{s+1/2} = \frac{1}{2}\left(\sigma_{s,i}\phi_i^s + Q_i\right)\Delta x_i, \tag{2.80a}$$

$$\theta_i \mu_m \left(\psi_{m,i+1/2}^{s+1/2} + \psi_{m,i-1/2}^{s+1/2} - 2\psi_{m,i}^{s+1/2}\right) + \sigma_{t,i}\Delta x_i \hat{\psi}_{m,i}^{s+1/2} = \frac{1}{2}\left(\sigma_{s,i}\hat{\phi}_i^{\,s} + \hat{Q}_i\right)\Delta x_i, \tag{2.80b}$$

$$\begin{cases} \psi_{m,i+1/2}^{s+1/2} = \psi_{m,i}^{s+1/2} + \hat{\psi}_{m,i}^{s+1/2}, & \mu_m > 0, \\ \psi_{m,i-1/2}^{s+1/2} = \psi_{m,i}^{s+1/2} - \hat{\psi}_{m,i}^{s+1/2}, & \mu_m < 0, \end{cases} \tag{2.80c}$$

$$\theta_i = \begin{cases} 3, & \sigma_{t,i}\Delta x_i \leq \tau^*, \\ 1, & \sigma_{t,i}\Delta x_i \geq \tau^*. \end{cases} \tag{2.80d}$$

Following this we calculate the second moment closure terms in the transport domains,

$$F_{i+1/2}^{s+1/2} = \sum_{m=1}^{M}\left(\frac{1}{3} - \mu_m^2\right)\psi_{m,i+1/2}^{s+1/2} w_m, \tag{2.81a}$$

$$F_i^{s+1/2} = \sum_{m=1}^{M}\left(\frac{1}{3} - \mu_m^2\right)\psi_{m,i}^{s+1/2} w_m, \tag{2.81b}$$

$$\Gamma_{n,i}^{s+1/2} = \frac{1}{2}\sum_{m=1}^{M}\mu_m^n \gamma_{m,i}\left(\psi_{m,i+1/2}^{s+1/2} - \psi_{m,i-1/2}^{s+1/2}\right) w_m, \text{ for } n = 0, 1. \tag{2.81c}$$

In diffusion subdomains, where we don't calculate the high order solution $\psi^{s+1/2}$, we set the closure terms to their diffusion values, i.e.

$$F_{i+1/2}^{s+1/2} = 0, \tag{2.82a}$$

$$F_i^{s+1/2} = 0, \tag{2.82b}$$

$$\Gamma_{n,i}^{s+1/2} = 0, \text{ for } n = 0, 1. \tag{2.82c}$$

From here we can now solve the LOSM equations in the entire problem domain,

$$J_{i+1/2}^{s+1} - J_{i-1/2}^{s+1} + \sigma_{a,i}\Delta x_i \phi_i^{s+1} = Q_i \Delta x_i, \tag{2.83a}$$

$$\theta_i \left(J_{i+1/2}^{s+1} + J_{i-1/2}^{s+1} - J_i \right) + \sigma_{a,i}\Delta x_i \hat{\phi}_i^{s+1} = \hat{Q}_i \Delta x_i, \tag{2.83b}$$

$$\frac{1}{3}\left(\phi_{i+1/2}^{s+1} - \phi_{i-1/2}^{s+1} \right) + \sigma_{t,i}\Delta x_i J_i^{s+1} = F_{i+1/2}^{s+1/2} - F_{i-1/2}^{s+1/2}, \tag{2.83c}$$

$$\frac{\theta_i}{3}\left(\phi_{i+1/2}^{s+1} + \phi_{i-1/2}^{s+1} - 2\phi_i^{s+1} \right) + \sigma_{t,i}\Delta x_i \hat{J}_i^{s+1} = \theta_i \left(F_{i+1/2}^{s+1/2} + F_{i-1/2}^{s+1/2} - 2F_i^{s+1/2} \right), \tag{2.83d}$$

$$\phi_i^{s+1} = \frac{1}{2}\left(\phi_{i+1/2}^{s+1} + \phi_{i-1/2}^{s+1} \right) + \frac{3}{2}\rho_i \left(J_{i+1/2}^{s+1} - J_{i-1/2}^{s+1} \right) + \Gamma_{0,i}^{s+1/2}, \tag{2.83e}$$

$$\begin{aligned} J_i^{s+1} = \frac{1}{2}\left(J_{i+1/2}^{s+1} + J_{i-1/2}^{s+1} \right) + \frac{\rho_i}{2}\left(\phi_{i+1/2}^{s+1} - \phi_{i-1/2}^{s+1} \right) \\ - \frac{3\rho_i}{2}\left(F_{i+1/2}^{s+1/2} - F_{i-1/2}^{s+1/2} \right) - \frac{\rho_i}{\sigma_{t,i}}\left(\sigma_{s,i}\hat{\phi}_i^{s+1} + \hat{Q}_i \right) + \Gamma_{1,i}^{s+1/2}, \end{aligned} \tag{2.83f}$$

$$\frac{1}{4}\phi_{1/2}^{s+1} + \frac{1}{2}J_{1/2}^{s+1} = J_{in}^{+} + \frac{1}{4}B_{left}, \tag{2.83g}$$

$$\frac{1}{4}\phi_{N+1/2}^{s+1} - \frac{1}{2}J_{N+1/2}^{s+1} = \frac{1}{4}B_{right} - J_{in}^{-}. \tag{2.83h}$$

The scalar flux from the solution of the LOSM equations are then used in the transport equations and iterated until a solution is found. The initial guess, ϕ^0, for the transport iterations comes from solving the LOSM equations, where $F = \Gamma_0 = \Gamma_1 = 0$. Notice that the LOSM equations are used everywhere in the problem domain for every iteration. To approximate the angular flux at the boundaries of these domains we use the asymptotic boundary conditions,

$$\psi_{m,i+1/2}^{s+1/2} = \begin{cases} \frac{1}{2}\left(\phi_i^s + \hat{\phi}_i^s \right) - \frac{\mu_m}{2\sigma_{t,i}\Delta x_i}\left(\phi_{i+1/2}^s - \phi_{i-1/2}^s \right), & \mu_m > 0, \\ \frac{1}{2}\left(\phi_{i+1}^s - \hat{\phi}_{i+1}^s \right) - \frac{\mu_m}{2\sigma_{t,i+1}\Delta x_{i+1}}\left(\phi_{i+3/2}^s - \phi_{i+1/2}^s \right), & \mu_m < 0. \end{cases} \tag{2.84}$$

This concludes our discussion of the equations and methodologies needed to solve transport problems in 1D slab geometry using the LD/LLD transport equations and the Low-Order Second Moment method.

Chapter 3

Numerical Results for 1D Problems

Here we analyze the numerical results from three test cases. Each test is designed specifically to explore certain aspects of the accuracy of the algorithm for various problems. These problems are tailored to show distinct diffusive domains and areas where transport effects dominate. All cases were run using the double S_4 Gauss-Legendre quadrature, with the pointwise convergence criteria of $\varepsilon = 10^{-15}$. We start by looking at the solution to the tests themselves without any domain decomposition. In the next section we analyze the metrics for each test developed in Sec. 2.4 to quantify transport effects. To fully utilize our methodology, we need to consider estimations of the metrics based off of one transport iteration and compare to the converged solution already presented. We also consider the boundary conditions applied between domains, developed in Sec. 2.6, where we look at the effects of imposing these approximations at domain interfaces without actually using a full domain decomposition. Finally, we conclude with an analysis of the error of a full domain decomposition method to one without any. In the final section we use the QD method in place of the LOSM method for a non-diffusive test.

3.1 Test Problems

We first consider the solution to the three problems where we analyze the scalar flux. The first test (Test A) is a two region problem with pure absorber $\sigma_t = 2$, for $0 \leq x \leq 1$, with $\Delta x = 0.1$, followed by a pure scattering medium $\sigma_t = 100$, $\sigma_s = 100$, for $1 \leq x \leq 11$ for $\Delta x = 1.0$. There is an incident flux on the left hand side of $\psi|_{x=0} = 1$, and vacuum boundary on the right. The scalar flux for Test A is given in Figure 3.1. This test has an optically thick, highly diffusive area on the right side of the domain where transport effects should be negligible. The left side of the domain is a pure absorber with an incident flux where we should see significant transport effects. This test highlights two distinctly different regions for diffusive and transport domains.

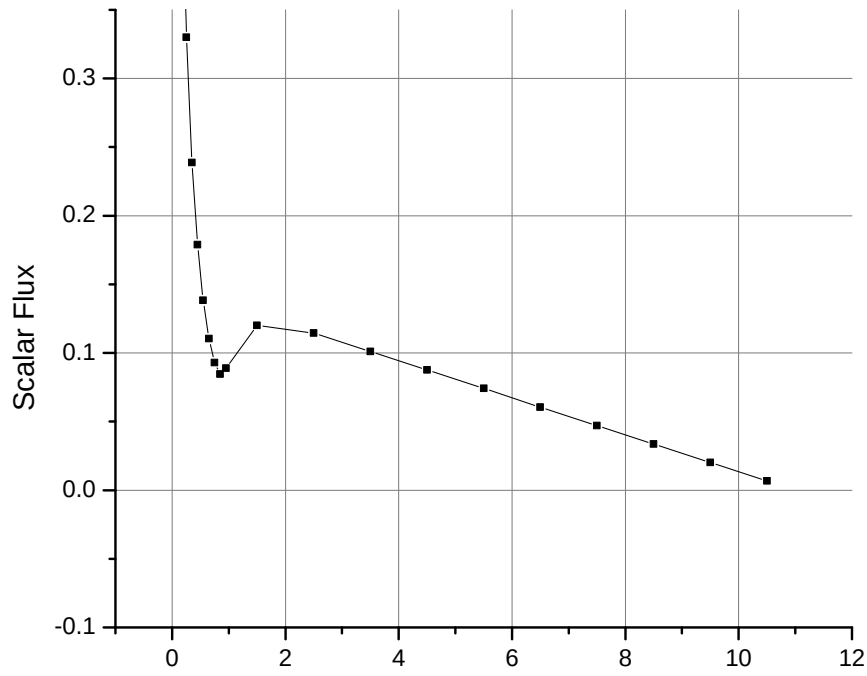

Figure 3.1: Test A Scalar Flux

Test B is characterized by two distinct regions. The left side of the domain is a weak absorber $\sigma_t = 1.0$ and $\sigma_s = 0.5$, with an external source $Q = 0.5$, for $0 \leq x \leq 10$ where $\Delta x = 1.0$. The right side of the problem is defined as a weak diffusive area with $\sigma_t = 10.0$ and $\sigma_s = 9.9$ with a weak external source $Q = 0.1$, for $10 \leq x \leq 30$ where $\Delta x = 0.5$. Test B has vacuum boundary conditions on both sides of the domain. The solution is given in Figure 3.2. Unlike Test A, this problem has an external source both in the absorption section, and another smaller one in the diffusive area. This test shows more of a 'gray' area between diffusive and transport subdomains.

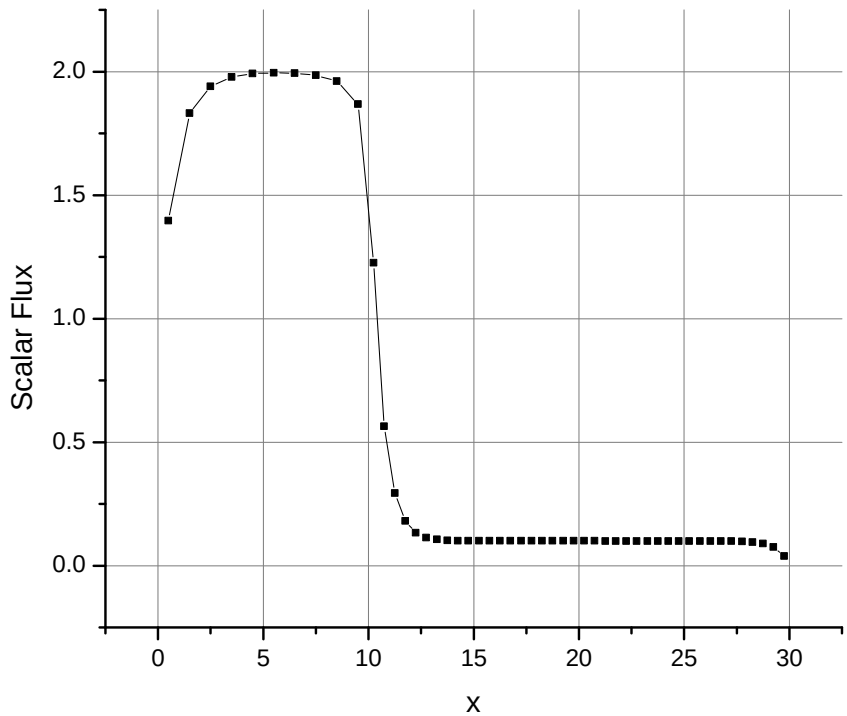

Figure 3.2: Test B Scalar Flux

Test C is very similar to Test B, however the source in the right hand side of the domain is removed, i.e. $q = 0.0$ for $10 \leq x \leq 30$. The solution to this problem is given in Figure 3.3, and notice it is given on a log scale. This allows for a small amount of absorption in the high-scattering area, though it still retains a large total cross section and scattering ratio of .99. This problem is not diffusive even though it shows several characteristics of a diffusive problem.

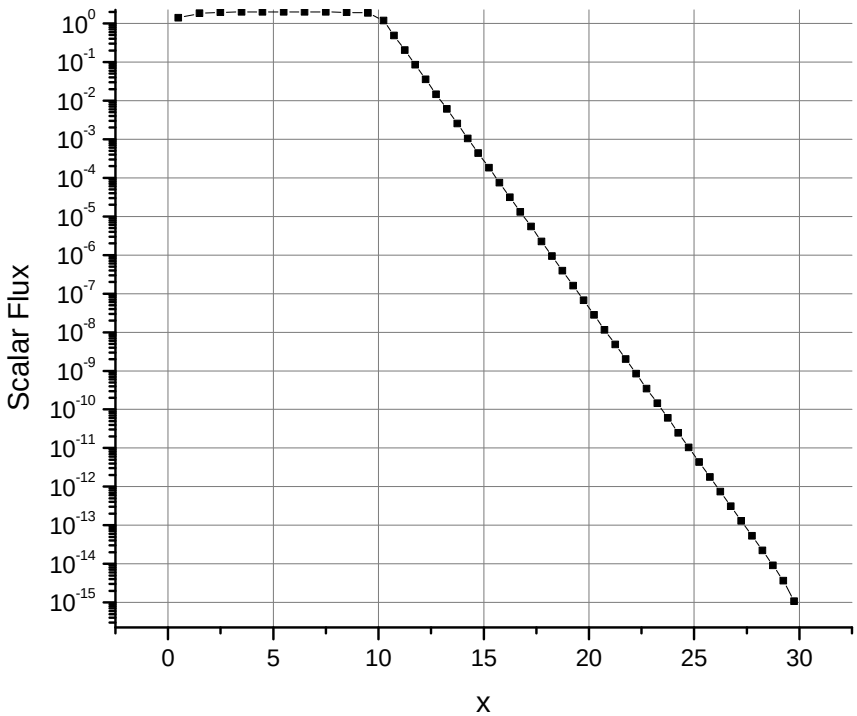

Figure 3.3: Test-C Scalar Flux

3.2 Metrics

Here we analyze how the metrics developed earlier quantify diffusive regions for each test case. Each metric shows something different and this is highlighted for each test. The metrics presented are calculated for the cell-average values using Eq. 2.50, Eq. 2.47a, and Eq. 2.58a for M_1, M_2, and M_3 respectively. Note that all the following metrics are calculated from the converged solution to the transport problem with no domain decomposition.

Figure 3.4 shows the various metrics for Test A. As stated earlier these values measure how diffusive a region in a problem is, so the smaller a metric is, the more diffusive that area is. Every metric gives the same general trend where it is large in the absorbing region and very small in the center of the 'diffusive' region. In the areas where the metrics are large, that is, near boundaries and in the first region, are areas where transport effects typically dominate. This test provides a good basis for what the extremes of how the metrics trend in diffusive areas.

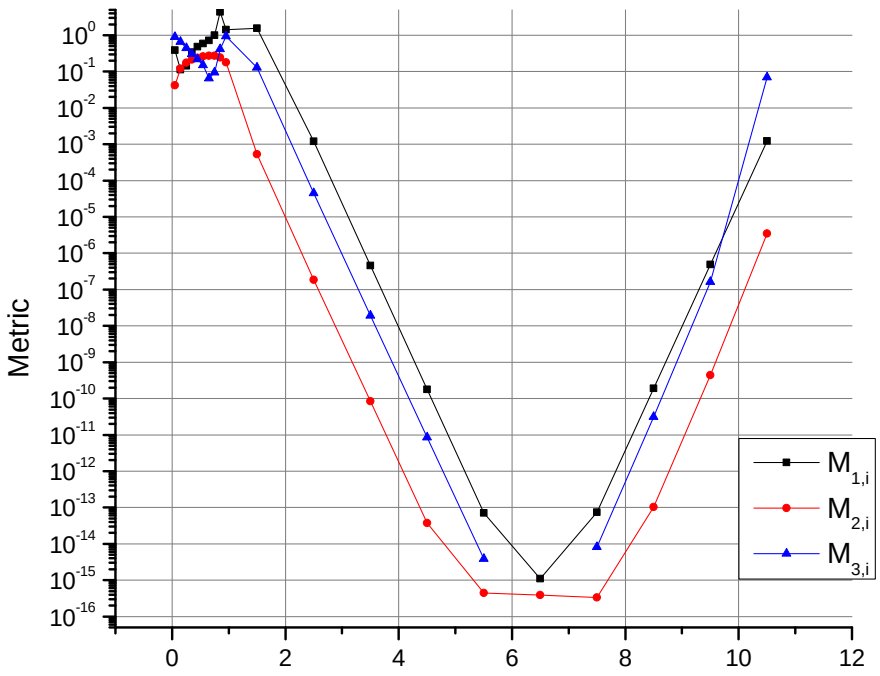

Figure 3.4: Test A Metrics

The results for the metric calculations in test B are shown in Figure 3.5. The first thing to notice is that all the metrics do not trend the same way as was the case in test A. Again we have a diffusive area on the right, which the metrics M_2 and M_3 show, however M_1 does not. This indicates that the first term in Eq. 2.40b is small, but not as small as it was previously in test A. Since M_2 is close to zero, this indicates that E is close to $\frac{1}{3}$. We can also conclude from M_3 that the second term in Eq. 2.44 is negligible as well, and that E is constant. Thus, there is a valid diffusion equation in this region.

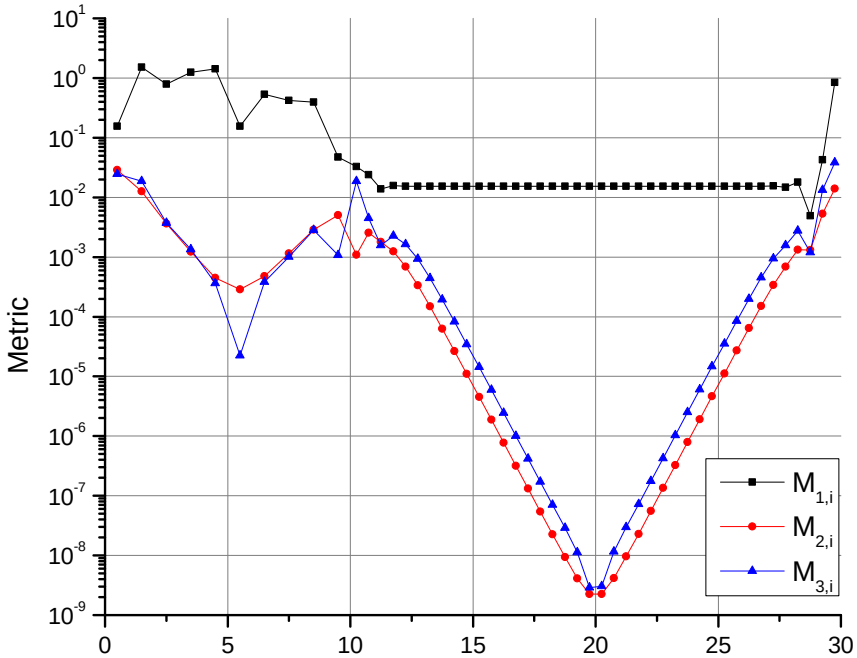

Figure 3.5: Test B Metrics

The results from test C show a similar trend to those in test B, however M_2 no longer indicates the right side of the problem is not diffusive. All of the metrics trend very similarly in the first (left) region of the domain as in test B indicating that the region is not diffusive. However, in the second (right) region M_2 remains fairly constant and M_3 is very small throughout this area. This means that the quasidiffusion factor E is constant however it is not equal to $\frac{1}{3}$ as it should be for the diffusion equation. Therefore, a modified diffusion equation can be valid if E were updated to be approximately 0.336037.

Each metric accurately predicts where diffusive areas are as seen by test A. Test B showed where M_1 is inconclusive in this problem for predicting a diffusive region, however M_2 and M_3 accurately predict and describe it. This shows how sensitive the metrics are, because test B is not that diffusive M_1 doesn't clearly show whether the diffusion approximation is accurate or not.

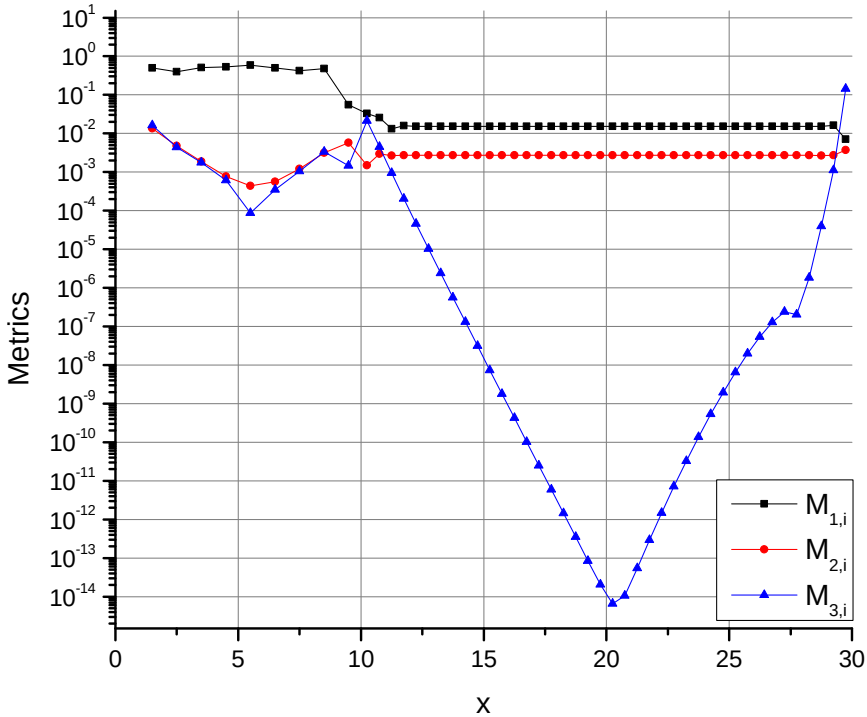

Figure 3.6: Test-C Metrics

3.3 Approximate Calculation of Metrics

The values presented for the metrics earlier in this paper for the test problems were all calculated using the converged solution of the transport problem without any domain decomposition. To effectively use the method proposed for solving transport problems one would have to estimate the metric values from a single transport iteration over the entire domain. This allows one to use the developed metrics to split the problem into subdomains without solving the transport problem everywhere. Here we present the results of the metrics when they are calculated from a single transport iteration, where the scattering source is calculated by means of the scalar flux that was obtained as a solution of the diffusion equations.

There will naturally be some loss in accuracy by estimating the metric values from one specific iteration vs. the converged transport solution. It can be seen in Figure 3.7 that the metrics are well estimated for test A even with one iteration. Comparing this plot to Figure 3.4, we see that all the metrics take the same shape, and same order of magnitude. One can note

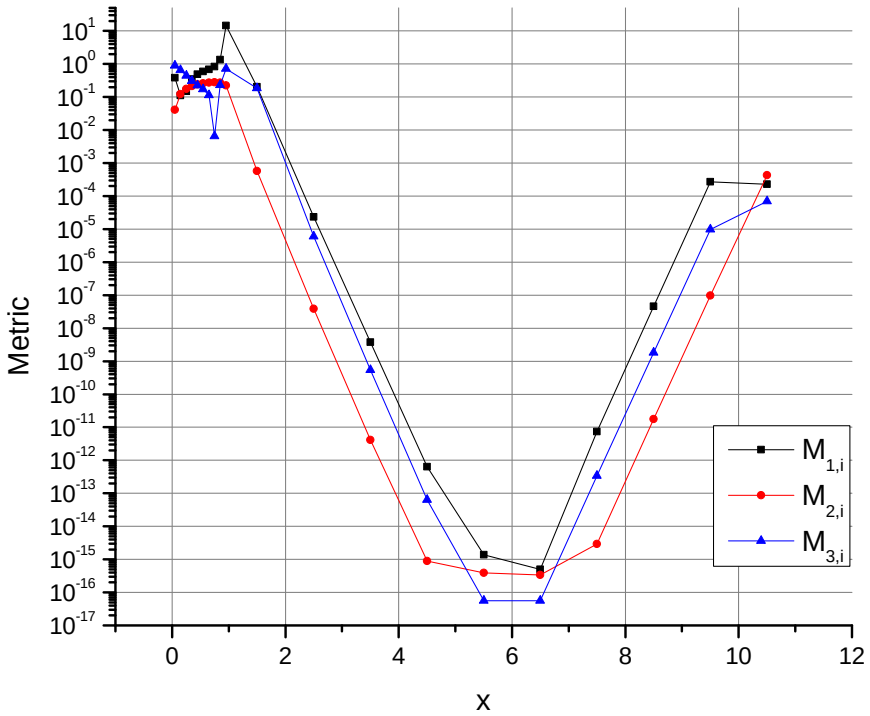

Figure 3.7: Test-A Metric Comparison

that the values for the metrics well inside the diffusion domain are marginally less than the values for those of the converged solution.

The results for test B show similar details to those in test A. Figure 3.8 shows again a similar trend to Figure 3.5 where the metrics have the same shape and closely approximates the values. Again, the values shown for one iteration tend to underestimate the converged solution. For test C, Figure 3.9, we see several of the same trends in the previous two tests. Comparing this figure to Figure 3.6 we see they are similar as well.

These results show that the metrics can accurately predict diffusive regions in the problem from only one transport iteration based on a diffusion-scattering source. All the metrics are small where the diffusive regions are, even if the shapes and values are slightly different. This means that one can set a tolerance for the metrics to define what a diffusive region is and the estimates of the metrics will do a similar job of defining diffusive regions compared to those calculated from converged solution. We can note that most of the estimates have a fairly large relative error, however the effect of this is negligible for our purposes.

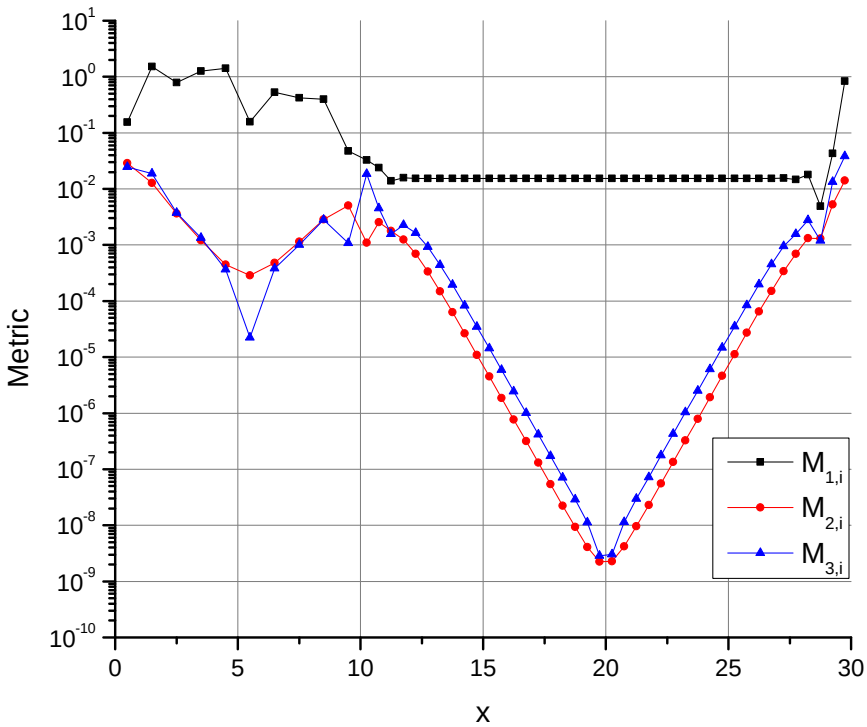

Figure 3.8: Test-B Metric Comparison

3.4 Discretization Methods for Calculating Metrics

Previously it was shown that there were multiple ways of calculating each of the metrics. Here we present the results of calculating the metrics for various methods based off one transport iteration. Most of them can be estimated for both cell-average and cell-edge values. Due to the discretization of the LD/LLD method, we can estimate the derivatives in several fashions. First we will consider M_1, which can be calculated at the cell center, using traditional finite differencing methods, Eq. 2.50, or by estimates using linear moments Eq. 2.55. Note that the indices in Eq. 2.50 can be modified to calculate M_1 at the cell edges, i.e.

$$M_{1,i+1/2} = 2\left|\frac{\phi_{2,i+1} - \phi_{2,i}}{\phi_{i+1} - \phi_i}\right| \tag{3.1}$$

Here we will only consider Test A because it is the test where M_1 is not constant. As seen in Figure 3.10, the alternate method of calculating M_1, as denoted by $M^*_{1,i}$, does have the same

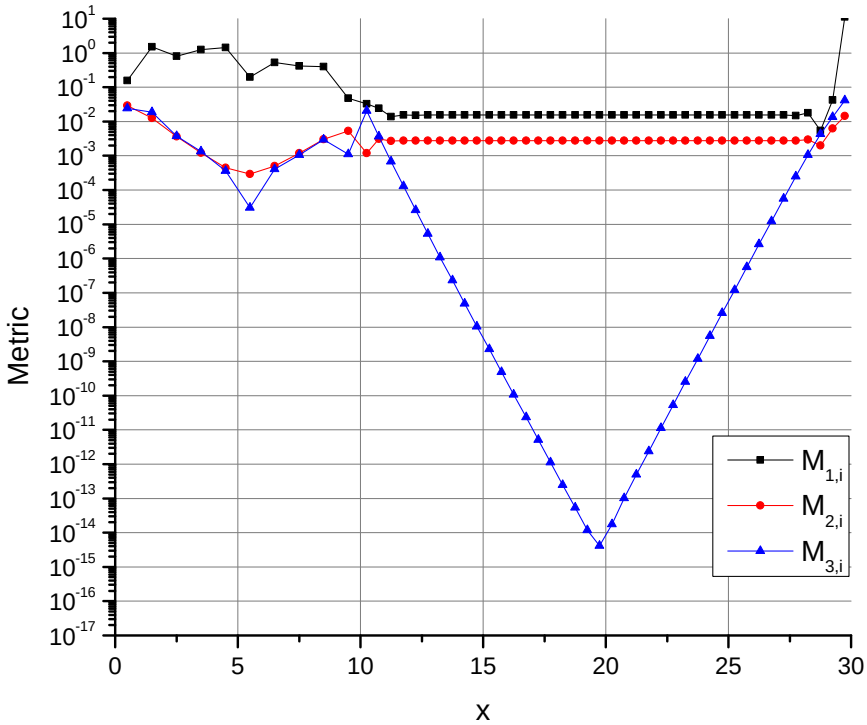

Figure 3.9: Test-C Metric Comparison

shape as the traditional finite difference method, however it is significantly lower at the same points in the diffusive region. Both the cell average and cell edge values for M_1 do fall along the same line as expected. This means the method using linear moments is more likely to predict a region as diffusive than the finite difference method.

M_2 can also be calculated for both cell-edge and cell-average values, using Eq. 2.47a or Eq. 2.47b respectively. Here we only consider Test B because it exhibits all the properties of the relationship between the cell edge and cell averages values. The most obvious characteristic in Figure 3.11 is that the values for cell-edge and cell-average do not line up in the diffusive region. We take note that there is a jump in the cell average line after the interface of the two regions at $x = 10$. This is an intrinsic property of the LLD method, where the angular shapes of the cell-edge and cell-average LLD angular fluxes differ in highly diffusive regions. This leads to the observed differences in the cell-edge and cell-average E.

Now consider M_3 where it can be calculated using a finite difference method, Eq. 2.58a, or using linear moments, Eq. 2.64, denoted by M_3^*. We notice in all cases, Figure 3.12, M_3 behaves

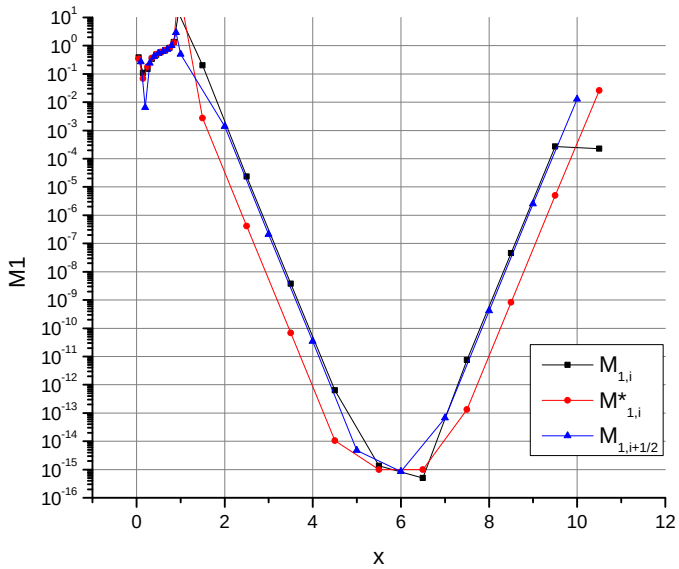

Figure 3.10: Test A M_1

differently for each test. Consider Test A shown in Figure 3.12a; the linear moment method of calculating the metric is not consistent with the finite differencing methods. The metric is typically lower in the diffusive region for all values. However, in test B, Figure 3.12b, we see that the cell-edge finite difference method and the linear moment method seem to be more consistent with one another than finite difference method for both the cell-edge and cell-average values. In Test C, we notice the same relation between the cell-average and cell-edge values as we do in Test A.

In case of a particular transport discretization method one needs metrics that will indicate subdomains where the second-moment terms in the low-order equations can be evaluated by their diffusion values. The analysis of the LSOM equations consistently discretized with the LD/LLD scheme shows that one should use metrics based on the cell-edge values of the QD factors. It is also possible to use metrics calculated by means of cell-average E.

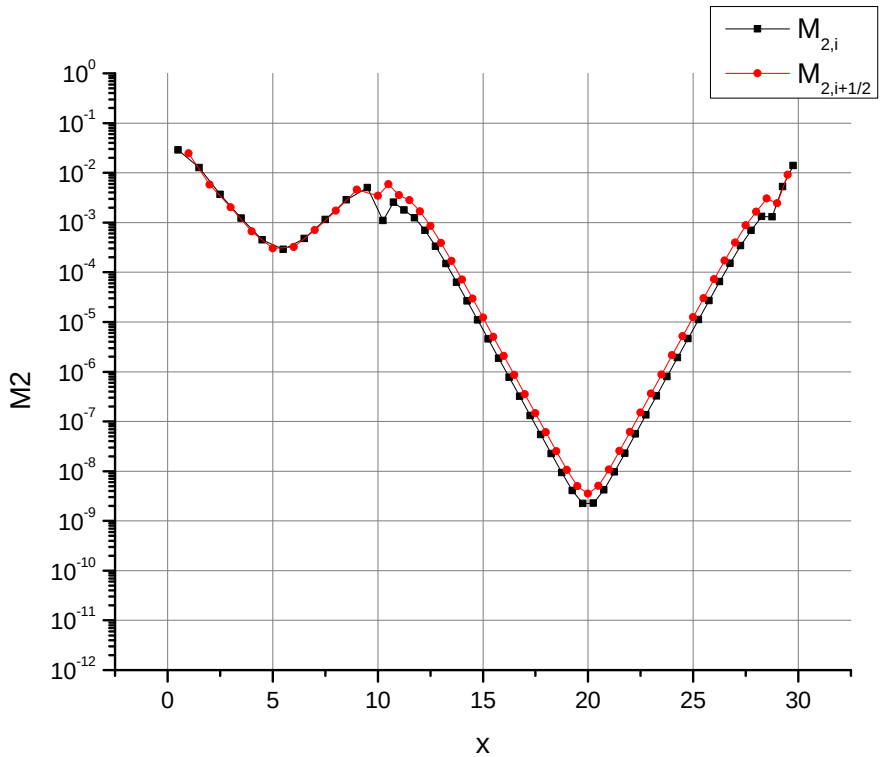

Figure 3.11: Test B M_2

3.5 Boundary Condition Effects

Now that a method for where to split the domains has been established, we must consider the effects of splitting the domain. Earlier we introduced two methods for applying boundary conditions for the transport subdomains based off of the P_1 expansion, Eq. 2.66, and the asymptotic diffusion limit, Eq. 2.79. We can see the effect of the boundary conditions themselves by dividing the domain into regions and injecting the approximate boundary (interface) conditions *into* the transport domain *from* the diffusion subdomain. We will still continue to solve the problem by doing transport sweeps through the whole domain, however we will be dividing the domains into multiple parts.

For Test A we will set a metric tolerance of 10^{-6} and 10^{-9} which will define a diffusion domain of $3 \leq x \leq 10$ and $4 \leq x \leq 9$ respectively. We will use Eq. 2.66, denoted by $[P_1]$, and Eq. 2.79, denoted by [Asy.], to apply an angular flux for $\mu_m \leq 0$ at $x = 3$ and 4, and for $\mu \geq 0$ at $x = 9$ and 10. The relative error of the problem solved with approximated boundary conditions compared to the converged solution is shown in Figure 3.13. Notice that for all cases

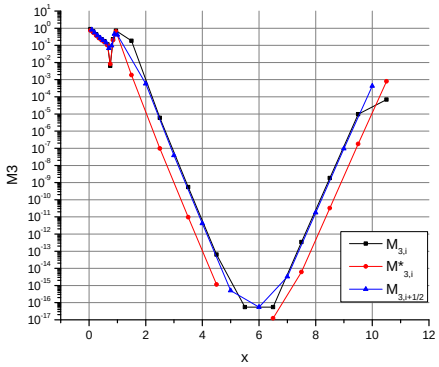

(a): Test A M_3

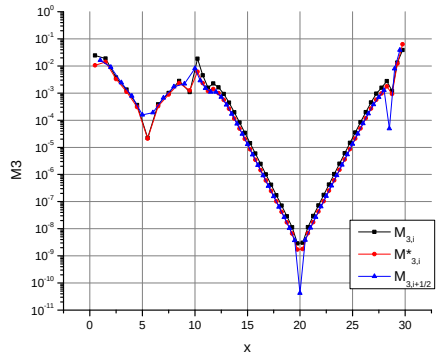

(b): Test B M_3

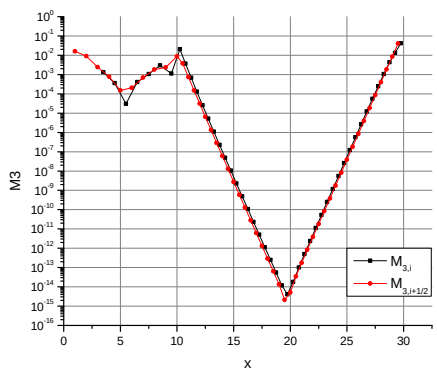

(c): Test C M_3

Figure 3.12: M_3 For All Test Cases

in the diffusion domain specified that the boundary conditions developed with the asymptotic diffusion limit always yield smaller error. It can also be noted that the error goes straight to this limit and remains constant in this domain for the most conservative case of $\varepsilon = 10^{-9}$, using asymptotic boundary conditions. The cases that were solved with the diffusion boundary conditions typically yield higher error throughout the domain than the asymptotic diffusion conditions. For all cases the further we go into the diffusion domain, or when the metric tolerance is decreased, then the error drops for the entire domain as well, regardless of the boundary condition.

A similar analysis was done for Test B. A metric tolerance of 10^{-4}, 10^{-5}, and 10^{-6} were selected which resulted in diffusion domains of $14 \leq x \leq 27.5$, $15.5 \leq x \leq 26$, $17 \leq x \leq 25$. This shows the same trends, Figure 3.14, as in Test A only a bit clearer. For the same diffusion

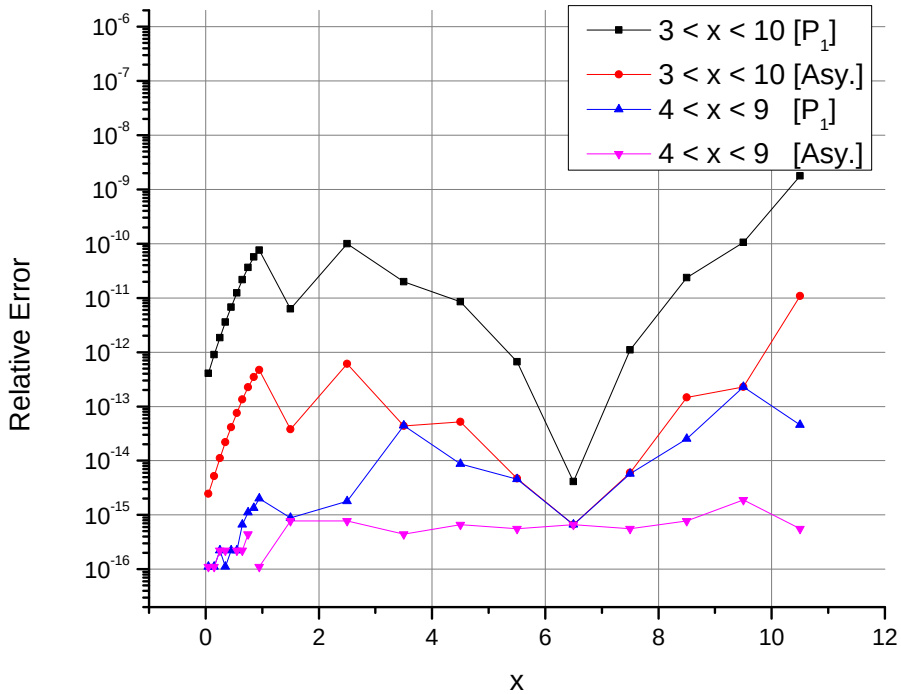

Figure 3.13: Test A Boundary Effects

domain, the asymptotic boundary conditions always provide a lower error than the P_1 expansion throughout the whole domain. Similarly, by increasing the tolerance and moving further into the diffusion domain, the error decreases everywhere.

In test C the weakly diffusive area is obtained by setting the tolerance for the metrics at 10^{-6} and 10^{-9} which yielded subdomains of $13.5 \leq x \leq 25.5$ and $15.5 \leq x \leq 23.5$, the results can be seen in Figure 3.15. Due to the small scalar flux in this domain, the solution is very sensitive to any errors introduced, hence the error increases so much on that side of the problem domain compared to the other tests. The asymptotic boundary conditions here show a reduction in error inside the diffusive domain, however the P_1 boundary conditions keep error at a constant level inside that area.

The main conclusions we can draw from these tests are that the boundary conditions do produce a small amount of error in the solution. Logically, this is greatest at interfaces between subdomains where the boundary condition is implemented. Error can be reduced throughout the entire domain by decreasing the size of a diffusion subregion, and as a result applying the boundary conditions further into the diffusion region. It is safe to conclude that using the

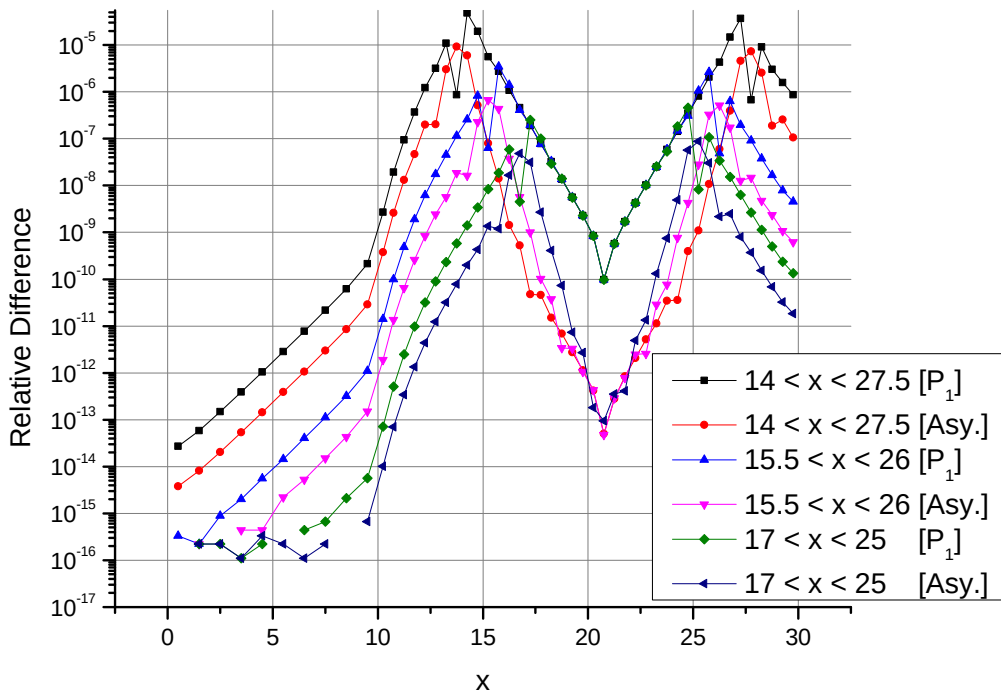

Figure 3.14: Test B Boundary Effects

boundary conditions derived using the asymptotic diffusion analysis in Eq. 2.79 provide much better approximation of the angular flux than the estimation based off the P_1 approximation.

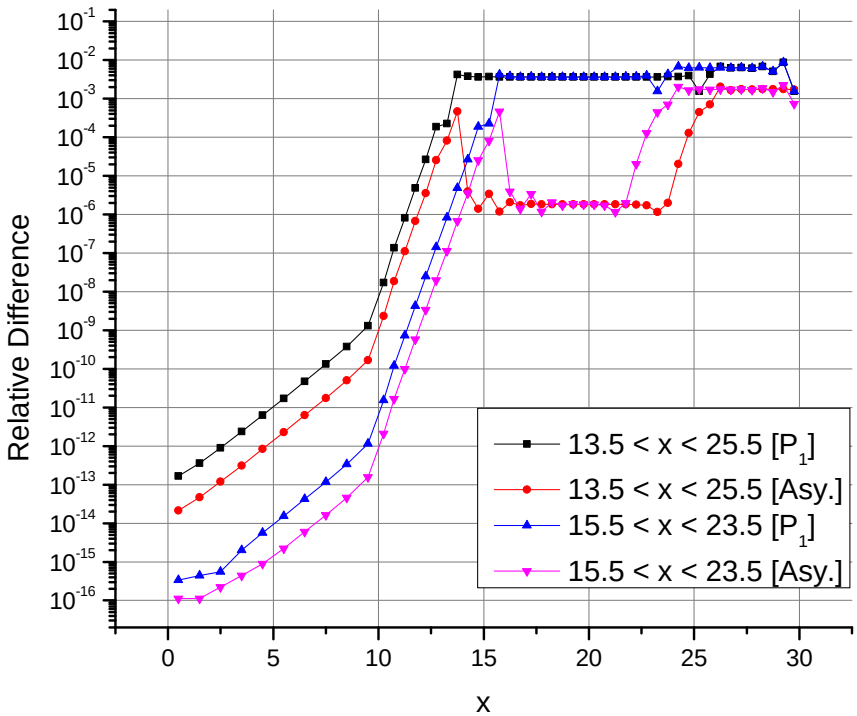

Figure 3.15: Test-C Boundary Effects

3.6 Domain Decomposition

In this section a full domain decomposition technique is applied, where unlike the last section, the transport equation will not be solved in the diffusive region. We use the same domains outlined in the previous section for each of the tests. Results will be compared to the transport solution calculated not using a domain decomposition. All problems were ran using the boundary conditions defined by the P_1 approximation and the asymptotic diffusion analysis.

From Figure 3.16 we see the error associated with applying the full domain decomposition methodology for Test A. Similar results to the boundary condition analysis show that by increasing the tolerance and making a smaller diffusion domain reduces the error throughout the problem. Missing points in the figure are due to zero error which can not be shown on a log scale. We see that the error remains well below 10^{-7} for both cases and well below 10^{-10} for the majority of the problem with a higher tolerance.

The results from Test B have similar characteristics as Test A, which are shown in Fig-

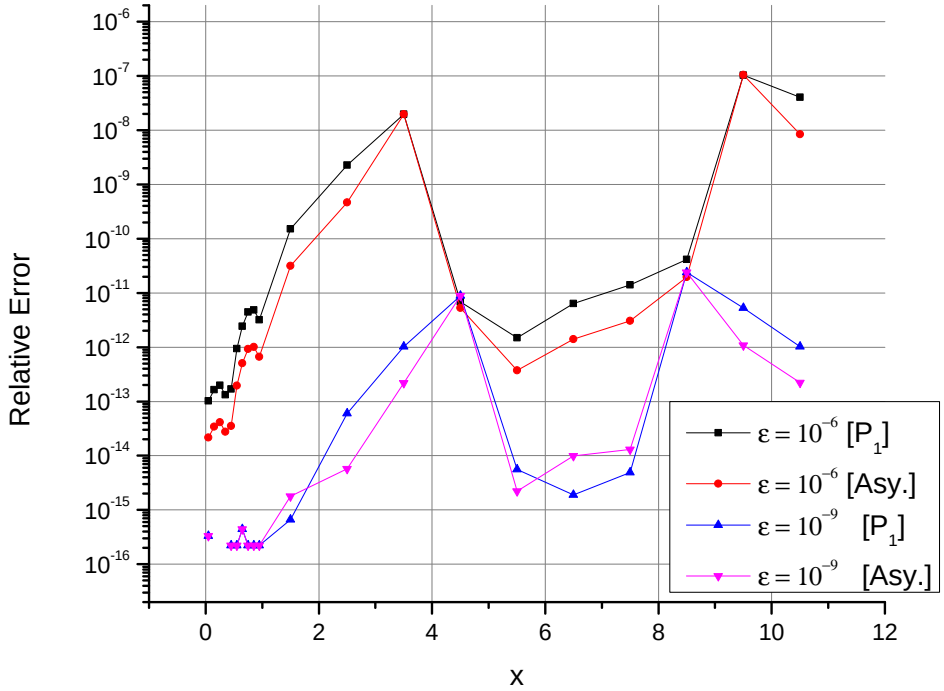

Figure 3.16: Test-A Domain Decomposition

ure 3.17. We note that going further into the diffusion domain reduces the error throughout the problem. Note that inside the determined diffusion domain the error tracks asymptotically along the same line regardless of how far into the diffusion domain the boundaries are set. The order of error is not significantly higher than that of the error found in only applying the boundary conditions. The associated error is consistent with the value of the metrics used to define the diffusion subregion. Hence, this result shows that one can control the error by optimizing domain decomposition.

In test C, Figure 3.18, there is a significant amount of error introduced using the domain decomposition method compared to the other two tests. Note that there are no diffusion domains in this test, so using the a diffusion approximation such as the second moment method would be incorrect. Thus using the method presented we should expect large errors since we are unable to reproduce the transport solution in these areas. It is possible to get the solution of this transport problem approximately using modified diffusion equations in the right subdomain as presented in Sec. 2.3. We discuss these results in the next section.

From these tests we can see that this method does accurately produce results similar to

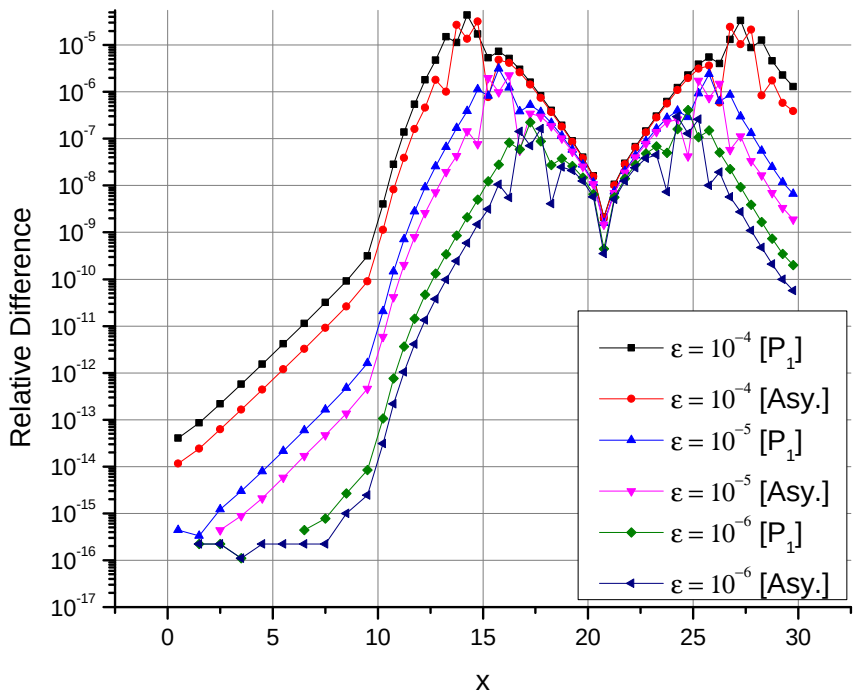

Figure 3.17: Test-B Domain Decomposition

a method solved not using domain decomposition. All results were converged for a pointwise convergence criteria of 10^{-15}. We note that in the diffusive areas of the domains, where we do not need to solve the transport equations, we modify the low order equations, Eq. 2.29, so they represent a true diffusion approximation. We do this by forcing the low order closure terms i.e. F, Γ_0, and Γ_1 to be 0.0 in the diffusion subdomain. Otherwise these terms, which depend on the angular flux, could only provide a solution as good as that obtained from the first iteration. This also provides us with a true diffusion approximation.

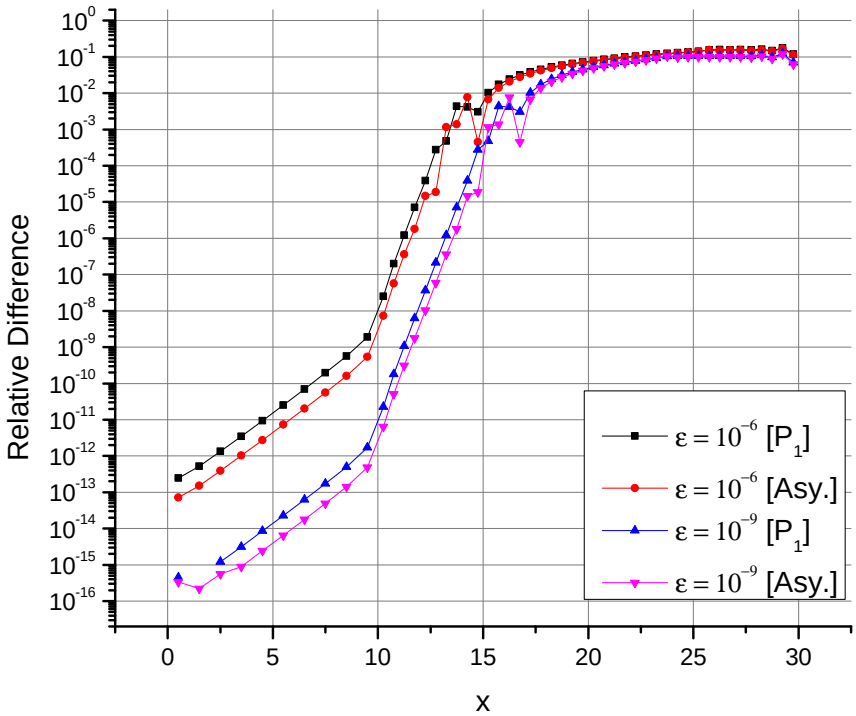

Figure 3.18: Test-C Domain Decomposition

3.7 Domain Decomposition using Quasidiffusion Low-Order Equations

To this point we have used the second moment method for the low-order equations. By using the Quasidiffusion method as an alternate set of low order equations, we can see an improvement in certain results. There are a few key points that should be noted in test C. First, is that from the metrics it can be seen that there are no diffusion regions but transport effects are weak on the right side of the domain. This is because the QD factor, although relatively constant as indicated by M_3, is not $\frac{1}{3}$. This can be seen in Figure 3.6. Therefore, using a modified diffusion equation can be considered as a good approximation for this transport problem.

From Figure 3.19 it can be seen that the approximate method based on the low-order quasidifussion equations does have a significant advantage over the method based on the low-order second moment equations in the right side of the domain. Looking at the set of equations used in Sec. 2.3, we note that they use Eddington factors instead of a value of $\frac{1}{3}$. However, like

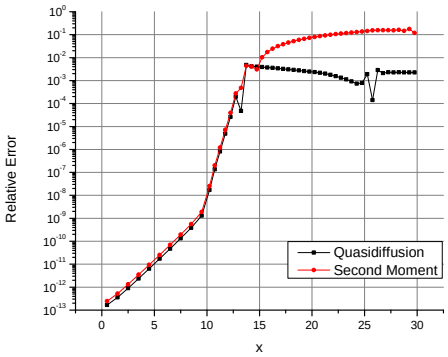

(a): Diffusion BC for $13.5 \leq x \leq 25.5$

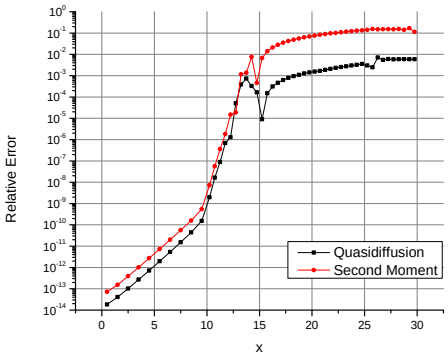

(b): Asymptotic BC for $13.5 \leq x \leq 25.5$

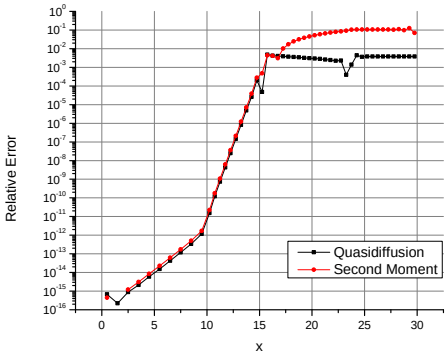

(c): Diffusion BC for $15.5 \leq x \leq 23.5$

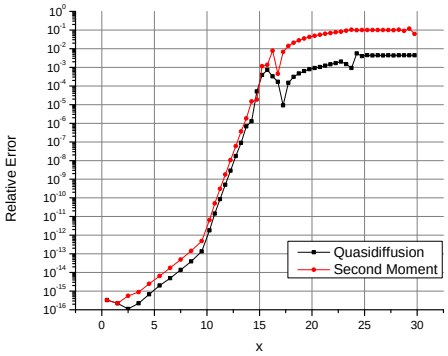

(d): Asymptotic BC for $15.5 \leq x \leq 23.5$

Figure 3.19: Test C Domain Decomposition using Quasidiffusion Method

the metrics, the Eddington factors, defined by Eq. 2.30, are calculated from the angular flux. Since this method does not calculate the angular flux in the "diffusion" region, these factors are based off a single transport iteration across the entire domain. Due to the accuracy limitations of only doing one transport iteration we can only get an estimate of what the modified diffusion coefficient should be. This will then propagate through, and is shown where this method generates the solution with the relative error, 10^{-2}, in the domain with weak transport effects.

Chapter 4

Methodology for SCB Scheme in 2D Cartesian Geometry

Only one dimensional problems have been considered so far. Here we present a look at two dimensional steady state problems. Using analogous techniques and metrics we will show how the method of domain splitting discussed earlier can be applied to higher dimensional problems. It is thought that by accomplishing this method in two dimensions, it can then be easily applied to three dimensional problems without any difficulty. We will use the simple corner balance (SCB) method for solving transport problems, and again develop the second moment equations for our set of diffusive low order equations.

4.1 Simple Corner Balance Scheme

In this section we look at the equations needed to solve the two dimensional steady state transport problem. [21]. We start with the time independent, two dimensional, fixed source, linear Boltzmann equation in Cartesian geometry, Eq. 1.7. Here we will use the following discretization by taking points from the four corners as represented in Figure 4.1 [3]. By integrating Eq. 1.7 over a corner of the cell, we can arrive at the set of balance equations for the Simple Corner Balance method, where the angular fluxes ψ_{1L}, ψ_{2B}, ψ_3, etc are at the locations defined in Figure 4.1. We present them here in matrix from and drop the (m, i, j) index for brevity.

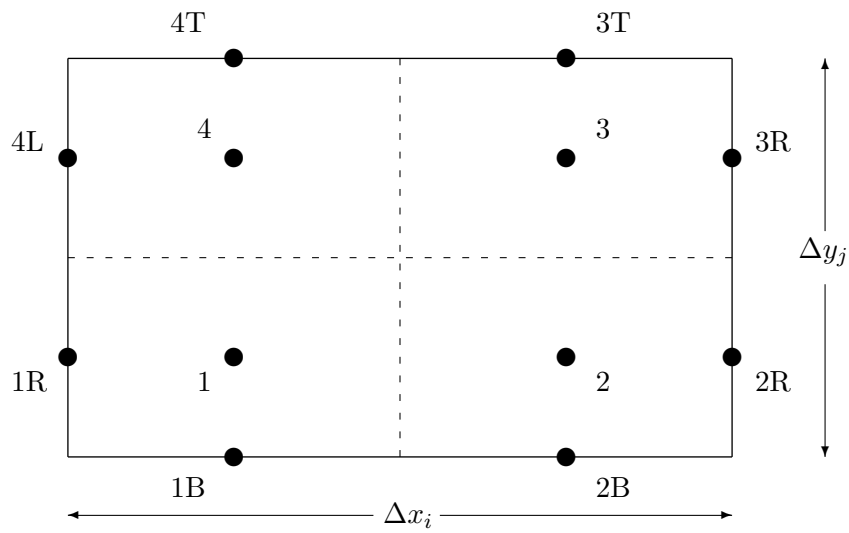

Figure 4.1: Location of points in Rectangular Cell For SCB

$$\frac{\mu\Delta y}{2}\begin{bmatrix}-\psi_{1L}\\ \psi_{2R}\\ \psi_{3R}\\ -\psi_{4L}\end{bmatrix}+\frac{\mu\Delta y}{4}\begin{bmatrix}1 & 1 & 0 & 0\\ -1 & -1 & 0 & 0\\ 0 & 0 & -1 & -1\\ 0 & 0 & 1 & 1\end{bmatrix}\begin{bmatrix}\psi_1\\ \psi_2\\ \psi_3\\ \psi_4\end{bmatrix}+\frac{\eta\Delta x}{2}\begin{bmatrix}-\psi_{1B}\\ -\psi_{2B}\\ \psi_{3T}\\ \psi_{4T}\end{bmatrix}$$
$$\frac{\eta\Delta x}{4}\begin{bmatrix}1 & 0 & 0 & 1\\ 0 & 1 & 1 & 0\\ 0 & -1 & -1 & 0\\ -1 & 0 & 0 & -1\end{bmatrix}\begin{bmatrix}\psi_1\\ \psi_2\\ \psi_3\\ \psi_4\end{bmatrix}+\frac{\sigma_t\Delta x\Delta y}{4}\begin{bmatrix}\psi_1\\ \psi_2\\ \psi_3\\ \psi_4\end{bmatrix}=\frac{\sigma_s\Delta x\Delta y}{(4\pi)4}\begin{bmatrix}\phi_1\\ \phi_2\\ \phi_3\\ \phi_4\end{bmatrix}+\frac{\Delta x\Delta y}{(4\pi)4}\begin{bmatrix}q_1\\ q_2\\ q_3\\ q_4\end{bmatrix} \quad (4.1)$$

Here, the points $\psi_{1L}, \psi_{1B}, \psi_{2L}, \psi_{2R} \ldots$ are defined by their downstream values, that is,

$$\psi_{1L} = \begin{cases} \psi_{1,i,j,m} & \mu_m < 0 \\ \psi_{3,i-1,j,m} & \mu_m > 0 \\ \psi^{in}_{1,i,j,m} & i = 1, \text{ for } \mu_m > 0 \end{cases} \qquad \psi_{1B} = \begin{cases} \psi_{1,i,j,m} & \eta_m < 0 \\ \psi_{4,i,j-1,m} & \eta_m > 0 \\ \psi^{in}_{1,i,j,m} & j = 1, \text{ for } \eta_m > 0 \end{cases} \tag{4.2a}$$

$$\psi_{2R} = \begin{cases} \psi_{1,i+1,j,m} & \mu_m < 0 \\ \psi_{2,i,j,m} & \mu_m > 0 \\ \psi^{in}_{2,i,j,m} & i = N_x, \text{ for } \mu_m < 0 \end{cases} \qquad \psi_{2B} = \begin{cases} \psi_{2,i,j,m} & \eta_m < 0 \\ \psi_{3,i,j-1,m} & \eta_m > 0 \\ \psi^{in}_{2,i,j,m} & j = 1, \text{ for } \eta_m > 0 \end{cases} \tag{4.2b}$$

$$\psi_{3R} = \begin{cases} \psi_{4,i+1,j,m} & \mu_m < 0 \\ \psi_{3,i,j,m} & \mu_m > 0 \\ \psi^{in}_{3,i,j,m} & i = N_x, \text{ for } \mu_m < 0 \end{cases} \qquad \psi_{3T} = \begin{cases} \psi_{2,i,j+1,m} & \eta_m < 0 \\ \psi_{3,i,j,m} & \eta_m > 0 \\ \psi^{in}_{3,i,j,m} & j = N_y, \text{ for } \eta_m < 0 \end{cases} \tag{4.2c}$$

$$\psi_{4L} = \begin{cases} \psi_{4,i,j,m} & \mu_m < 0 \\ \psi_{3,i-1,j,m} & \mu_m > 0 \\ \psi^{in}_{4,i,j,m} & i = 1, \text{ for } \mu_m > 0 \end{cases} \qquad \psi_{4T} = \begin{cases} \psi_{1,i,j+1,m} & \eta_m < 0 \\ \psi_{4,i,j,m} & \eta_m > 0 \\ \psi^{in}_{4,i,j,m} & j = N_y, \text{ for } \eta_m < 0 \end{cases} \tag{4.2d}$$

We can note that this set of equations is consistent with the fully lumped Bilinear Discontinuous Equations. [14] Here we have defined the Simple corner balance equations for 2D rectangular geometry, with Eq. 4.1. The downstream values are defined by Eq. 4.2, with boundary conditions Eq. 4.3.

$$\psi_m|_{i=1} = \psi^{in}_{left}(\vec{\Omega}), \text{ for } \mu > 0, \tag{4.3a}$$

$$\psi_m|_{i=N_x} = \psi^{in}_{right}(\vec{\Omega}), \text{ for } \mu < 0, \tag{4.3b}$$

$$\psi_m|_{j=1} = \psi^{in}_{bottom}(\vec{\Omega}), \text{ for } \eta > 0, \tag{4.3c}$$

$$\psi_m|_{j=N_y} = \psi^{in}_{top}(\vec{\Omega}), \text{ for } \eta < 0. \tag{4.3d}$$

4.2 Second Moment Method for SCB

Here we will develop a low-order set of equations for the Simple Corner Balance equations based off the second moment method. [15], [22] We start by taking the zeroth angular moment and integrating the balance equation, Eq. 4.1 in discrete form i.e. using a quadrature set. The

result is,

$$\frac{\Delta y}{2}\begin{bmatrix}-J_{x,1L}\\ J_{x,2R}\\ J_{x,3R}\\ -J_{x,4L}\end{bmatrix}+\frac{\Delta y}{4}\begin{bmatrix}1&1&0&0\\-1&-1&0&0\\0&0&-1&-1\\0&0&1&1\end{bmatrix}\begin{bmatrix}J_{x,1}\\J_{x,2}\\J_{x,3}\\J_{x,4}\end{bmatrix}+\frac{\Delta x}{2}\begin{bmatrix}-J_{y,1B}\\-J_{y,2B}\\J_{y,3T}\\J_{y,4T}\end{bmatrix}$$
$$\frac{\Delta x}{4}\begin{bmatrix}1&0&0&1\\0&1&1&0\\0&-1&-1&0\\-1&0&0&-1\end{bmatrix}\begin{bmatrix}J_{y,1}\\J_{y,2}\\J_{y,3}\\J_{y,4}\end{bmatrix}+\frac{\sigma_a\Delta x\Delta y}{4}\begin{bmatrix}\phi_1\\\phi_2\\\phi_3\\\phi_4\end{bmatrix}=\frac{\Delta x\Delta y}{4}\begin{bmatrix}q_1\\q_2\\q_3\\q_4\end{bmatrix} \tag{4.4}$$

We now integrate, in discrete form, the balance equation with weight μ_m to get,

$$\frac{\Delta y}{2}\begin{bmatrix}-\tilde{E}_{xx,1L}\\ \tilde{E}_{xx,2R}\\ \tilde{E}_{xx,3R}\\ -\tilde{E}_{xx,4L}\end{bmatrix}+\frac{\Delta y}{4}\begin{bmatrix}1&1&0&0\\-1&-1&0&0\\0&0&-1&-1\\0&0&1&1\end{bmatrix}\begin{bmatrix}\tilde{E}_{xx,1}\\\tilde{E}_{xx,2}\\\tilde{E}_{xx,3}\\\tilde{E}_{xx,4}\end{bmatrix}+\frac{\Delta x}{2}\begin{bmatrix}-\tilde{E}_{xy,1B}\\-\tilde{E}_{xy,2B}\\\tilde{E}_{xy,3T}\\\tilde{E}_{xy,4T}\end{bmatrix}$$
$$\frac{\Delta x}{4}\begin{bmatrix}1&0&0&1\\0&1&1&0\\0&-1&-1&0\\-1&0&0&-1\end{bmatrix}\begin{bmatrix}\tilde{E}_{xy,1}\\\tilde{E}_{xy,2}\\\tilde{E}_{xy,3}\\\tilde{E}_{xy,4}\end{bmatrix}+\frac{\sigma_t\Delta x\Delta y}{4}\begin{bmatrix}J_{x,1}\\J_{x,2}\\J_{x,3}\\J_{x,4}\end{bmatrix}=0, \tag{4.5}$$

where,

$$\tilde{E}_{\alpha\beta}=\sum_m \Omega_{\alpha,m}\Omega_{\beta,m}\psi_m w_m. \tag{4.6}$$

Now we integrate the balance equation with weight η_m.

$$\frac{\Delta y}{2}\begin{bmatrix}-\tilde{E}_{xy,1L}\\ \tilde{E}_{xy,2R}\\ \tilde{E}_{xy,3R}\\ -\tilde{E}_{xy,4L}\end{bmatrix}+\frac{\Delta y}{4}\begin{bmatrix}1&1&0&0\\-1&-1&0&0\\0&0&-1&-1\\0&0&1&1\end{bmatrix}\begin{bmatrix}\tilde{E}_{xy,1}\\\tilde{E}_{xy,2}\\\tilde{E}_{xy,3}\\\tilde{E}_{xy,4}\end{bmatrix}+\frac{\Delta x}{2}\begin{bmatrix}-\tilde{E}_{yy,1B}\\-\tilde{E}_{yy,2B}\\\tilde{E}_{yy,3T}\\\tilde{E}_{yy,4T}\end{bmatrix}$$
$$\frac{\Delta x}{4}\begin{bmatrix}1&0&0&1\\0&1&1&0\\0&-1&-1&0\\-1&0&0&-1\end{bmatrix}\begin{bmatrix}\tilde{E}_{yy,1}\\\tilde{E}_{yy,2}\\\tilde{E}_{yy,3}\\\tilde{E}_{yy,4}\end{bmatrix}+\frac{\sigma_t\Delta x\Delta y}{4}\begin{bmatrix}J_{y,1}\\J_{y,2}\\J_{y,3}\\J_{y,4}\end{bmatrix}=0, \tag{4.7}$$

We now introduce,

$$\hat{E}_{\alpha\beta} = \sum_m \left(\frac{1}{3}\delta_{\alpha\beta} - \Omega_\alpha\Omega_\beta\right)\psi_m w_m \tag{4.8}$$

and the obtain the following low-order second moment equations

$$\frac{\Delta y}{6}\begin{bmatrix}-\phi_{1L}\\ \phi_{2R}\\ \phi_{3R}\\ -\phi_{4L}\end{bmatrix} + \frac{\Delta y}{12}\begin{bmatrix}1 & 1 & 0 & 0\\ -1 & -1 & 0 & 0\\ 0 & 0 & -1 & -1\\ 0 & 0 & 1 & 1\end{bmatrix}\begin{bmatrix}\phi_1\\ \phi_2\\ \phi_3\\ \phi_4\end{bmatrix} + \frac{\sigma_t\Delta x\Delta y}{4}\begin{bmatrix}J_{x,1}\\ J_{x,2}\\ J_{x,3}\\ J_{x,4}\end{bmatrix} = \frac{\Delta y}{2}\begin{bmatrix}-\hat{E}_{xx,1L}\\ \hat{E}_{xx,2R}\\ \hat{E}_{xx,3R}\\ -\hat{E}_{xx,4L}\end{bmatrix} +$$
$$\frac{\Delta y}{4}\begin{bmatrix}1 & 1 & 0 & 0\\ -1 & -1 & 0 & 0\\ 0 & 0 & -1 & -1\\ 0 & 0 & 1 & 1\end{bmatrix}\begin{bmatrix}\hat{E}_{xx,1}\\ \hat{E}_{xx,2}\\ \hat{E}_{xx,3}\\ \hat{E}_{xx,4}\end{bmatrix} + \frac{\Delta x}{2}\begin{bmatrix}-\hat{E}_{xy,1B}\\ -\hat{E}_{xy,2B}\\ \hat{E}_{xy,3T}\\ \hat{E}_{xy,4T}\end{bmatrix} + \frac{\Delta x}{4}\begin{bmatrix}1 & 0 & 0 & 1\\ 0 & 1 & 1 & 0\\ 0 & -1 & -1 & 0\\ -1 & 0 & 0 & -1\end{bmatrix}\begin{bmatrix}\hat{E}_{xy,1}\\ \hat{E}_{xy,2}\\ \hat{E}_{xy,3}\\ \hat{E}_{xy,4}\end{bmatrix}, \tag{4.9a}$$

$$\frac{\Delta x}{6}\begin{bmatrix}-\phi_{1B}\\ -\phi_{2B}\\ \phi_{3T}\\ \phi_{4T}\end{bmatrix} + \frac{\Delta x}{12}\begin{bmatrix}1 & 0 & 0 & 1\\ 0 & 1 & 1 & 0\\ 0 & -1 & -1 & 0\\ -1 & 0 & 0 & -1\end{bmatrix}\begin{bmatrix}\phi_1\\ \phi_2\\ \phi_3\\ \phi_4\end{bmatrix} + \frac{\sigma_t\Delta x\Delta y}{4}\begin{bmatrix}J_{y,1}\\ J_{y,2}\\ J_{y,3}\\ J_{y,4}\end{bmatrix} = \frac{\Delta y}{2}\begin{bmatrix}-\hat{E}_{xy,1L}\\ \hat{E}_{xy,2R}\\ \hat{E}_{xy,3R}\\ -\hat{E}_{xy,4L}\end{bmatrix} +$$
$$\frac{\Delta y}{4}\begin{bmatrix}1 & 1 & 0 & 0\\ -1 & -1 & 0 & 0\\ 0 & 0 & -1 & -1\\ 0 & 0 & 1 & 1\end{bmatrix}\begin{bmatrix}\hat{E}_{xy,1}\\ \hat{E}_{xy,2}\\ \hat{E}_{xy,3}\\ \hat{E}_{xy,4}\end{bmatrix} + \frac{\Delta x}{2}\begin{bmatrix}-\hat{E}_{yy,1B}\\ -\hat{E}_{yy,2B}\\ \hat{E}_{yy,3T}\\ \hat{E}_{yy,4T}\end{bmatrix} + \frac{\Delta x}{4}\begin{bmatrix}1 & 0 & 0 & 1\\ 0 & 1 & 1 & 0\\ 0 & -1 & -1 & 0\\ -1 & 0 & 0 & -1\end{bmatrix}\begin{bmatrix}\hat{E}_{yy,1}\\ \hat{E}_{yy,2}\\ \hat{E}_{yy,3}\\ \hat{E}_{yy,4}\end{bmatrix}. \tag{4.9b}$$

Here $\delta_{\alpha\beta}$ is the Kronecker delta function, and $\alpha, \beta = x.y$.

Now, consider the face average values defined in Eq. 4.2. These are defined by their downstream values, and thus when integrating over them, they can be split into two components for $\Omega_\alpha \geq 0$ and $\Omega_\alpha \leq 0$. Consider ψ_{1L}, the lower left face,

$$J^{i,j}_{x,1L} = \sum_m \mu_m \psi^{i,j}_{1L,m} w_m = \sum_{\mu_m \geq 0} \mu_m \psi^{i-1,j}_{3,m} w_m + \sum_{\mu_m \leq 0} \mu_m \psi^{i,j}_{1,m} w_m.$$

By using the P_1 approximation for the angular flux, we can rewrite the equation as,

$$
\begin{aligned}
J^{i,j}_{x,1L} &= \sum_{\mu_m \geq 0} \mu_m \psi^{i-1,j}_{2,m} w_m + \sum_{\mu_m \leq 0} \mu_m \psi^{i,j}_{1,m} w_m \\
&= \sum_{\mu_m \geq 0} \mu_m \frac{1}{4\pi} \left(\phi^{i-1,j}_2 + 3 \left[\mu_m J^{i-1,j}_{x,2} + \eta_m J^{i-1,j}_{y,2} \right] \right) w_m + \\
&\quad \sum_{\mu_m \leq 0} \mu_m \frac{1}{4\pi} \left(\phi^{i,j}_1 + 3 \left[\mu_m J^{i,j}_{x,1} + \eta_m J^{i,j}_{y,1} \right] \right) w_m + \\
&\quad \sum_{\mu_m \geq 0} \mu_m \left[\psi^{i-1,j}_{2,m} - \frac{1}{4\pi} \left(\phi^{i-1,j}_2 + 3 \left[\mu_m J^{i-1,j}_{x,2} + \eta_m J^{i-1,j}_{y,2} \right] \right) \right] w_m + \\
&\quad \sum_{\mu_m \leq 0} \mu_m \left[\psi^{i,j}_{m,1} - \frac{1}{4\pi} \left(\phi^{i,j}_1 + 3 \left[\mu_m J^{i,j}_{x,1} + \eta_m J^{i,j}_{y,1} \right] \right) \right] w_m \\
&= \sum_{\mu_m \geq 0} \mu_m \frac{1}{4\pi} \left(\phi^{i-1,j}_2 + 3\mu_m J^{i-1,j}_{x,2} \right) w_m + \sum_{\mu_m \leq 0} \mu_m \frac{1}{4\pi} \left(\phi^{i,j}_1 + 3\mu_m J^{i,j}_{x,1} \right) w_m + r^{i,j}_{1L} \\
&= \alpha_x \left(\phi^{i-1,j}_2 - \phi^{i,j}_1 \right) + \beta_x \left(J^{i-1,j}_{x,2} + J^{i,j}_{x,1} \right) + r^{i,j}_{1L}
\end{aligned}
$$

Here we have defined,

$$\alpha_x = \frac{1}{4\pi} \sum_{\mu_m \geq 0} \mu_m w_m, \tag{4.10}$$

$$\beta_x = \frac{3}{4\pi} \sum_{\mu_m \geq 0} \mu_m^2 w_m, \tag{4.11}$$

and the residual from the P_1 approximation as:

$$r^{i,j}_{1L} = \sum_{\mu_m \geq 0} \mu_m \psi^{i-1,j}_{2,m} + \sum_{\mu_m \leq 0} \mu_m \psi^{i,j}_{1,m} w_m - \alpha_x \left(\tilde{\phi}^{i-1,j}_2 - \tilde{\phi}^{i,j}_1 \right) - \beta_x \left(\tilde{J}^{i-1,j}_{x,2} + \tilde{J}^{i,j}_{x,1} \right). \tag{4.12}$$

Here $\tilde{\phi}$ and $\tilde{J}$ represent the scalar flux, and current obtained from the high-order transport equations. A similar method can be used for the other seven cell face values.

$$J^{i,j}_{y,1B} = \alpha_y \left(\phi^{i,j-1}_4 - \phi^{i,j}_1 \right) + \beta_y \left(J^{i,j-1}_{y,4} + J^{i,j}_{y,1} \right) + r^{i,j}_{1B} \tag{4.13a}$$

$$J^{i,j}_{x,2R} = \alpha_x \left(\phi^{i,j}_2 - \phi^{i+1,j}_1 \right) + \beta_x \left(J^{i,j}_{x,2} + J^{i+1,j}_{x,1} \right) + r^{i,j}_{2R} \tag{4.13b}$$

$$J^{i,j}_{y,2B} = \alpha_y \left(\phi^{i,j-1}_3 - \phi^{i,j}_2 \right) + \beta_y \left(J^{i,j-1}_{y,3} + J^{i,j}_{y,2} \right) + r^{i,j}_{2B} \tag{4.13c}$$

$$J^{i,j}_{x,3R} = \alpha_x \left(\phi^{i,j}_3 - \phi^{i+1,j}_4 \right) + \beta_x \left(J^{i,j}_{x,3} + J^{i+1,j}_{x,4} \right) + r^{i,j}_{3R} \tag{4.13d}$$

$$J^{i,j}_{y,3T} = \alpha_y \left(\phi^{i,j}_3 - \phi^{i,j+1}_2 \right) + \beta_y \left(J^{i,j}_{y,3} + J^{i,j+1}_{y,2} \right) + r^{i,j}_{3T} \tag{4.13e}$$

$$J_{x,4L}^{i,j} = \alpha_x \left(\phi_3^{i-1,j} - \phi_4^{i,j}\right) + \beta_x \left(J_{x,3}^{i-1,j} + J_{x,4}^{i,j}\right) + r_{4R}^{i,j} \tag{4.13f}$$

$$J_{y,4T}^{i,j} = \alpha_y \left(\phi_4^{i,j} - \phi_1^{i,j+1}\right) + \beta_y \left(J_{y,4}^{i,j} + J_{y,1}^{i,j+1}\right) + r_{4T}^{i,j} \tag{4.13g}$$

Similarly, we have

$$\alpha_y = \frac{1}{4\pi} \sum_{\eta_m \geq 0} \eta_m w_m \tag{4.14}$$

$$\beta_y = \frac{3}{4\pi} \sum_{\eta_m \geq 0} \eta_m^2 w_m \tag{4.15}$$

The residuals for Eq. 4.13 are defined as:

$$r_{1B}^{i,j} = \sum_{\eta_m \geq 0} \eta_m \psi_{4,m}^{i,j-1} + \sum_{\eta_m \leq 0} \eta_m \psi_{1,m}^{i,j} w_m - \alpha_y \left(\tilde{\phi}_4^{i,j-1} - \tilde{\phi}_1^{i,j}\right) - \beta_y \left(\tilde{J}_{y,4}^{i,j-1} + \tilde{J}_{y,1}^{i,j}\right), \tag{4.16a}$$

$$r_{2R}^{i,j} = \sum_{\mu_m \geq 0} \mu_m \psi_{2,m}^{i,j} + \sum_{\mu_m \leq 0} \mu_m \psi_{m,1}^{i+1,j} w_m - \alpha_x \left(\tilde{\phi}_2^{i,j} - \tilde{\phi}_1^{i+1,j}\right) - \beta_x \left(\tilde{J}_{x,2}^{i,j} + \tilde{J}_{x,1}^{i+1,j}\right), \tag{4.16b}$$

$$r_{2B}^{i,j} = \sum_{\eta_m \geq 0} \eta_m \psi_{3,m}^{i,j-1} + \sum_{\eta_m \leq 0} \eta_m \psi_{2,m}^{i,j} w_m - \alpha_y \left(\tilde{\phi}_3^{i,j-1} - \tilde{\phi}_2^{i,j}\right) - \beta_y \left(\tilde{J}_{y,3}^{i,j-1} + \tilde{J}_{y,2}^{i,j}\right), \tag{4.16c}$$

$$r_{3R}^{i,j} = \sum_{\mu_m \geq 0} \mu_m \psi_{3,m}^{i,j} + \sum_{\mu_m \leq 0} \mu_m \psi_{4,m}^{i+1,j} w_m - \alpha_x \left(\tilde{\phi}_3^{i,j} - \tilde{\phi}_4^{i+1,j}\right) - \beta_x \left(\tilde{J}_{x,3}^{i,j} + \tilde{J}_{x,4}^{i+1,j}\right), \tag{4.16d}$$

$$r_{3T}^{i,j} = \sum_{\eta_m \geq 0} \eta_m \psi_{3,m}^{i,j} + \sum_{\eta_m \leq 0} \eta_m \psi_{2,m}^{i,j+1} w_m - \alpha_y \left(\tilde{\phi}_3^{i,j} - \tilde{\phi}_2^{i,j+1}\right) - \beta_y \left(\tilde{J}_{y,3}^{i,j} + \tilde{J}_{y,2}^{i,j+1}\right), \tag{4.16e}$$

$$r_{4L}^{i,j} = \sum_{\mu_m \geq 0} \mu_m \psi_{3,m}^{i-1,j} + \sum_{\mu_m \leq 0} \mu_m \psi_{4,m}^{i,j} w_m - \alpha_x \left(\tilde{\phi}_3^{i-1,j} - \tilde{\phi}_4^{i,j}\right) - \beta_x \left(\tilde{J}_{x,3}^{i-1,j} + \tilde{J}_{x,4}^{i,j}\right), \tag{4.16f}$$

$$r_{4T}^{i,j} = \sum_{\eta_m \geq 0} \eta_m \psi_{4,m}^{i,j} + \sum_{\eta_m \leq 0} \eta_m \psi_{1,m}^{i,j+1} w_m - \alpha_y \left(\tilde{\phi}_4^{i,j} - \tilde{\phi}_1^{i,j+1}\right) - \beta_y \left(\tilde{J}_{y,4}^{i,j} + \tilde{J}_{y,1}^{i,j+1}\right). \tag{4.16g}$$

Using a similar method to that of above we can now expand the the face average $\tilde{E}$ in Eq. 4.5,

and Eq. 4.7 using the P_1 equations as well.

$$
\begin{aligned}
\tilde{E}^{i,j}_{xx,1L} &= \sum_{\mu_m \geq 0} \mu_m^2 \psi^{i-1,j}_{2,m} w_m + \sum_{\mu_m \leq 0} \mu_m^2 \psi^{i,j}_{1,m} w_m \\
&= \sum_{\mu_m \geq 0} \mu_m^2 \frac{1}{4\pi} \left(\phi_2^{i-1,j} + 3 \left[\mu_m J^{i-1,j}_{x,2} + \eta_m J^{i-1,j}_{y,2} \right] \right) w_m + \\
&\quad \sum_{\mu_m \leq 0} \mu_m^2 \frac{1}{4\pi} \left(\phi_1^{i,j} + 3 \left[\mu_m J^{i,j}_{x,1} + \eta_m J^{i,j}_{y,1} \right] \right) w_m + \\
&\quad \sum_{\mu_m \geq 0} \mu_m^2 \left[\psi^{i-1,j}_{2,m} - \frac{1}{4\pi} \left(\phi_2^{i-1,j} + 3 \left[\mu_m J^{i-1,j}_{x,2} + \eta_m J^{i-1,j}_{y,2} \right] \right) \right] w_m + \\
&\quad \sum_{\mu_m \leq 0} \mu_m^2 \left[\psi^{i,j}_{m,1} - \frac{1}{4\pi} \left(\phi_1^{i,j} + 3 \left[\mu_m J^{i,j}_{x,1} + \eta_m J^{i,j}_{y,1} \right] \right) \right] w_m \\
&= \sum_{\mu_m \geq 0} \mu_m^2 \frac{1}{4\pi} \left(\phi_2^{i-1,j} + 3\mu_m J^{i-1,j}_{x,2} \right) w_m + \sum_{\mu_m \leq 0} \mu_m^2 \frac{1}{4\pi} \left(\phi_1^{i,j} + 3\mu_m J^{i,j}_{x,1} \right) w_m + R^{i,j}_{xx,1L}
\end{aligned}
$$

By making the following definitions,

$$\xi_{xxx} = \frac{3}{4\pi} \sum_{\mu_m \geq 0} \mu_m^3 w_m, \tag{4.17a}$$

$$\xi_{xyx} = \frac{3}{4\pi} \sum_{\eta_m \geq 0} \mu_m^2 \eta_m w_m, \tag{4.17b}$$

$$\xi_{yyy} = \frac{3}{4\pi} \sum_{\eta_m \geq 0} \eta_m^3 w_m, \tag{4.17c}$$

$$\xi_{xyy} = \frac{3}{4\pi} \sum_{\mu_m \geq 0} \eta_m^2 \mu_m w_m, \tag{4.17d}$$

$$\rho_{xx} = \frac{1}{4\pi} \sum_{\mu_m \geq 0} \mu_m^2 w_m, \tag{4.17e}$$

$$\rho_{yy} = \frac{1}{4\pi} \sum_{\eta_m \geq 0} \eta_m^2 w_m. \tag{4.17f}$$

we can now write the face average $\tilde{E}$ in terms of the P_1 expansion for the left and right sides of the cell,

$$\tilde{E}^{i,j}_{xx,1L} = \rho_{xx} \left(\phi_2^{i-1,j} + \phi_1^{i,j} \right) + \xi_{xxx} \left(J^{i-1,j}_{x,2} - J^{i,j}_{x,1} \right) + R^{i,j}_{xx,1L} \tag{4.18a}$$

$$\tilde{E}^{i,j}_{xx,4L} = \rho_{xx}\left(\phi^{i-1,j}_3 + \phi^{i,j}_4\right) + \xi_{xxx}\left(J^{i-1,j}_{x,3} - J^{i,j}_{x,4}\right) + R^{i,j}_{xx,4L} \tag{4.18b}$$

$$\tilde{E}^{i,j}_{xx,2R} = \rho_{xx}\left(\phi^{i,j}_2 + \phi^{i+1,j}_1\right) + \xi_{xxx}\left(J^{i,j}_{x,2} - J^{i+1,j}_{x,1}\right) + R^{i,j}_{xx,2R} \tag{4.18c}$$

$$\tilde{E}^{i,j}_{xx,3R} = \rho_{xx}\left(\phi^{i,j}_3 + \phi^{i+1,j}_4\right) + \xi_{xxx}\left(J^{i,j}_{x,3} - J^{i+1,j}_{x,4}\right) + R^{i,j}_{xx,3R} \tag{4.18d}$$

Where the residuals are defined as:

$$R^{i,j}_{xx,1L} = \sum_{\mu_m \geq 0} \mu_m^2 \psi^{i-1,j}_{2,m} w_m + \sum_{\mu_m \leq 0} \mu_m^2 \psi^{i,j}_{1,m} w_m - \rho_{xx}\left(\tilde{\phi}^{i-1,j}_2 + \tilde{\phi}^{i,j}_1\right) - \xi_{xxx}\left(\tilde{J}^{i-1,j}_{x,2} - \tilde{J}^{i,j}_{x,1}\right) \tag{4.19a}$$

$$R^{i,j}_{xx,4L} = \sum_{\mu_m \geq 0} \mu_m^2 \psi^{i-1,j}_{3,m} w_m + \sum_{\mu_m \leq 0} \mu_m^2 \psi^{i,j}_{4,m} w_m - \rho_{xx}\left(\tilde{\phi}^{i-1,j}_3 + \tilde{\phi}^{i,j}_4\right) - \xi_{xxx}\left(\tilde{J}^{i-1,j}_{x,3} - \tilde{J}^{i,j}_{x,4}\right) \tag{4.19b}$$

$$R^{i,j}_{xx,2R} = \sum_{\mu_m \geq 0} \mu_m^2 \psi^{i,j}_{2,m} w_m + \sum_{\mu_m \leq 0} \mu_m^2 \psi^{i+1,j}_{1,m} w_m - \rho_{xx}\left(\tilde{\phi}^{i,j}_2 + \tilde{\phi}^{i+1,j}_1\right) - \xi_{xxx}\left(\tilde{J}^{i,j}_{x,2} - \tilde{J}^{i+1,j}_{x,1}\right) \tag{4.19c}$$

$$R^{i,j}_{xx,3R} = \sum_{\mu_m \geq 0} \mu_m^2 \psi^{i,j}_{3,m} w_m + \sum_{\mu_m \leq 0} \mu_m^2 \psi^{i+1,j}_{4,m} w_m - \rho_{xx}\left(\tilde{\phi}^{i,j}_3 + \tilde{\phi}^{i+1,j}_4\right) - \xi_{xxx}\left(\tilde{J}^{i,j}_{x,3} - \tilde{J}^{i+1,j}_{x,4}\right) \tag{4.19d}$$

For the top and bottom of the cells we have

$$\tilde{E}^{i,j}_{yy,1B} = \rho_{yy}\left(\phi^{i,j-1}_4 + \phi^{i,j}_1\right) + \xi_{yyy}\left(J^{i,j-1}_{y,4} - J^{i,j}_{y,1}\right) + R^{i,j}_{yy,1B} \tag{4.20a}$$

$$\tilde{E}^{i,j}_{yy,2B} = \rho_{yy}\left(\phi^{i,j-1}_3 + \phi^{i,j}_2\right) + \xi_{yyy}\left(J^{i,j-1}_{y,3} - J^{i,j}_{y,2}\right) + R^{i,j}_{yy,2B} \tag{4.20b}$$

$$\tilde{E}^{i,j}_{yy,3T} = \rho_{yy}\left(\phi^{i,j}_3 + \phi^{i,j+1}_2\right) + \xi_{yyy}\left(J^{i,j}_{y,3} - J^{i,j+1}_{y,2}\right) + R^{i,j}_{yy,3T} \tag{4.20c}$$

$$\tilde{E}^{i,j}_{yy,4T} = \rho_{yy}\left(\phi^{i,j}_4 + \phi^{i,j+1}_1\right) + \xi_{yyy}\left(J^{i,j}_{y,4} - J^{i,j+1}_{y,1}\right) + R^{i,j}_{yy,4T} \tag{4.20d}$$

Where the residuals here are defined as

$$R^{i,j}_{1B,yy} = \sum_{\eta_m \geq 0} \eta_m^2 \psi^{i,j-1}_{4,m} w_m + \sum_{\eta_m \leq 0} \eta_m^2 \psi^{i,j}_{1,m} w_m - \rho_{yy} \left(\tilde{\phi}^{i,j-1}_4 + \tilde{\phi}^{i,j}_1 \right) + \xi_{yyy} \left(\tilde{J}^{i,j-1}_{y,4} - \tilde{J}^{i,j}_{y,1} \right) \tag{4.21a}$$

$$R^{i,j}_{2B,yy} = \sum_{\eta_m \geq 0} \eta_m^2 \psi^{i,j-1}_{3,m} w_m + \sum_{\eta_m \leq 0} \eta_m^2 \psi^{i,j}_{2,m} w_m - \rho_{yy} \left(\tilde{\phi}^{i,j-1}_3 + \tilde{\phi}^{i,j}_2 \right) + \xi_{yyy} \left(\tilde{J}^{i,j-1}_{y,3} - \tilde{J}^{i,j}_{y,2} \right) \tag{4.21b}$$

$$R^{i,j}_{3T,yy} = \sum_{\eta_m \geq 0} \eta_m^2 \psi^{i,j}_{3,m} w_m + \sum_{\eta_m \leq 0} \eta_m^2 \psi^{i,j+1}_{2,m} w_m - \rho_{yy} \left(\tilde{\phi}^{i,j}_3 + \tilde{\phi}^{i,j+1}_2 \right) + \xi_{yyy} \left(\tilde{J}^{i,j}_{y,3} - \tilde{J}^{i,j+1}_{y,2} \right) \tag{4.21c}$$

$$R^{i,j}_{4T,yy} = \sum_{\eta_m \geq 0} \eta_m^2 \psi^{i,j}_{4,m} w_m + \sum_{\eta_m \leq 0} \eta_m^2 \psi^{i,j+1}_{1,m} w_m - \rho_{yy} \left(\tilde{\phi}^{i,j}_4 + \tilde{\phi}^{i,j+1}_1 \right) + \xi_{yyy} \left(\tilde{J}^{i,j}_{y,4} - \tilde{J}^{i,j+1}_{y,1} \right) \tag{4.21d}$$

Now looking at the cross terms, $\tilde{E}_{xy}$ we see

$$\tilde{E}^{i,j}_{xy,1L} = \xi_{xyy} \left(J^{i-1,j}_{y,2} - J^{i,j}_{y,1} \right) + R^{i,j}_{xy,1L} \tag{4.22a}$$

$$\tilde{E}^{i,j}_{xy,1B} = \xi_{xyx} \left(J^{i,j-1}_{x,4} - J^{i,j}_{x,1} \right) + R^{i,j}_{xy,1B} \tag{4.22b}$$

$$\tilde{E}^{i,j}_{xy,2R} = \xi_{xyy} \left(J^{i,j}_{y,2} - J^{i+1,j}_{y,1} \right) + R^{i,j}_{xy,2R} \tag{4.22c}$$

$$\tilde{E}^{i,j}_{xy,2B} = \xi_{xyx} \left(J^{i,j-1}_{x,3} - J^{i,j}_{x,2} \right) + R^{i,j}_{xy,2B} \tag{4.22d}$$

$$\tilde{E}^{i,j}_{xy,3R} = \xi_{xyy} \left(J^{i,j}_{y,3} - J^{i+1,j}_{y,4} \right) + R^{i,j}_{xy,3R} \tag{4.22e}$$

$$\tilde{E}^{i,j}_{xy,3T} = \xi_{xyx} \left(J^{i,j}_{x,3} - J^{i,j+1}_{x,2} \right) + R^{i,j}_{xy,3T} \tag{4.22f}$$

$$\tilde{E}^{i,j}_{xy,4L} = \xi_{xyy} \left(J^{i-1,j}_{y,3} - J^{i,j}_{y,4} \right) + R^{i,j}_{xy,4L} \tag{4.22g}$$

$$\tilde{E}^{i,j}_{xy,4T} = \xi_{xyx} \left(J^{i,j}_{x,4} - J^{i,j+1}_{x,1} \right) + R^{i,j}_{xy,4T} \tag{4.22h}$$

Here the residuals are defined as:

$$R^{i,j}_{xy,1L} = \sum_{\mu_m \geq 0} \mu_m \eta_m \psi^{i-1,j}_{2,m} w_m + \sum_{\mu_m \leq 0} \mu_m \eta_m \psi^{i,j}_{1,m} w_m - \xi_{xyy} \left(\tilde{J}^{i-1,j}_{y,2} - \tilde{J}^{i,j}_{y,1} \right) \tag{4.23a}$$

$$R^{i,j}_{xy,1B} = \sum_{\eta_m \geq 0} \mu_m \eta_m \psi^{i,j-1}_{4,m} w_m + \sum_{\eta_m \leq 0} \mu_m \eta_m \psi^{i,j}_{1,m} w_m - \xi_{xyx} \left(\tilde{J}^{i,j-1}_{x,4} - \tilde{J}^{i,j}_{x,1} \right) \tag{4.23b}$$

$$R^{i,j}_{xy,2R} = \sum_{\mu_m \geq 0} \mu_m \eta_m \psi^{i,j}_{2,m} w_m + \sum_{\mu_m \leq 0} \mu_m \eta_m \psi^{i+1,j}_{1,m} w_m - \xi_{xyy} \left(\tilde{J}^{i,j}_{y,2} - \tilde{J}^{i+1,j}_{y,1} \right) \tag{4.23c}$$

$$R^{i,j}_{xy,2B} = \sum_{\eta_m \geq 0} \mu_m \eta_m \psi^{i,j-1}_{3,m} w_m + \sum_{\eta_m \leq 0} \mu_m \eta_m \psi^{i,j}_{2,m} w_m - \xi_{xyx} \left(\tilde{J}^{i,j-1}_{x,3} - \tilde{J}^{i,j}_{x,2} \right) \tag{4.23d}$$

$$R^{i,j}_{xy,3R} = \sum_{\mu_m \geq 0} \mu_m \eta_m \psi^{i,j}_{3,m} w_m + \sum_{\mu_m \leq 0} \mu_m \eta_m \psi^{i+1,j}_{4,m} w_m - \xi_{xyy} \left(\tilde{J}^{i,j}_{y,3} - \tilde{J}^{i+1,j}_{y,4} \right) \tag{4.23e}$$

$$R^{i,j}_{xy,3T} = \sum_{\eta_m \geq 0} \mu_m \eta_m \psi^{i,j}_{3,m} w_m + \sum_{\eta_m \leq 0} \mu_m \eta_m \psi^{i+1,j}_{2,m} w_m - \xi_{xyx} \left(\tilde{J}^{i,j}_{x,3} - \tilde{J}^{i+1,j}_{x,2} \right) \tag{4.23f}$$

$$R^{i,j}_{xy,4L} = \sum_{\mu_m \geq 0} \mu_m \eta_m \psi^{i-1,j}_{3,m} w_m + \sum_{\mu_m \leq 0} \mu_m \eta_m \psi^{i,j}_{4,m} w_m - \xi_{xyy} \left(\tilde{J}^{i-1,j}_{y,3} - \tilde{J}^{i,j}_{y,4} \right) \tag{4.23g}$$

$$R^{i,j}_{xy,4T} = \sum_{\eta_m \geq 0} \mu_m \eta_m \psi^{i,j}_{4,m} w_m + \sum_{\eta_m \leq 0} \mu_m \eta_m \psi^{i,j+1}_{1,m} w_m - \xi_{xyx} \left(\tilde{J}^{i,j}_{x,4} - \tilde{J}^{i,j+1}_{x,1} \right) \tag{4.23h}$$

We now have a complete set of equations that can be substituted into Eq. 4.4, Eq. 4.5, and Eq. 4.7, to solve for the scalar flux, x- and y- components of the current for all cells in the interior of the domain. To solve along the edges and corners of the domain, we will need to modify the factors developed above. In the case of the boundary conditions defined in Eq. 4.3, we can define the incoming current at any point by

$$J^{in}_{r,*} = \sum_{\Omega \cdot n \leq 0} \Omega_{r,m} \psi^{in}_{*,m} w_m \tag{4.24}$$

Here $r = x$ or y and $* = 1L, 2B, 3R, 4T \ldots$. One can then use this definition to rewrite Eq. 4.13, and their associated residuals Eq. 4.16. For the bottom cells, $* = 1, 2$ we would have

$$J^{i,1}_{y,*B} = -\alpha_y \phi^{i,1}_* + \beta_y J^{i,1}_{y,*} + J^{in,i}_{y,*} + r^{i,1}_{*B} \tag{4.25a}$$

$$r^{i,1}_{*B} = \sum_{\eta_m \leq 0} \eta_m \psi^{i,1}_{*,m} w_m + \alpha_y \tilde{\phi}^{i,1}_* - \beta_y \tilde{J}^{i,1}_{y,*} \tag{4.25b}$$

$$J^{in,i}_{y,*} = \sum_{\eta_m \geq 0} \eta_m \psi^{in}_{*B,m} w_m \tag{4.25c}$$

For the top cells, $* = 3, 4$ we would have

$$J^{i,n_y}_{y,*T} = \alpha_y \phi^{i,n_y}_* + \beta_y J^{i,n_y}_{y,*} + J^{in,i}_{y,*} + r^{i,n_y}_{*T} \tag{4.26a}$$

$$r^{i,n_y}_{*T} = \sum_{\eta_m \geq 0} \eta_m \psi^{i,n_y}_{*,m} w_m - \alpha_y \tilde{\phi}^{i,n_y}_* - \beta_y \tilde{J}^{i,n_y}_{y,*} \tag{4.26b}$$

$$J^{in,i}_{y,*} = \sum_{\eta_m \leq 0} \eta_m \psi^{in}_{*T,m} w_m \tag{4.26c}$$

For the left cells, $* = 1, 4$ we would have

$$J^{1,j}_{x,*L} = -\alpha_x \phi^{1,j}_* + \beta_x J^{1,j}_{x,*} + J^{in,j}_{x,*} + r^{1,j}_{*L} \tag{4.27a}$$

$$r^{1,j}_{*L} = \sum_{\mu_m \leq 0} \mu_m \psi^{1,j}_{*,m} w_m + \alpha_x \tilde{\phi}^{1,j}_* - \beta_x \tilde{J}^{1,j}_{x,*} \tag{4.27b}$$

$$J^{in,j}_{x,*} = \sum_{\mu_m \geq 0} \mu_m \psi^{in}_{*L,m} w_m \tag{4.27c}$$

For the right cells, $* = 2, 3$ we would have

$$J^{n_x,j}_{x,*R} = \alpha_x \phi^{n_x,j}_* + \beta_x J^{n_x,j}_{x,*} + J^{in,j}_{x,*} + r^{n_x,j}_{*R} \tag{4.28a}$$

$$r^{n_x,j}_{*R} = \sum_{\mu_m \geq 0} \mu_m \psi^{n_x,j}_{*,m} w_m - \alpha_x \tilde{\phi}^{n_x,j}_* - \beta_x \tilde{J}^{n_x,j}_{x,*} \tag{4.28b}$$

$$J^{in,j}_{x,*} = \sum_{\mu_m \leq 0} \mu_m \psi^{in}_{*R,m} w_m \tag{4.28c}$$

We now look at the boundary conditions needed for the first moment equations. For the left cells, $i = 1$, and $* = 1, 4$, the boundary equations would be

$$\tilde{E}^{1,j}_{xx,*L} = \rho_{xx} \phi^{1,j}_* - \xi_{xxx} J^{1,j}_{x,*} + R^{1,j}_{xx,*L} + \epsilon^{in,j}_{xx,*L} \tag{4.29a}$$

$$\tilde{E}^{1,j}_{xy,*L} = -\xi_{xyy} J^{1,j}_{y,*} + R^{1,j}_{xy,*L} + \epsilon^{in,j}_{xy,*L} \tag{4.29b}$$

$$R^{1,j}_{xx,*L} = \sum_{\mu_m \leq 0} \mu_m^2 \psi^{1,j}_{*,m} w_m - \rho_{xx} \tilde{\phi}^{1,j}_* + \xi_{xxx} \tilde{J}^{1,j}_{x,*} \tag{4.29c}$$

$$R^{1,j}_{xy,*L} = \sum_{\mu_m \leq 0} \mu_m \eta_m \psi^{1,j}_{*,m} w_m + \xi_{xyy} \tilde{J}^{1,j}_{y,*} \tag{4.29d}$$

$$\epsilon^{1,j}_{xx,*L} = \sum_{\mu_m \geq 0} \mu_m^2 \psi^{in}_{*L,m} w_m \tag{4.29e}$$

$$\epsilon_{xy,*L}^{1,j} = \sum_{\mu_m \geq 0} \mu_m \eta_m \psi_{*L,m}^{in} w_m \tag{4.29f}$$

For the right cells, where $i = n_x$, and $* = 3, 4$, we would have

$$\tilde{E}_{xx,*R}^{n_x,j} = \rho_{xx} \phi_*^{n_x,j} + \xi_{xxx} J_{x,*}^{n_x,j} + R_{xx,*R}^{n_x,j} + \epsilon_{xx,*R}^{in,j} \tag{4.30a}$$

$$\tilde{E}_{xy,*R}^{n_x,j} = \xi_{xyy} J_{y,*}^{n_x,j} + R_{xy,*L}^{n_x,j} + \epsilon_{xy,*R}^{in,j} \tag{4.30b}$$

$$R_{xx,*R}^{n_x,j} = \sum_{\mu_m \geq 0} \mu_m^2 \psi_{*,m}^{n_x,j} w_m - \rho_{xx} \tilde{\phi}_*^{n_x,j} - \xi_{xxx} \tilde{J}_{x,*}^{n_x,j} \tag{4.30c}$$

$$R_{xy,*R}^{n_x,j} = \sum_{\mu_m \geq 0} \mu_m \eta_m \psi_{*,m}^{n_x,j} w_m - \xi_{xyy} \tilde{J}_{y,*}^{n_x,j} \tag{4.30d}$$

$$\epsilon_{xx,*R}^{n_x,j} = \sum_{\mu_m \leq 0} \mu_m^2 \psi_{*R,m}^{in} w_m \tag{4.30e}$$

$$\epsilon_{xy,*R}^{n_x,j} = \sum_{\mu_m \leq 0} \mu_m \eta_m \psi_{*R,m}^{in} w_m \tag{4.30f}$$

For the bottom cells, $j = 1$, and $* = 1, 2$, the boundary equations would be

$$\tilde{E}_{yy,*B}^{i,1} = \rho_{yy} \phi_*^{i,1} - \xi_{yyy} J_{y,*}^{i,1} + R_{yy,*B}^{i,1} + \epsilon_{yy,*B}^{in,i} \tag{4.31a}$$

$$\tilde{E}_{xy,*B}^{i,1} = -\xi_{xyx} J_{x,*}^{i,1} + R_{xy,*B}^{i,1} + \epsilon_{xy,*B}^{in,i} \tag{4.31b}$$

$$R_{yy,*B}^{i,1} = \sum_{\eta_m \leq 0} \eta_m^2 \psi_{*,m}^{i,1} w_m - \rho_{yy} \tilde{\phi}_*^{i,1} + \xi_{yyy} \tilde{J}_{y,*}^{i,1} \tag{4.31c}$$

$$R_{xy,*B}^{i,1} = \sum_{\eta_m \leq 0} \mu_m \eta_m \psi_{*,m}^{i,1} w_m + \xi_{xyx} \tilde{J}_{x,*}^{i,1} \tag{4.31d}$$

$$\epsilon_{yy,*B}^{i,1} = \sum_{\eta_m \geq 0} \eta_m^2 \psi_{*B,m}^{in} w_m \tag{4.31e}$$

$$\epsilon_{xy,*B}^{i,1} = \sum_{\eta_m \geq 0} \mu_m \eta_m \psi_{*B,m}^{in} w_m \tag{4.31f}$$

For the top cells, $j = n_y$, $* = 3, 4$

$$\tilde{E}_{yy,*T}^{i,n_y} = \rho_{yy} \phi_*^{i,n_y} + \xi_{yyy} J_{y,*}^{i,n_y} + R_{yy,*T}^{i,n_y} + \epsilon_{yy,*T}^{in,i} \tag{4.32a}$$

$$\tilde{E}_{xy,*T}^{i,n_y} = \xi_{xyx} J_{x,*}^{i,n_y} + R_{xy,*T}^{i,n_y} + \epsilon_{xy,*T}^{in,i} \tag{4.32b}$$

$$R_{yy,*T}^{i,n_y} = \sum_{\eta_m \geq 0} \eta_m^2 \psi_{*,m}^{i,n_y} w_m - \rho_{yy} \tilde{\phi}_*^{i,n_y} - \xi_{yyy} \tilde{J}_{y,*}^{i,n_y} \tag{4.32c}$$

$$R^{i,n_y}_{xy,*T} = \sum_{\eta_m \geq 0} \mu_m \eta_m \psi^{i,n_y}_{*,m} w_m - \xi_{xyx} \tilde{J}^{i,n_y}_{x,*} \tag{4.32d}$$

$$\epsilon^{i,n_y}_{yy,*T} = \sum_{\eta_m \leq 0} \eta_m^2 \psi^{in}_{*T,m} w_m \tag{4.32e}$$

$$\epsilon^{i,n_y}_{xy,*R} = \sum_{\eta_m \leq 0} \mu_m \eta_m \psi^{in}_{*T,m} w_m \tag{4.32f}$$

We now have a fully developed set of equations for describing the face average cell values that can be used in Eq. 4.4 - Eq. 4.7. This set of low order equations can be further simplified from twelve equations and unknowns (ϕ, J_x, and J_y in each corner) to eliminate currents. By doing this we reduce the computational power needed to solve this coupled set of equations.

4.3 Metrics in Two Dimensions

Previously we have developed metrics that measure transport effects. For now we will only consider the metrics M_2 and M_3 that are based off the quasidiffusion factor E. Looking at a more general version of Eq. 2.43c, [23] we would have:

$$\bar{\bar{E}} = \frac{\int_{4\pi} \vec{\Omega}\vec{\Omega}\psi(\vec{r},\vec{\Omega})d\Omega}{\int_{4\pi} \psi(\vec{r},\vec{\Omega})d\Omega}. \tag{4.33}$$

We see that the quasidiffusion factor E is now a tensor, with multiple components: E_{xx}, E_{yy}, and $E_{xy} = E_{yx}$. Consequently, M_2, and M_3, now have multiple components as well. M_2 would be defined:

$$\bar{\bar{M}}_2 = \bar{\bar{I}}\frac{1}{3} - \bar{\bar{E}} \tag{4.34}$$

The individual components of M_2 would be:

$$M_{2,xx}(x,y) = \frac{1}{3} - E_{xx}(x,y), \tag{4.35a}$$

$$M_{2,yy}(x,y) = \frac{1}{3} - E_{yy}(x,y), \tag{4.35b}$$

$$M_{2,xy}(x,y) = M_{2,yx}(x,y) = E_{xy}(x,y). \tag{4.35c}$$

For M_3 we would now have,

$$\bar{\bar{M}}_3 = \nabla\bar{\bar{E}}, \tag{4.36}$$

where its components would be,

$$M_{3,xx}(x,y) = \frac{\partial}{\partial x} E_{xx}(x,y), \tag{4.37a}$$

$$M_{3,yy}(x,y) = \frac{\partial}{\partial y} E_{yy}(x,y), \tag{4.37b}$$

$$M_{3,xy}(x,y) = \frac{\partial}{\partial x} E_{xy}(x,y), \tag{4.37c}$$

$$M_{3,yx}(x,y) = \frac{\partial}{\partial y} E_{yx}(x,y). \tag{4.37d}$$

To calculate these metrics numerically, based on the SCB discretization, we would simply calculate the quasidiffusion factor E for each corner point by

$$E^{i,j}_{k,xx} = \frac{\sum_m \mu_m^2 \psi^{i,j}_{k,m} w_m}{\sum_m \psi^{i,j}_{k,m} w_m}, \tag{4.38a}$$

$$E^{i,j}_{k,yy} = \frac{\sum_m \eta_m^2 \psi^{i,j}_{k,m} w_m}{\sum_m \psi^{i,j}_{k,m} w_m}, \tag{4.38b}$$

$$E^{i,j}_{k,xy} = \frac{\sum_m \mu_m \eta_m \psi^{i,j}_{k,m} w_m}{\sum_m \psi^{i,j}_{k,m} w_m}, \tag{4.38c}$$

where $k = 1 \ldots 4$, is the corner index. We can then calculate M_2 for each corner easily by

$$M^{i,j}_{k,2xx} = \left| \frac{1}{3} - E^{i,j}_{k,xx} \right|, \tag{4.39a}$$

$$M^{i,j}_{k,2yy} = \left| \frac{1}{3} - E^{i,j}_{k,yy} \right|, \tag{4.39b}$$

$$M^{i,j}_{k,2xy} = \left| E^{i,j}_{k,xy} \right|. \tag{4.39c}$$

For M_3 we need to consider partial derivatives. To obtain these values we use finite difference approximation across two adjacent corners in the same cell.

$$M^{i,j}_{k,3x*} = \frac{2}{\Delta x_i} \left| E^{i,j}_{k'',x*} - E^{i,j}_{k',x*} \right|, \tag{4.40a}$$

$$M^{i,j}_{k,3y*} = \frac{2}{\Delta y_j} \left| E^{i,j}_{k'',x*} - E^{i,j}_{k',x*} \right| . \tag{4.40b}$$

We generalize $* = x, y$, and $k = 1, 2$, because of the discretization. k' and k'' would be two adjacent corners, for the first equation where we calculate the x-derivative, $k' = 1, 4$, and $k'' = 1, 3$ respectively. For the second equation for the y-derivative, we would have $k' = 1, 2$, and $k'' = 3, 4$.

4.4 2D Boundary Conditions

Here we develop the boundary conditions to couple the transport and diffusion subdomains. Similar to the one dimensional version, we approximate the angular flux as a linearly anisotropic function and expand the angular flux using the P_1 approximation,

$$\psi_m(x, y) = \frac{1}{4\pi} \left(\phi(x, y) + 3\mu_m J_x(x, y) + 3\eta_m J_y(x, y) \right) . \tag{4.41}$$

Chapter 5

Numerical Results for 2D Problem

In this chapter we look at the numerical results to two test problems. In the first section we outline test problems and their solutions. These test cases are extensions of the ones done for the 1D results and expanded to multiple dimensions. We then look at the metrics developed in Sec. 4.3, for the converged solution. We compare these metrics to those estimated from the solution of a single transport iteration. The Second Moment residual terms are presented as another measure of how far the flux is from being linearly anisotropic. All these results help to define what areas in the problem domain can be considered diffusive to define the different domains. The final domain decomposition results are presented last where diffusion subdomains are imposed, and the relative error of the method is presented compared to a solution obtained without any domain decomposition.

5.1 Test Problems

In this section we consider tests which are analogous to the one dimensional problems. We start with a two dimensional version of Test A, which can be seen in Figure 5.1a. This is a two region problem defined by a pure absorbing region on the bottom and left sides of the domain $\sigma_t = 2$ cm^{-1} and $\sigma_s = 0$ cm^{-1}. This area is defined by $\Delta x = 0.1$ cm for $0 \leq x \leq 1$, and $\Delta y = 0.1$ cm for $0 \leq y \leq 1$. The interior of the domain is a pure scattering media where $\sigma_t = \sigma_s = 100$ cm^{-1}. The spacial mesh for $1 \leq x \leq 11$ is $\Delta x = 1$ cm, and $1 \leq y \leq 11$ is $\Delta y = 1$ cm. There is an incident flux on the left and bottom sides of the domain where $\psi^{in} = 1.0$. The scalar flux solution to this problem is presented in Figure 5.1a.

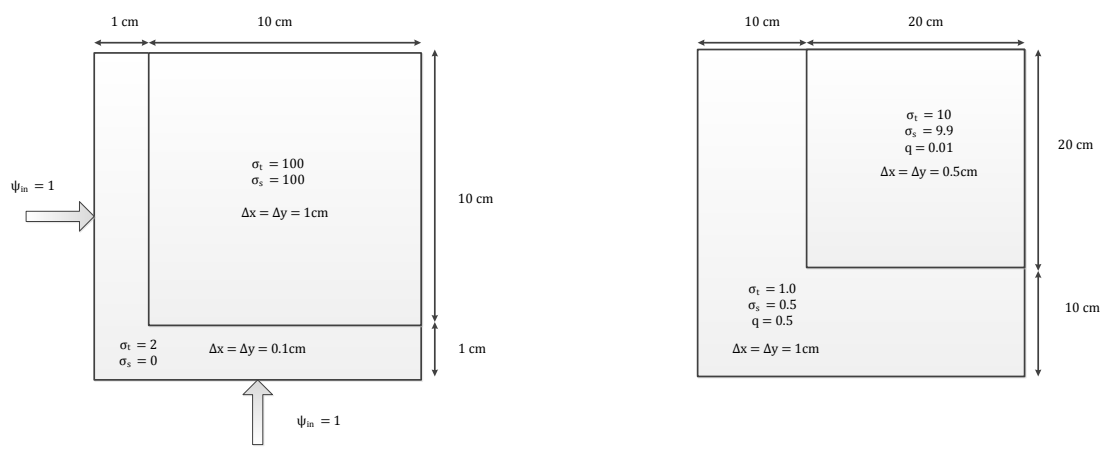

(a): Test-A Map

(b): Test-B Map

Another test, analogous to Test B, in two dimensions is again defined by a two region problem, shown in Figure 5.1b. The absorbing area domain, $0 \leq x \leq 10$, and $0 \leq y \leq 10$, has cross sections $\sigma_t = 1.0$ and $\sigma_s = 0.5$, and a external source $q = 0.5$. Each spatial cell is one mean free path thick in the x- and y- directions where $\Delta x = \Delta y = 1$. The highly scattering domain, $10 \leq x \leq 30$, and $10 \leq y \leq 30$, are defined by cell widths $\Delta x = 0.5$ and $\Delta y = 0.5$. Here the cross sections are $\sigma_t = 10$ and $\sigma_s = 9.9$, with a very small external source of $q = 0.01$. The scalar flux for this problem is given in Figure 5.1b. For these problems we ran with a point-wise convergence criteria of $\varepsilon = 10^{-12}$ and used the Abu-Shumay's q461214 quadrature set. [24].

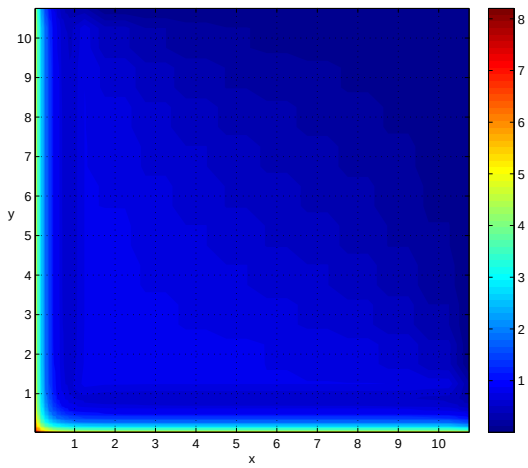

(a): Test-A Scalar Flux

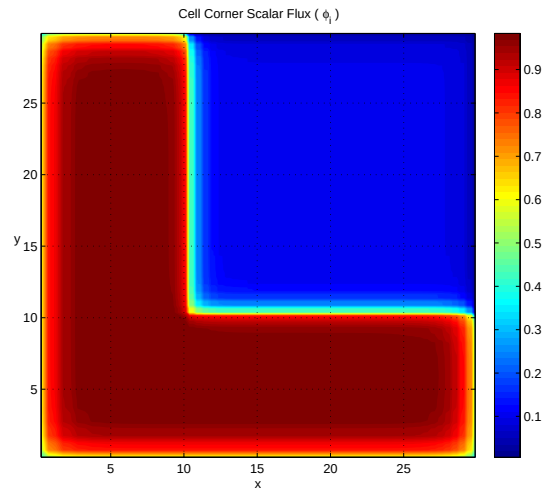

(b): Test-B Scalar Flux

5.2 2D Metric Results

In this section we analyze the metrics developed in Section 4.3. These metrics provide a way of determining what areas in a problem domain are diffusive. From Test A, we know the high scattering domain to be the definition of a diffusive area, so we expect that in that area the metrics will be small. The results presented here represent the metrics calculated without domain decomposition and from the final solution. The graphs for M_2 can be seen in Figure 5.1.

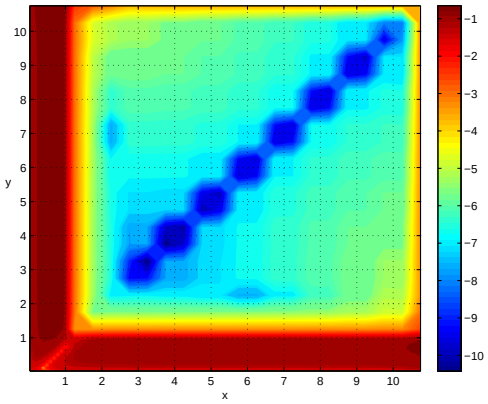

(a): $\log_{10}(M_{2,xx})$

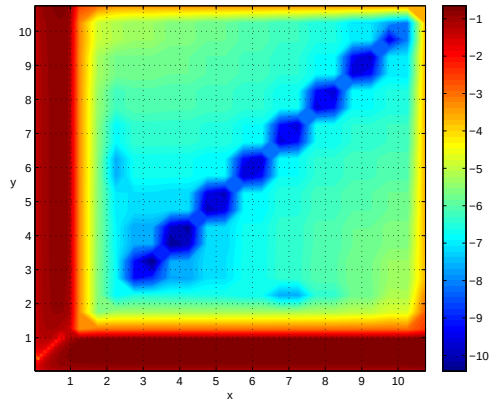

(b): $\log_{10}(M_{2,yy})$

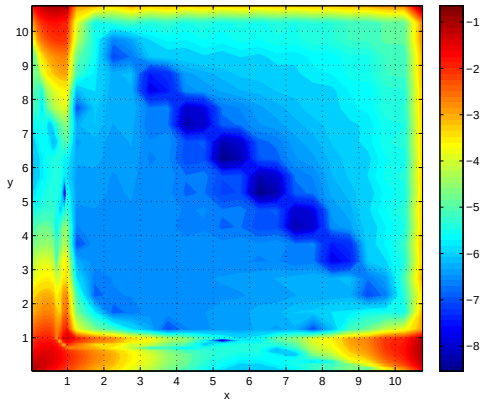

(c): $\log_{10}(M_{2,xy})$

Figure 5.1: M_2 for Test A

From these graphs we can see that the metrics are small in the pure scattering region, noticing that most of the values for the metrics are below 10^{-5}. Another obvious fact about these graphs is that they are symmetric and show that the smallest values are well within the diffusive area along the line of symmetry for the xx and yy moments. For the xy moment, we see that the smallest values are perpendicular to the axis of symmetry.

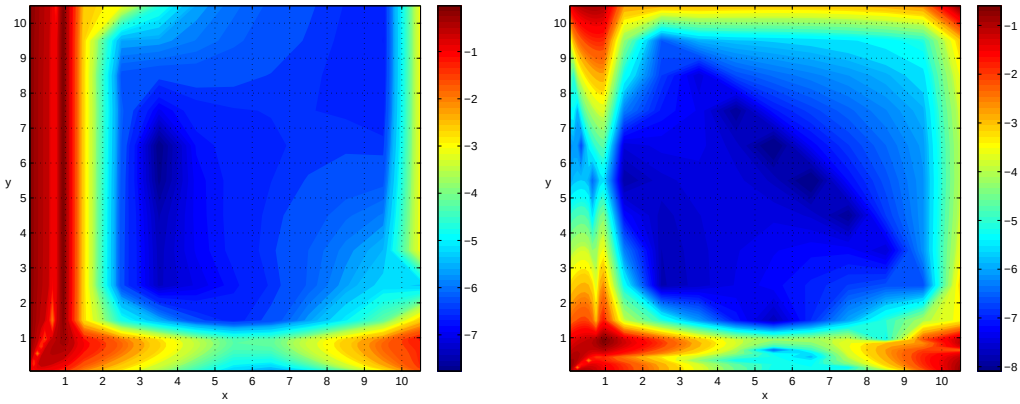

(a): $\log_{10}(M_{3,xx})$

(b): $\log_{10}(M_{3,xy})$

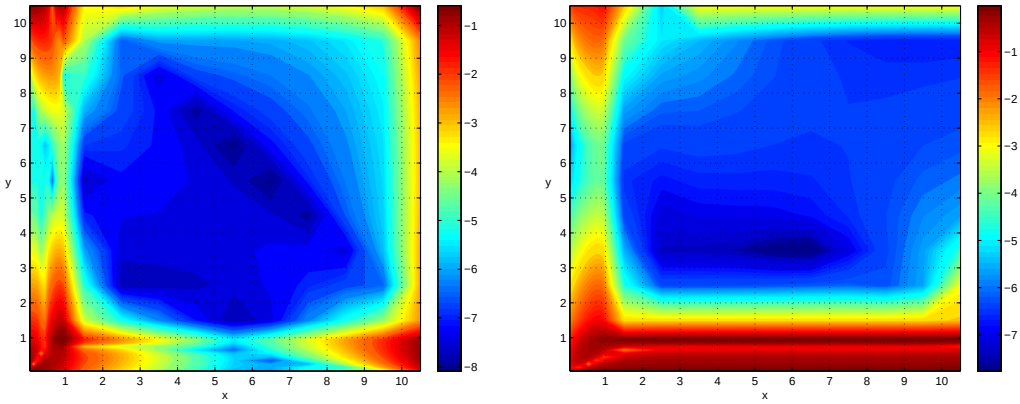

(c): $\log_{10}(M_{3,yx})$

(d): $\log_{10}(M_{3,yy})$

Figure 5.2: M_3 for Test A

Figure 5.2 shows M_3 calculated for Test A. The upper two graphs Figure 5.2a and Figure 5.2b, show the x-derivatives of the components of $\bar{\bar{E}}$, from Eq. 4.35, while the lower two graphs, Figure 5.2c and Figure 5.2d show the y-derivatives.

The results for Test B are not quite as dramatic as those in Test A, which can be seen in Figure 5.3 and Figure 5.4. For M_2 we notice that the diffusive domain, where $M_{2,xx}$ and $M_{2,yy} \leq 10^{-5}$, does not occur until $x, y = 15$ which is approximately 100 mean free paths into the domain. This is true too for Test A, where each cell is 100 mean free paths and the gradient for the metric is much steeper.

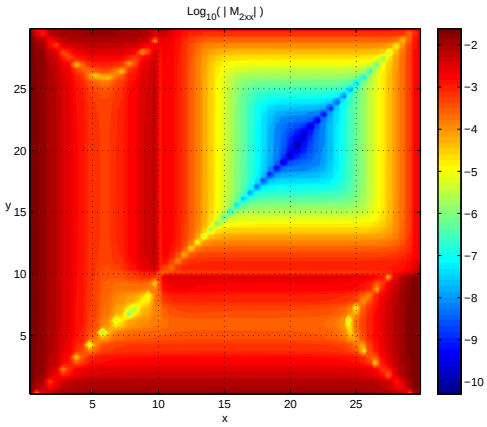

(a): $\log_{10}(M_{2,xx})$

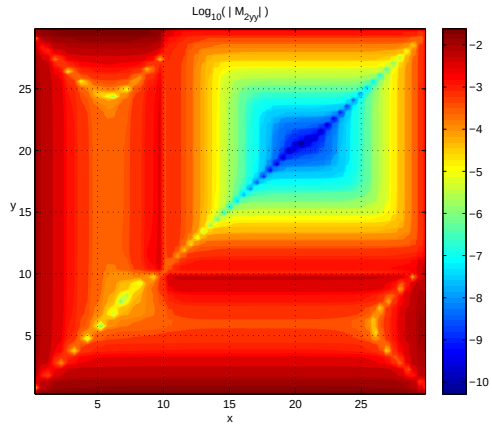

(b): $\log_{10}(M_{2,yy})$

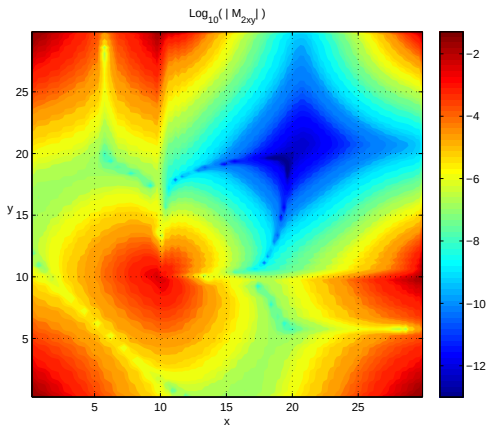

(c): $\log_{10}(M_{2,xy})$

Figure 5.3: M_2 for Test B

Figure 5.4 shows M_3 calculate for test B. The upper two graphs show the x-derivatives of the E_{xx} and E_{xy}, while the bottom two show the y-derivatives of E_{yy} and E_{yx}. We note that these metrics identify diffusive regions next to the boundary, which is why we consider all metrics presented rather than any single one.

Each of these plots shows the metrics calculated from the converged transport solution with no domain decomposition. These graphs accurately show where all the diffusive domains are, and highlight areas of strong transport effects. Compared to 1D, there are more effects here, which is why we must consider many different versions of the metrics to accurately define the diffusive domains. This estimate can not be based off the converged solution however, the

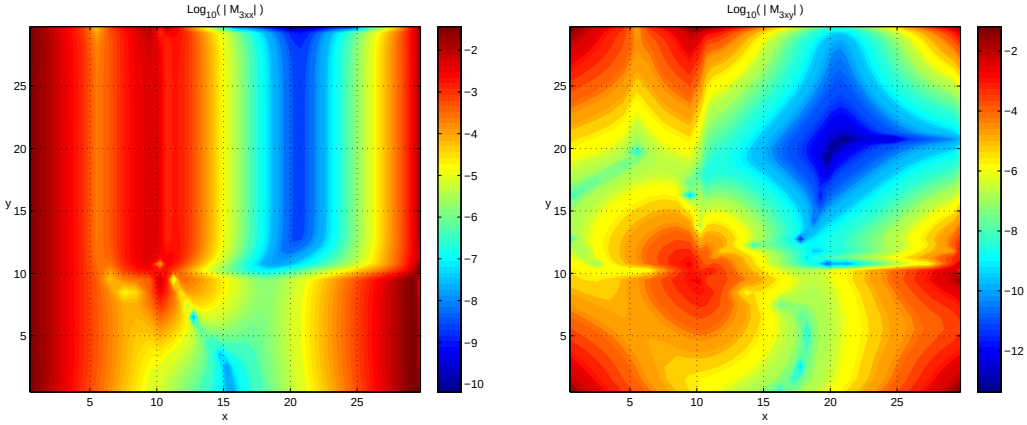

(a): $\log_{10}(M_{3,xx})$ (b): $\log_{10}(M_{3,xy})$

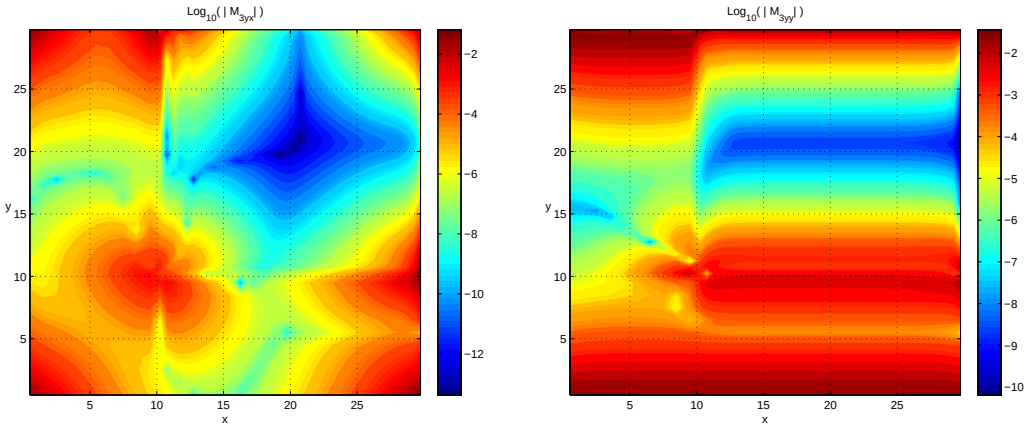

(c): $\log_{10}(M_{3,yx})$ (d): $\log_{10}(M_{3,yy})$

Figure 5.4: M_3 for Test B

metrics will need to be calculated after a single transport iteration to utilize the full methodology presented.

5.3 Metric Estimations in 2D

Here we look at the metrics that are calculated using only one transport iteration. The scattering term on the right hand side of the transport equation is based off a diffusion approximation of the whole domain. This approximation will allow us to estimate the location of diffusive areas for establishing subdomains. We first consider Test A.

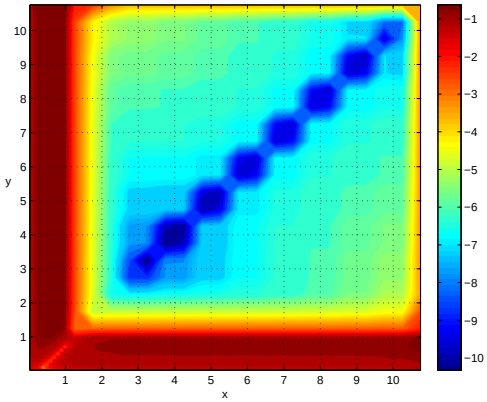

(a): $\log_{10}(M_{2,xx})$

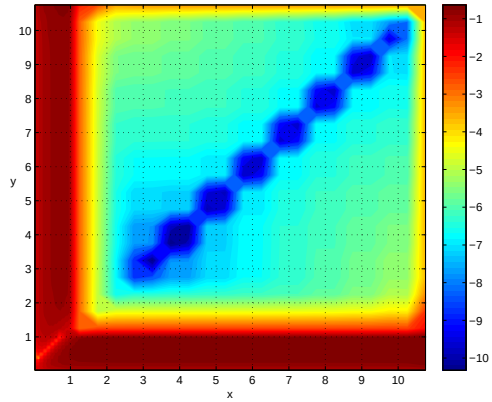

(b): $\log_{10}(M_{2,yy})$

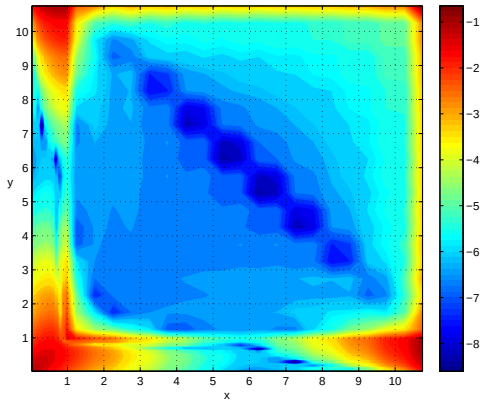

(c): $\log_{10}(M_{2,xy})$

Figure 5.5: M_2 Estimation for Test A

The metrics presented in Figure 5.5 and Figure 5.6 are the metrics estimated after one iteration. These figures can be compared to Figure 5.1 and Figure 5.2 respectively. We see

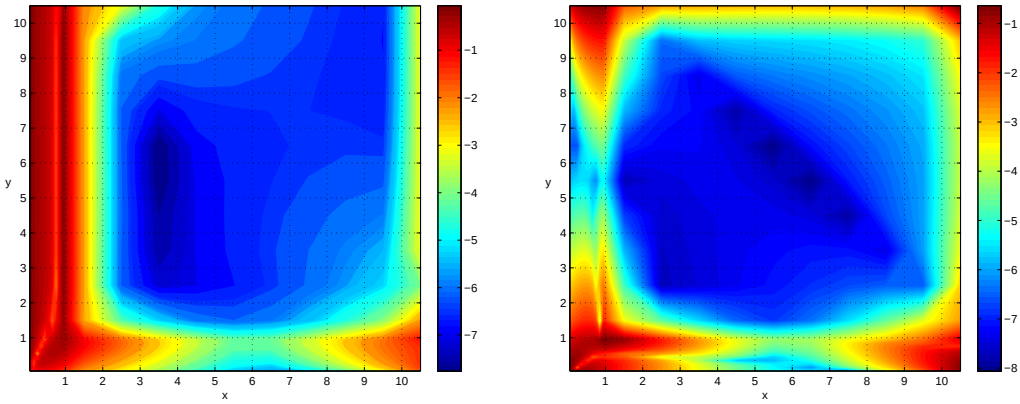

(a): $\log_{10}(M_{3,xx})$

(b): $\log_{10}(M_{3,xy})$

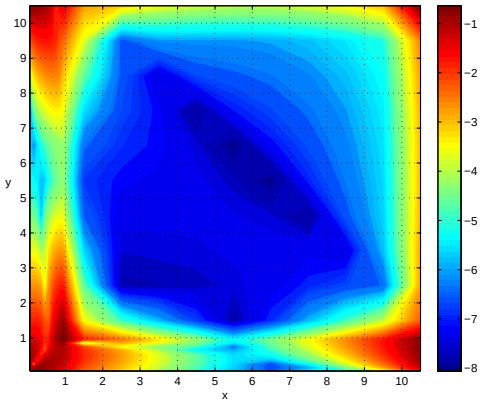

(c): $\log_{10}(M_{3,yx})$

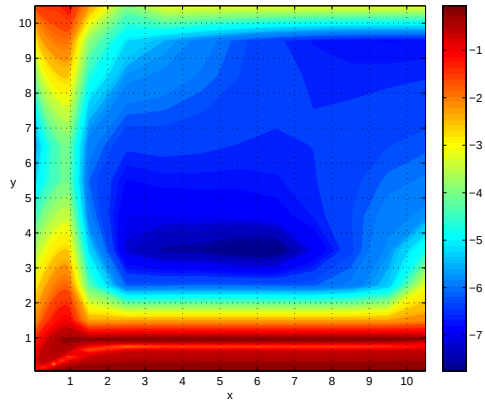

(d): $\log_{10}(M_{3,yy})$

Figure 5.6: M_3 Estimate for Test A

many of the same trends in both sets of figures, showing that this is an accurate estimation. To quantitatively evaluate the relative errors in the metrics we will use a L_1-norm,

$$\frac{\|M - M_{tr}\|_{L_1}}{\|M_{tr}\|_{L_1}}. \tag{5.1}$$

M_{tr} is a metric computed by a known solution obtained from a converged solution of the transport problem with no domain decomposition. The relative errors of M_2 and M_3 can be seen in Table 5.1. Notice that many of the values, e.g. $M_{2,xx}$ and $M_{2,yy}$ have the same error, this is because these metrics are symmetric to one another so it should follow that their error would be the same too.

Table 5.1: Error in Test A Metrics

Metric	$\|M - M_{tr}\|_{L_1} / \|M_{tr}\|_{L_1}$
$M_{2,xx}$	0.0482656
$M_{2,yy}$	0.0482656
$M_{2,xy}$	0.107730
$M_{3,xx}$	0.659710
$M_{3,xy}$	0.165611
$M_{3,yy}$	0.659710
$M_{3,yx}$	0.165611

Table 5.2: Error in Test B Metrics

Metric	$\|M - M_{tr}\|_{L_1} / \|M_{tr}\|_{L_1}$
$M_{2,xx}$	0.0168471
$M_{2,yy}$	0.0168471
$M_{2,xy}$	0.0225931
$M_{3,xx}$	0.0788289
$M_{3,xy}$	0.231046
$M_{3,yy}$	0.0788289
$M_{3,yx}$	0.231046

The results for estimating the metrics in test B can be seen in Figure 5.7 and Figure 5.8. These values represent the metrics calculated after one iteration and can be compared with those from the converged transport solution in Figure 5.3 and Figure 5.4 respectively. The error in these metrics is shown in Table 5.2.

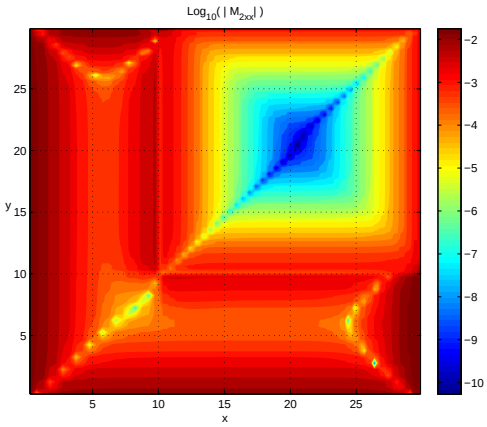

(a): $\log_{10}(M_{2,xx})$

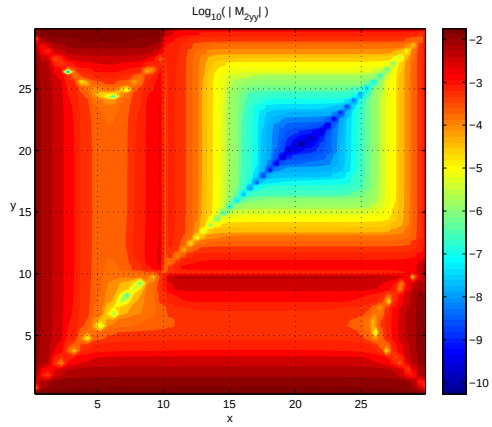

(b): $\log_{10}(M_{2,yy})$

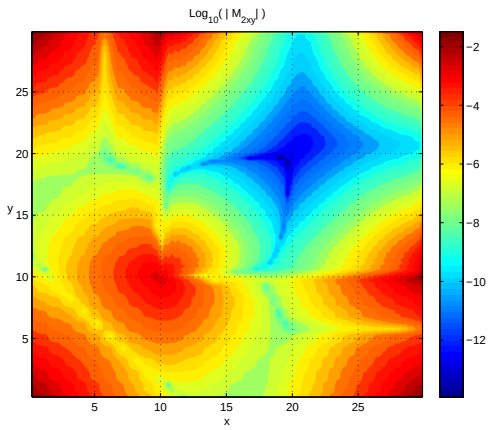

(c): $\log_{10}(M_{2,xy})$

Figure 5.7: M_2 Estimate for Test B

We can see from these results that our estimates of the metrics are sufficiently accurate for our purpose. The most important thing we need from these metrics is that they show the correct order, so that they can be captured by some user defined tolerance. This allows us to determine where the diffusive areas are for a domain decomposition method.

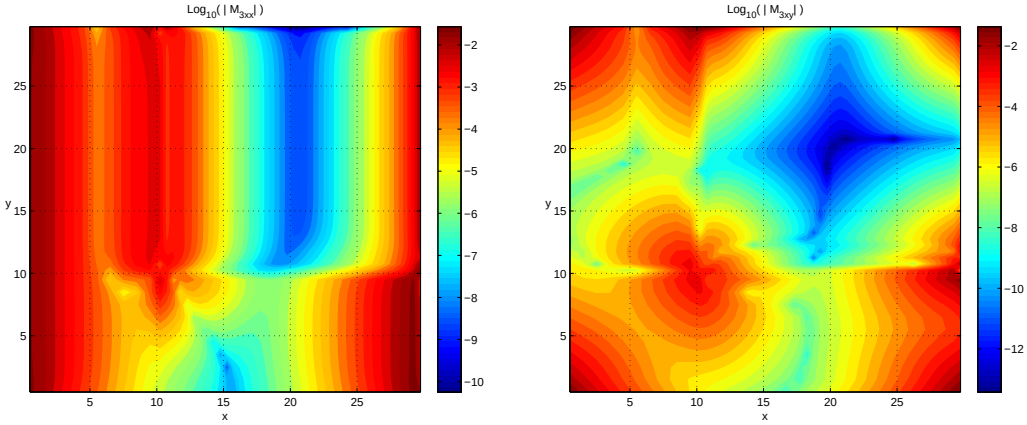

(a): $\log_{10}(M_{3,xx})$ (b): $\log_{10}(M_{3,xy})$

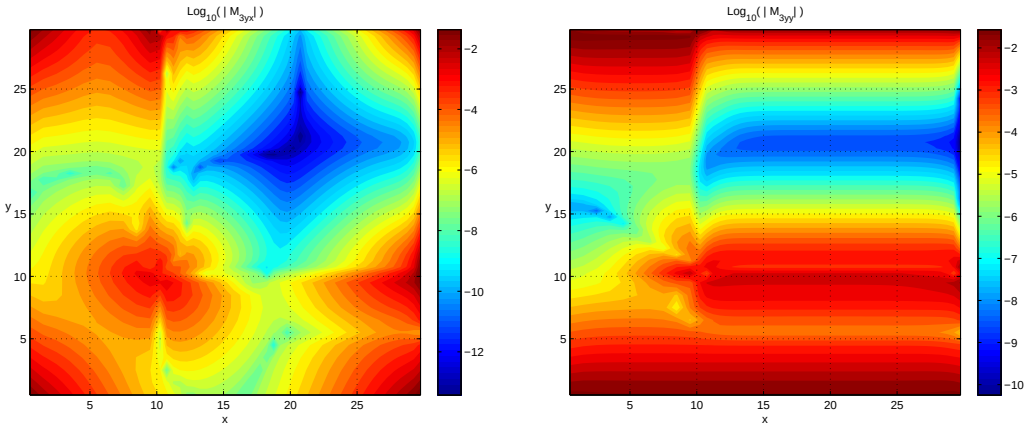

(c): $\log_{10}(M_{3,yx})$ (d): $\log_{10}(M_{3,yy})$

Figure 5.8: M_3 Estimate for Test B

5.4 Second Moment and Residual Terms

To evaluate the quality of the developed metrics, we can analyze the second moment and residual terms. These terms would be close to zero if the angular flux is linearly anisotropic. The residuals defined in Eq. 4.8, Eq. 4.16, Eq. 4.19, Eq. 4.21, and Eq. 4.23, can confirm our metric values in determining if a region is diffusive.

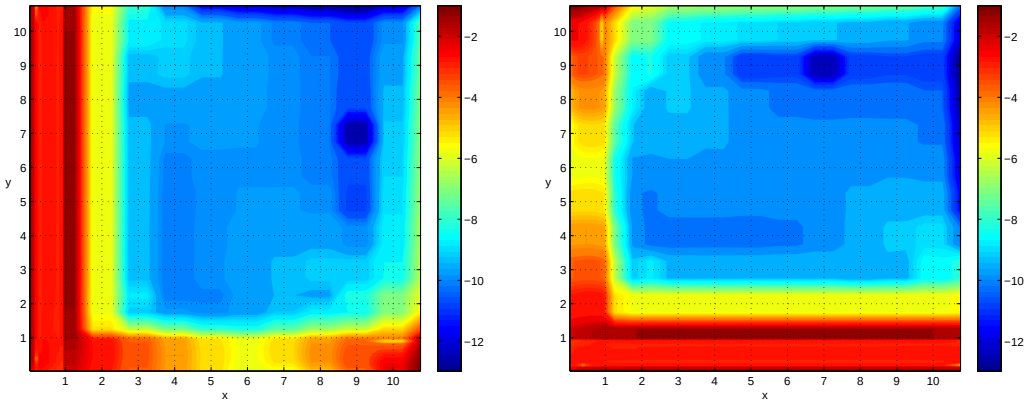

(a): $\log_{10}(r_{i,j})$ for Top and Bottom Face Values (b): $\log_{10}(r_{i,j})$ for Left and Right Face Values

Figure 5.9: $r_{i,j}$ for Test A

Figure 5.9 shows the residuals used in Eq. 4.4. The graph on the left shows the residuals calculated for r_{1B}, r_{2B}, r_{3T}, and r_{4T}, while the graph on the right shows r_{1L}, r_{2R}, r_{3R}, and r_{4L}. This plot shows the $log_{10}(r)$, so the values corresponding to different colors show what order of magnitude the value is. Notice that the center of the domain is typically well below 10^{-8}, indicating that this area is fairly diffusive.

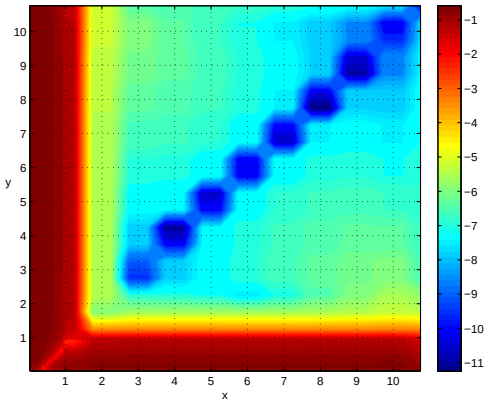

(a): $\log_{10}(R_{xx})$

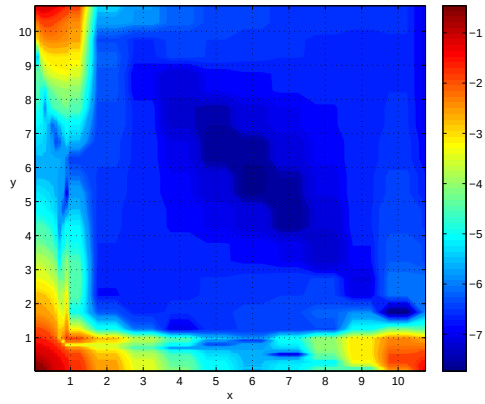

(b): $\log_{10}(R_{xy})$ for Left and Right Face Values

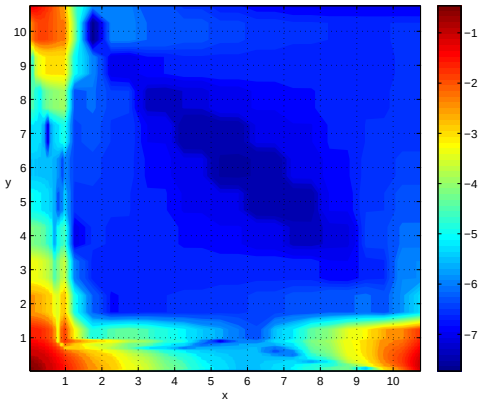

(c): $\log_{10}(R_{xy})$ for Top and Bottom Face Values

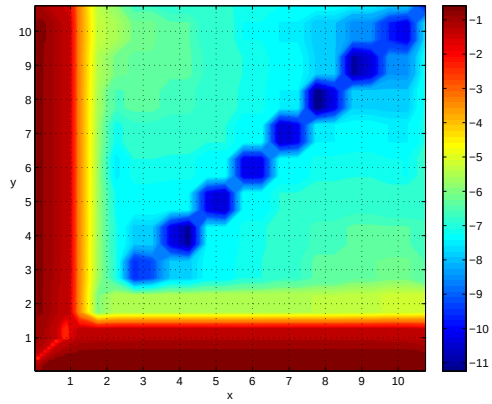

(d): $\log_{10}(R_{yy})$

Figure 5.10: $r_{i,j}$ for Test A

The residual terms, R, calculated to be used in Eq. 4.5 are presented in Figure 5.10a and Figure 5.10b, likewise the residuals used in Eq. 4.7 are presented in Figure 5.10c and Figure 5.10d. These all show trends similar to the metrics, indicating which areas can be considered diffusive. The last set of terms, $\hat{E}$, are shown in Figure 5.11. These Eddington-like terms are described by Eq. 4.8, and show the same trends as one sees for M_2 in Figure 5.1.

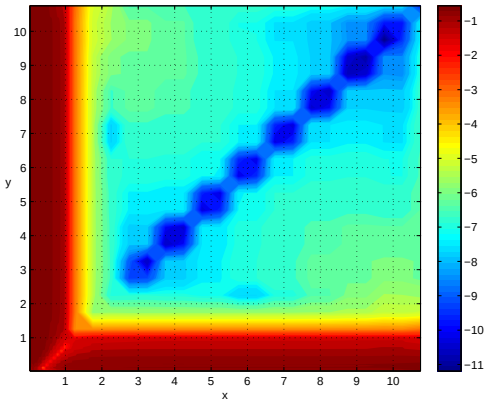

(a): $\log_{10}(\hat{E}_{xx})$

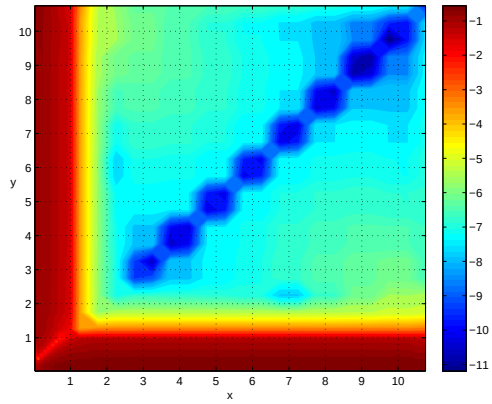

(b): $\log_{10}(\hat{E}_{yy})$

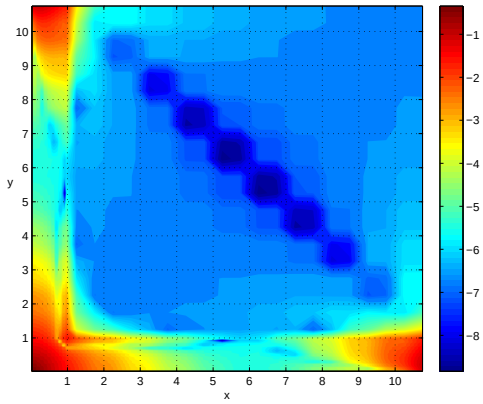

(c): $\log_{10}(\hat{E}_{xy})$

Figure 5.11: $\hat{E}_{i,j}$ for Test A

For all figures, we see that for cells inside the diffusion domain, most of the values are relatively small $< 10^{-5}$. This means that the right hand side of most of the low-order equations is relatively small well inside a diffusion domain. This indicates that one could set these values to 0.0 if it is known beforehand what areas are diffusive. Doing this will transform the SM equations into a diffusion approximation, and save the effort of having to solve the transport equation in these areas.

5.5 Domain Decomposition

Here we look at the effects of splitting the problem into multiple areas to see the effects of not solving transport in diffusive areas. We do not use the metrics to divide the domain, but rather to use them as verification of where we impose the diffusion areas. We use the same bounds as in the 1D case only extend them for both x and y bounds.

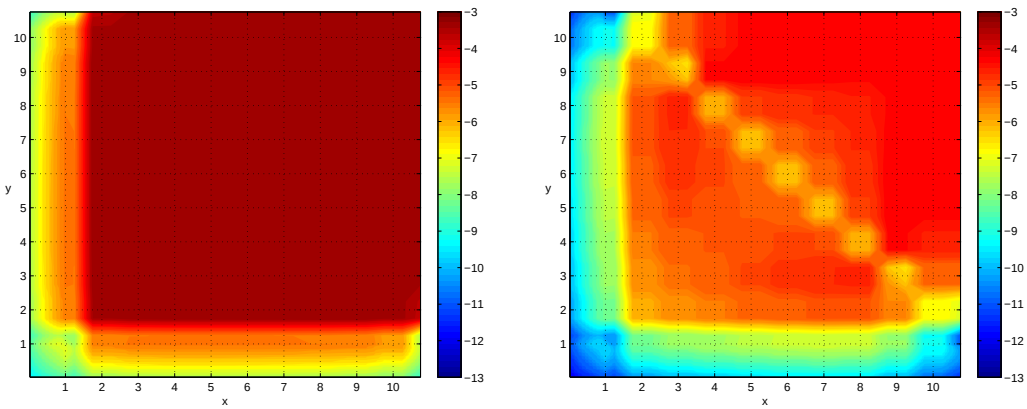

(a): $2 \leq x, y \leq 10$, P_1 Boundary Conditions (b): $3 \leq x, y \leq 9$, P_1 Boundary Conditions

Figure 5.12: Domain Decomposition of Test A, 2D

In Figure 5.12 we see the effects of imposing a diffusion subdomain in each problem at (a) $3 \leq x, y \leq 10$, and (b) $4 \leq x, y \leq 9$. The plots show the relative error of the scalar flux on a log scale. The areas of greatest error are at the subdomain boundaries and attenuate from there. We evaluate the relative error associated with each test in the L_1 norm. The results for Test A are shown in Table 5.3. We note that moving further inside the diffusive domain does reduce both the overall error and the maximum error. In Table 5.4, we see the largest metrics found in the diffusion domain for each case. Notice that the values decrease for smaller diffusion domains, indicating that we have a better approximation for the diffusion area, therefore error should decrease throughout the problem domain.

Table 5.3: Error in Test A Domain Decomposition

Diffusive Domain	$\|\phi - \phi_{tr}\|_{L_1} / \|\phi_{tr}\|_{L_1}$	$\max \|\phi_{error}\|$
$2 \leq x, y \leq 10$	5.97743×10^{-4}	2.55427×10^{-4}
$3 \leq x, y \leq 9$	5.64821×10^{-6}	5.54038×10^{-6}

Table 5.4: $\max |M|$ in Test A Diffusion Domain

Metric	$2 \leq x, y \leq 10$	$3 \leq x, y \leq 9$
$M_{2,xx}$	4.3568×10^{-6}	1.2602×10^{-6}
$M_{2,yy}$	4.3568×10^{-6}	1.2602×10^{-6}
$M_{2,xy}$	7.2996×10^{-6}	2.0778×10^{-6}
$M_{3,xx}$	7.9641×10^{-6}	1.6577×10^{-6}
$M_{3,xy}$	9.6736×10^{-6}	1.6416×10^{-6}
$M_{3,yy}$	7.9641×10^{-6}	1.6577×10^{-6}
$M_{3,xy}$	9.6736×10^{-6}	1.6416×10^{-6}

Figure 5.13 shows the results of imposing a diffusion subdomain in test B for diffusion regions defined by (a) $14 \leq x, y \leq 27.5$, (b) $15.5 \leq x, y \leq 26$, and (c) $17 \leq x, y \leq 25$. The integral norm, and maximal values can be seen in Table 5.5. All the figures are on the same scale, for each test, so it is easy to see the effects of splitting the boundary. We note that the largest source of error is always right at the interface of the regions, and this in turn affects the solution of the rest of the problem. Therefore, pushing the subdomain boundaries further into the diffusion area makes the approximations for the boundary conditions more accurate, and subsequently reduces error. In Table 5.6, we see the maximum error found in the diffusion domains. Here we observe the same trends as test A, where the metrics decrease the further we go into the diffusion domain, and making the diffusion approximation more accurate.

Table 5.5: Error in Test B Domain Decomposition

Diffusive Domain	$\|\phi - \phi_{tr}\|_{L_1} / \|\phi_{tr}\|_{L_1}$	$\max \|\phi_{error}\|$
$14 \leq x, y \leq 27.5$	5.97743×10^{-4}	2.55427×10^{-4}
$15.5 \leq x, y \leq 26$	1.75911×10^{-8}	2.15391×10^{-6}
$17 \leq x, y \leq 25$	1.90811×10^{-9}	3.85300×10^{-7}

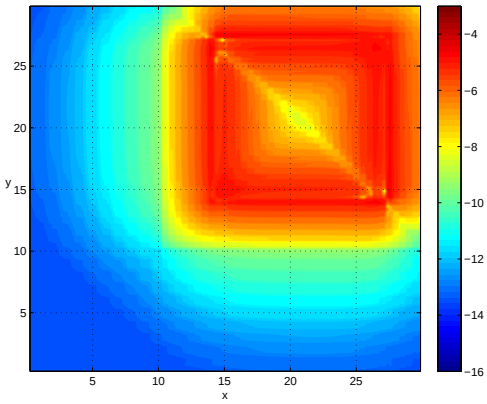

(a): $14 \leq x, y \leq 27.5$, P_1 Boundary Conditions

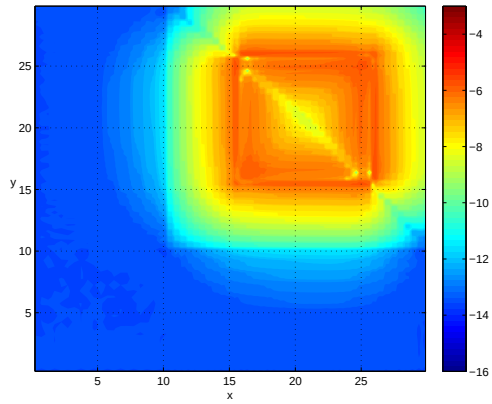

(b): $15.5 \leq x, y \leq 26$, P_1 Boundary Conditions

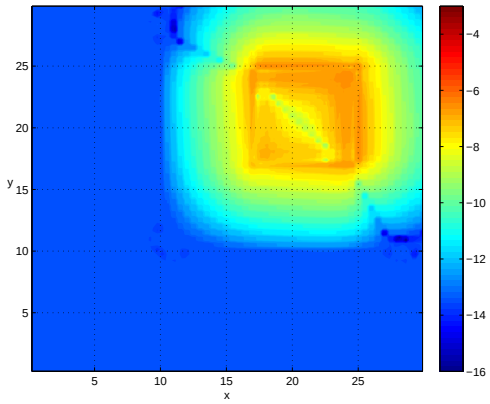

(c): $17 \leq x, y \leq 25$, P_1 Boundary Conditions

Figure 5.13: Domain Decomposition of Test A, 2D

Table 5.6: $\max |M|$ in Test B Diffusion Domain

Metric	$14 \leq x, y \leq 27.5$	$15.5 \leq x, y \leq 26$	$17 \leq x, y \leq 25$
$M_{2,xx}$	3.6464×10^{-5}	3.0585×10^{-6}	4.9750×10^{-7}
$M_{2,yy}$	3.6464×10^{-5}	3.0585×10^{-6}	4.9750×10^{-7}
$M_{2,xy}$	1.4903×10^{-6}	3.8417×10^{-8}	2.5764×10^{-9}
$M_{3,xx}$	7.5525×10^{-5}	6.2211×10^{-6}	1.1925×10^{-6}
$M_{3,xy}$	1.2313×10^{-6}	3.1407×10^{-8}	1.8503×10^{-9}
$M_{3,yy}$	7.5525×10^{-5}	6.2211×10^{-6}	1.1925×10^{-6}
$M_{3,yx}$	1.2313×10^{-6}	3.1407×10^{-8}	1.8503×10^{-9}

Chapter 6

Conclusions

In this study we analyzed how transport problems can be decomposed into multiple transport and diffusion domains to improve efficiency while still maintaining a required level of accuracy. 1D problems were studied using the Linear Discontinuous method, and 2D problems were solved using the Simple Corner Balance method. The Second Moment method was used to develop a set of low-order equations that would provide a solution everywhere and accelerate the convergence of the transport solution. Metrics for measuring transport effects were developed to determine how to split the domain, and different boundary conditions were used to couple the different kinds of domains.

In the 1D problems we saw a variety of results that showed a proof of concept. We determined in test A that a domain that is highly scattering can be successfully decomposed, while still generating a solution that is close to what is expected. It should be noted that test A is diffusive in terms of an asymptotic analysis, with scaling parameter 10^{-2}, meaning that even better results can be generated if the problem were more optically thick (i.e. corresponds to a smaller scaling parameter). These ideas were expanded for 2D transport and similar results were obtained. The results show that the greatest error in the domains always took place at the boundaries of the domain. This tells us that the limiting factor for not generating better results are the boundary conditions that couple transport and diffusion domains.

Test B in both 1D and 2D was meant to represent another type of problem where domains may only be slightly diffusive. Here the results show that we still get adequate solutions to the transport problem using the proposed domain decomposition method. We note that in our methodology we used a true diffusion equation for our low-order equations. That is, we modified our low order equations so that any second-moment terms would be set to zero.

We showed the proposed metrics enable one to quantify transport effects and determine the spatial range of diffusive domains.The algorithm developed in this paper can be applied to many production codes because it consists of a set of low order equations used in conjunction

with whatever transport method is being used. This set of low order equations can be solved everywhere and provide boundary conditions to the transport solver to limit where it is used. This will increase the efficiency of the transport calculations by not having to solve the transport problem everywhere, while still maintaining a desirable level of accuracy.

6.1 Future Work

This study can be expanded upon especially in terms of the 2D results. The discretized second moment low-order equations used can be simplified by eliminating part of the unknowns. This can significantly reduce the size of the matrix that is needed to be inverted, thus reducing the computational load in terms of execution time and the memory needed.

Better boundary conditions can be determined in the 2D case. The next step is to reproduce some necessary details of the asymptotic diffusion analysis on the SCB method. This derivation should improve the interface conditions coupling the different regions based on the asymptotic expansion of the angular flux. An analysis using different quadratures can be used to see if any one shows a significant advantage.

REFERENCES

[1] Marvin L. Adams and Edward W. Larsen. Fast iterative methods for discrete-ordinates particle transport calculations. *Progress in Nuclear Energy*, 40(1):3 – 159, 2002.

[2] Edward W. Larsen. Unconditionally stable diffusion-synthetic acceleration methods for the slab geometry discrete ordinates equations. part i: Theory. *Nuclear Science and Engineering*, 82(1):47 – 63, 1982.

[3] ML Adams. Discontinuous Finite Element Transport Solutions in Thick Diffusive Problems. *Nuclear Science and Engineering*, 137(3):298–333, MAR 2001.

[4] A. Klar and N. Siedow. Boundary layers and domain decomposition for radiative heat transfer and diffusion equations: Applications to glass manufacturing processes. *European J. Appl. Math*, 9:351–372, 1998.

[5] Edward W. Larsen. Asymptotic diffusion limit of discretized transport problems. *Nuclear Science and Engineering*, 112(4):336 – 346, 1992. Asymptotic diffusion limit;Transport problems;.

[6] Musa Yavuz and Edward W. Larsen. Spatial domain decomposition for neutron transport problems. *Transport Theory and Statistical Physics*, 18(2):205–219, 1989.

[7] Y. Y. Azmy. Communication strategies for angular domain decomposition of transport calculations on message passing multiprocessors. *Proceedings of the Joint International Conference on Mathematical Methods and Supercomputing for Nuclear Applications*, 1:404, 1997.

[8] Alireza Haghighat. Spatial and angular domain decomposition algorithms for the curvilinear s_n transport theory method. *Transport Theory and Statistical Physics*, 22(2&3):391–417, 1993.

[9] H. Neunzert A. Klar and J. Struckmeier. Transition from kinetic theory to macroscopic fluid equations: A problem for domain decomposition and a source for new algorithms. *Transport Theory and Statistical Physics*, 29(1&2):93–106, 2000.

[10] N. Stehle and D.Y. Anistratov. Methodology for decomposition into transport and diffusive subdomains for the linear discontinuous method. In *The 22nd International conference on Transport Theory (ICTT-22)*, Portland, Oregon, 2011.

[11] Nicholas D. Stehle, Dmitriy Y. Anistratov, and Marvin L. Adams. Domain decomposition method for the simple corner balance scheme in problems with diffusive regions. *Transactions of American Nuclear Society*, 105, 2011.

[12] James J. Duderstadt and Louis J. Hamilton. *Nuclear reactor analysis.* Wiley, New York, 1976.

[13] R. Vaidyanathan. A finite moments algorithm for particle transport problems. *Nuclear Science and Engineering*, 71:46–54, 1979.

[14] Marvin L. Adams. Subcell balance methods for radiative transfer on arbitrary grids. *Transport Theory and Statistical Physics*, 26(4-5):385–431, 1997.

[15] T. A. Wareing. New diffusion-synthetic acceleration methods for the s_n equations with corner balance spatial differencing. *Joint International Conference on Mathematical Methods and Supercomputing in Nuclear Applications*, 2:500–511, 1993.

[16] E. E. Lewis and W. F. Miller. A comparison of p_1 synthetic acceleration techniques. *Transactions of the American Nuclear Society*, 23:202, 1976.

[17] Edward W Larsen and J.E. Morel. Asymptotic solutions of numerical transport problems in optically thick, diffusive regimes ii. *Journal of Computational Physics*, 83(1):212 – 236, 1989.

[18] V. Ya. Gol'din. A quasi-diffusion method of solving the kinetic equation. *USSR Computational Mathematics and Mathematical Physics*, 4(6):136 – 149, 1964.

[19] Dmitriy Y. Anistratov. Evaluation of transport effects and spatial domain decomposition into transport and diffusive subdomains in 1d geometry. *Transactions of the American Nuclear Society*, 101:390 – 393, 2009.

[20] G.I. Bell and S. Glasstone. *Nuclear Reactor Theory.* R. E. Krieger Pub. Co., 1979.

[21] J.E. Denedy J.E. Morel and T.A. Wareing. Diffusion-Accelerated Solution of the 2-Dimensional S_n Equations with Bilinear-Discontinuous Differencing. *Nuclear Science and Engineering*, 115(4):304–319, Dec 1993.

[22] Marvin L. Adams. Private Communication, 2011.

[23] M. Miften and E.W. Larsen. A symmetrized quasidiffusion method for solving transport problems in multidimensional geometries. *Proc. ANS Topical Meeting, Mathematical Methods and Supercomputing in Nuclear Applications*, 1:707–717, 1993.

[24] I. Abu-Shumays. Angular quadratures for improved transport computations. *Transport Theory & Statistical Physics*, 30(2/3):169, 2001.